

## 8. SITE 1005<sup>1</sup>

### Shipboard Scientific Party<sup>2</sup>

#### HOLE 1005A

**Position:** 24°33.772'N, 79°14.141'W  
**Start hole:** 2000 hr, 7 March 1996  
**End hole:** 2030 hr, 10 March 1996  
**Time on hole:** 3 days, 30 min  
**Seafloor (drill pipe measurement from rig floor, mbrf):** 362  
**Total depth (drill pipe measurement from rig floor, mbrf):** 824.4  
**Distance between rig floor and sea level (m):** 11.3  
**Water depth (drill pipe measurement from sea level, m):** 350.7  
**Penetration (mbsf):** 462.4  
**Coring totals:**  
Type: APC; No: 9; Cored: 67.5 m; Recovered: 101.3%  
Type: XCB; No: 44; Cored: 394.9 m; Recovered: 20.6%  
**Formation:**  
Unit I: 0–261.7 mbsf, Quaternary to early Pliocene in age  
Unlithified to partially lithified peloidal wackestones  
Unit II: 261.7–360.9 mbsf, early Pliocene in age  
Partially lithified and dolomitized mudstones to wackestones  
Unit III: 360.9–462.4 mbsf, early Pliocene to late Miocene in age  
Partially dolomitized foraminifer wackestones with moderate to heavy bioturbation

#### HOLE 1005B

**Position:** 24°33.766'N, 79°14.142'W  
**Start hole:** 2030 hr, 10 March 1996  
**End hole:** 1300 hr, 11 March 1996  
**Time on hole:** 16 hr, 30 min  
**Seafloor (drill pipe measurement from rig floor, mbrf):** 363  
**Total depth (drill pipe measurement from rig floor, mbrf):** 424.7  
**Distance between rig floor and sea level (m):** 11.3  
**Water depth (drill pipe measurement from sea level, m):** 351.7  
**Penetration (mbsf):** 61.7  
**Coring totals:**  
Type: APC; No: 7; Cored: 51.0 m; Recovered: 81.4%  
Type: XCB; No: 2; Cored: 10.7 m; Recovered: 74.0%  
**Formation:**  
Unit I: 0–61.7 mbsf, Quaternary in age  
Unlithified to partially lithified peloidal wackestones

#### HOLE 1005C

**Position:** 24°33.755'N, 79°14.141'W  
**Start hole:** 1300 hr, 11 March 1996  
**End hole:** 0900 hr, 15 March 1996  
**Time on hole:** 3 days, 20 hr  
**Seafloor (drill pipe measurement from rig floor, mbrf):** 363  
**Total depth (drill pipe measurement from rig floor, mbrf):** 1063  
**Distance between rig floor and sea level (m):** 11.4  
**Water depth (drill pipe measurement from sea level, m):** 351.6  
**Penetration (mbsf):** 700.0  
**Coring totals:**  
Type: RCB; No: 34; Cored: 313.4 m; Recovered: 34.1%  
**Formation:**  
Unit III: 360.9–534.3 mbsf; early Pliocene to late Miocene in age  
Partially dolomitized foraminifer wackestones with moderate to heavy bioturbation  
Unit IV: 534.3 to 700 mbsf; middle to late Miocene in age  
Foraminifer wackestones that are heavily dolomitized and bioturbated

**Principal results:** Site 1005 is the most proximal site of five sites along the Bahamas Transect from the western margin of the Great Bahama Bank (GBB) into the Straits of Florida. Site 1005 is located in 352 m water depth, approximately 1150 m from the modern platform edge on the upper slope, 30 shot points southwest of the crossing of seismic Lines 106 and 107. It is positioned on the thickest portion of the prograding Neogene sequences seen on the seismic line. The target depth of 700 m was designed to penetrate nine seismic sequences. The sea-level objectives of Site 1005 were to (1) date precisely the sequence boundaries, (2) determine the facies within the different systems tracts, especially the nature of the onlapping units that were interpreted as lowstand deposits, and (3) retrieve a high-resolution record of climate and sea-level fluctuations for the Quaternary and late Pliocene. This site served also as the proximal site for the fluid-flow transect. A logging suite was collected to provide a continuous record of the sedimentary succession. In addition, a vertical seismic profile (VSP) was shot for an accurate time-depth conversion of the seismic reflections for a precise correlation of the cores to the seismic data.

A 700-m-thick Holocene to upper middle Miocene section was recovered at Site 1005. The sedimentary succession consists of a periplatform sedimentary section of mixed pelagic and bank-derived carbonates, with a carbonate content of 72%–99%. The section is composed of unlithified to partially lithified wackestones and slightly coarser grained intervals consisting of packstones and grainstones. Compositional variations document an alternating pattern of bank flooding, concomitant shedding to the slope with periods of exposed banks, a shutdown of shallow-water carbonate production, and largely pelagic sedimentation that is recorded in alternating high and low sedimentation rates. Periods of increased input of bank-derived material coincide with the progradation periods characterized by the seismic data as seismic sequences. This sedimentation pattern indicates that sea-level changes exert the major control on the development of the seismic sequences. Foraminifer and nannofossil biostratigra-

<sup>1</sup>Eberli, G.P., Swart, P.K., Malone, M.J., et al., 1997. *Proc. ODP, Init. Repts.*, 166: College Station, TX (Ocean Drilling Program).

<sup>2</sup>Shipboard Scientific Party is given in the list preceding the Table of Contents.

phy yielded precise ages of the lithologic units and seismic sequence boundaries. One of the seismic sequence boundaries coincides with a hiatus that probably straddles the Miocene/Pliocene boundary. Three other boundaries correlate to changes in sedimentation rates, whereas with the remaining boundaries no biostratigraphic hiatus is detected. The biostratigraphic data from Site 1005 confirm the ages that were carried along seismic reflections from Sites 1003 to 1005. This consistency gives a first indication that the seismic sequence boundaries (SSB) along the Bahamas Transect are indeed time lines. The cores, in combination with the logging data, provide the facies information in the seismic sequences and systems tracts. We found few mass gravity flow deposits in this proximal site, even less than at Site 1003. Obviously most of the platform-derived turbidites bypassed the upper slope. The thick Pleistocene section is characterized by sedimentation cycles that have all the characteristics of the periplatform aragonite cycles found in the basin surrounding the Bahamian platforms. These cycles are interpreted to have formed as a result of the high-frequency Pleistocene sea-level changes.

As observed at Sites 1003 and 1004, pore-water chemistry profiles at Site 1005 display normal seawater concentrations of all constituents in the upper 45 mbsf, indicating rapid exchange with the water column. Below this zone, organic matter remineralization reactions dominate the diagenetic changes. These reactions are a result of the high in situ abundance of organic material trapped within these marginal sediments during rapid Pliocene/Pleistocene platform shedding events, and provide the fuel that drives the early carbonate alteration reactions in these shallow sediments. Deeper (i.e., below 400 mbsf) increased salinity suggests the influence of deep-seated saline fluids. Some indications of fluid derived from the platform surface are shown by positive salinity anomalies between 50 and 150 mbsf.

The sedimentary succession of Site 1005 can be subdivided into four units. Although these sediments were deposited in a proximal position on the slopes of the GBB, they are generally fine-grained. Their main components are aragonite mud, platform-derived skeletal debris, and pelagic foraminifers and nannofossil ooze.

Unit I (0–261.7 mbsf) is of Holocene to late Pliocene age. The basal boundary of this unit is placed at the onset of peloids and aragonite mud. Variations in abundance of these two components were used to further subdivide the unit. Only a few turbidite layers are preserved as a result of heavy bioturbation that has obliterated many primary sedimentary structures. The sediments consist of unlithified to partially lithified mudstones, peloidal wackestones, and packstones. Components in the silt and sand fraction are peloids, benthic foraminifers, *Halimeda*, and other skeletal debris. Unit IA shows a cyclic sedimentation pattern with aragonite-rich intervals alternating with more pelagic intervals. Turbidites are concentrated in the aragonite intervals. Subunit IB is partially dolomitized and has a similar composition, but it does not display the pronounced cyclicality of Subunit IA. Subunit IC is also slightly dolomitized and consists mostly of partially lithified mudstones and wackestones with thin layers of clay- to silt-sized laminated intervals. The silt-rich layers are enriched in pelagic and benthic foraminifers and pellets.

Unit II (261.7–360.9 mbsf, early Pliocene in age) is a homogeneous section of partially lithified and dolomitized mudstones to wackestones. The constituents are predominantly pelagic foraminifers, with minor amounts of benthic foraminifers, lithoclasts, and unidentifiable bioclasts.

In Unit III (360.9–462.4 mbsf, early Pliocene to late Miocene in age) aragonite needles or pellets are no longer observed. The succession of partially dolomitized foraminifer wackestones displays a cyclic pattern. Gray to light gray well-cemented biowackestones alternate with less cemented gray to olive gray wackestones with compacted burrows. The boundary between the two lithologies is generally sharp. The average thickness of the compacted intervals in this unit is approximately 44 cm, but these intervals are thickest in the bottom portion of the succession.

In the middle to upper Miocene Unit IV (534.3–700 mbsf), the compacted interval of the cycles is nearly 80 cm thick, but also shows an increase in thickness downcore. The top of Unit IV is marked by a series of thin-bedded turbidites that are intercalated in the cycles. The cycles are in-

terpreted as being formed by variations in the amount of platform-derived material. The gray well-cemented intervals have a higher abundance of platform-derived clasts, whereas, the darker layers have more planktonic foraminifers and a higher organic content.

The sediments of Site 1005 document that the upper slope environment of the prograding margin of the GBB is dominated by fine-grained sediments. The variations in these mudstones and wackestones are subtle, but nevertheless give a record of platform shedding as a result of high-frequency sea-level changes. The observed trend of increasing thickness of the gray lithologies of the cycles within Units III and IV indicates an increase of progradation in these units.

Although Site 1005 was only 1.5 km from the modern platform edge of the GBB on the upper slope, biostratigraphic dating was possible, and there was good agreement between the nannofossil and planktonic foraminifer biostratigraphic events. Biostratigraphy indicates continuous sedimentation from the Pleistocene to the lower Pliocene. A major hiatus occurs in the upper Miocene that reaches from 5.6 back to 8.6 Ma. A hiatus of similar duration was also found farther downslope at Site 1003. In the previously drilled shallow-water platform sites Unda and Clino, the hiatus is not as extensive as more of the upper Miocene section is preserved. At Site 1005, the faunal assemblages below this unconformity are early late to late middle Miocene in age.

The benthic foraminifer assemblages indicate an upper bathyal paleodepth for Site 1005. The diversity and abundance of platform-derived benthic foraminifers provide an additional record of platform progradation and flooding events. In much of the Pleistocene section, there is a diverse and abundant benthic fauna, whereas only a depauperate assemblage is found in the upper Pliocene. In the lower Pliocene and the Miocene, a low diversity shallow-water assemblage is diluted in the monotonous sediments.

Variations in sedimentation rates reflect the export of bank-derived material to the upper slope. The late Pleistocene sedimentation rate was high (15 cm/k.y.), but it was reduced during the late Pliocene and early Pleistocene (3.5–1.2 Ma) to approximately 2 cm/k.y. This latter rate is characteristic of normal pelagic carbonate sedimentation with little to no addition of platform-derived material. The early Pliocene sedimentation rate was also high (10 cm/k.y.), indicating that the leeward side of the GBB received large amounts of platform-derived material during this period. A hiatus that spans nannofossil Zone NN11 (5.6–8.6 Ma) was probably caused by the combination of large-scale slope erosion associated with lower sea level and increased current activity, as there is little to no pelagic sedimentation recorded. An expanded lower upper Miocene section was recovered below the hiatus. The high sedimentation rate of 11 cm/k.y. during nannofossil Zones NN9 and NN10 reflects another period of platform shedding, consisting mostly of fine carbonate mud to the upper slope. There is minimal input from the platform during nannofossil Zone NN8. Another high input of platform-derived material occurred during the late middle Miocene yielding sedimentation rates of 13 cm/k.y. The sedimentation rates are in concert with long-term sea-level changes. The two largest known long-term sea-level falls straddle the middle/late Miocene and early/late Pliocene boundaries and are clearly expressed in the sedimentation rates at Site 1005 and also at Site 1003. Higher-frequency sea-level changes are indicated in the sedimentation patterns but beyond the resolution of biostratigraphic dating.

After logging, a check shot survey (VSP) was performed that allows for the correlation of the cores with the seismic data. Three of the six seismic sequence boundaries coincide with abrupt changes in sedimentation rate, and the late Miocene hiatus coincides with sequence Boundary G. In addition, the thick seismic sequences coincide with the periods of high sedimentation rates. There is also a good correlation of the seismic sequence boundaries with changes in mineralogy. In the Pleistocene section, the sequence boundaries coincide with low contents of high-magnesium calcite (HMC) and aragonite that record reduced platform-derived sediment input. In the Pliocene and Miocene section, the boundaries are either associated with high amounts of insoluble residues or peaks of dolomite. The overall monotonous sediments do not yield dramatic facies changes

at sequence boundaries. The sequence boundaries generally correlate to mudstone intervals that contain a larger amount of nannofossil ooze. The oldest sequence boundary recovered on the middle Miocene is marked by a firmground.

The log data correlate well with the sedimentary succession and can be used to fill in gaps in low recovery zones. The strong cyclic nature of the data is the most notable feature recorded in all the logs, specifically from 700 to 385 mbsf (middle Miocene to lowest Pliocene) and from 260 to 90 mbsf (upper Pliocene to Pleistocene). The intervening section from 385 to 260 mbsf (lower Pliocene) is marked by an apparent stark diminution of the intensity of the cycles, as reflected in particular by the monotony of the resistivity curve. Between 260 and 90 mbsf, the sharp increases in gamma-ray intensity correlate with increased density, resistivity, and velocity and decreased porosity. This association is indicative of more indurated sediment deposited during periods with a reduced sedimentation rate leading to hardground formation. The logs clearly display that the sedimentation pattern was punctuated by periods of decreased sediment input marked by the formation of better cemented layers. The log data correlate well with the seismic sequence boundaries. Not surprisingly, the velocity log has the strongest correlation.

In summary, the sedimentary, mineralogical, geophysical, and stratigraphic data provide the record of a sedimentary system characterized by variable input of platform-derived sediment that is most likely caused by changing sea level. These input fluctuations occur on several levels. A high-frequency cyclic alternation is seen in the sedimentary and the log data, while the sedimentation rates monitor the long-term changes. The seismic sequences provide a record on an intermediate scale.

The interstitial water chemistry at Site 1005 yielded interesting geochemical profiles that can be subdivided into four zones. The top 45 mbsf displays no change in most measured constituents. This zone probably experiences pervasive flushing of seawater that prevents diffusional gradients from developing between the overlying seawater and the underlying saline fluid. Zone 2 extends to a depth of 190 mbsf and is characterized by a sharp change in the gradient of all major and minor pore-water constituents.  $\text{Cl}^-$  is enriched in this zone, which might either reflect an intrusion of saline, sulfate-rich water derived from the shallow platform or indicate penetration of bottom water into the sediments deeper in the core. High rates of microbial sulfate reduction within this zone reduce the sulfate concentration to zero and give all major ion profiles an anomalous appearance. In the two underlying zones, most constituents display a steady change to the bottom of the hole. A shift in many profiles marks the boundary between Zones 3 and 4. At this time it is not known to what extent the shifts are influenced by diagenetic alterations within lithologic units.

The cores and data collected at Site 1005 provide the necessary information to answer several of the questions addressed before drilling this site. In regard to the sea-level objectives, the data corroborated the results of the more distal Site 1003. Site 1005 also yielded abundant biostratigraphic markers that allow for the precise age dating of the sequence boundaries. Furthermore, the ages can be carried along the seismic reflection horizons to Site 1003, where they fall on the same stratigraphic level. This consistency documents that the seismic reflections are indeed time lines and have a chronostratigraphic significance. The impedance that causes seismic reflections is controlled by both original sediment composition and the diagenetic overprint. In these carbonate slope sediments, sediment composition itself is largely controlled by the input of platform-derived sediment, which in turn is related to sea-level fluctuations. Early diagenetic alteration is strongest during reduced sedimentation rates when the platform is exposed. Thus, both facies and diagenesis are related to sea level, which leaves its expression in physical properties and finally in the seismic sequences.

In regard to the fluid-flow objectives, the geochemical profiles of Site 1005, in conjunction with Sites 1003 and 1004, provided further evidence for fluid flow through the slopes of the GBB. In particular, the upper flushed zone seen at Sites 1003 and 1004 extended to Site 1005, and there was evidence of the intrusion of lower salinity bottom water into the sediments.

## BACKGROUND AND OBJECTIVES

Site 1005 is the most proximal of five sites along the Bahamas Transect from the western margin of the Great Bahama Bank (GBB) into the Straits of Florida. Site 1005 is located in 352 m water depth, approximately 1150 m from the modern platform edge on the upper slope (Fig. 1), and positioned on the thickest portion of the prograding Neogene sequences seen on the seismic data. Based on a set of single-channel seismic lines, Wilber et al. (1990) mapped the Holocene sediment thickness along the western margin of GBB and predicted approximately 20 m of Holocene sediments in the area of Site 1005. On our seismic data, the upper Pliocene–Quaternary package (Sequences *a* through *e*) is nearly 200 m thick, forming a downlapping wedge that thins basinward (see Fig. 2). Below this wedge, the seismic data show a package of transparent facies overlying continuous seismic reflections and intervals with channelized and discontinuous reflections. A 700-m hole was planned to penetrate nine seismic sequences that were deposited between the upper middle Miocene and Holocene.

The thick sedimentary section at Site 1005 indicates high rates of sedimentation that make this site suitable for a detailed analysis of high-frequency climate and sea-level changes. High-frequency fluctuations in sea level are recorded in sediments on the slopes of the GBB as cyclic variations in aragonite content and as variations in turbidite composition and abundance, which can be compared to the oxygen isotope record (Droxler et al., 1983; Reymer et al., 1988; Haddad et al., 1993). During highstands, the periplatform ooze is rich in bank-derived aragonite, while during lowstands the aragonite content decreases as a result of reduced input and possibly increased dissolution (Droxler et al., 1983; Reymer et al., 1988). The sedimentation rates for bulk sediment and turbidite accumulation, as well as turbidite frequency, are consistently higher during interglacials than during glacials (Droxler and Schlager, 1985). In contrast, lowstand deposits are white, aragonite-poor intervals, including intervals indicating starvation and hiatus (Kier and Pilkey, 1971). Turbidites deposited during sea-level lowstands are dominated by skeletal material, whereas highstand turbidites show a dominance of nonskeletal material such as ooids, pellets, and grainstone lumps (Haak and Schlager, 1989).

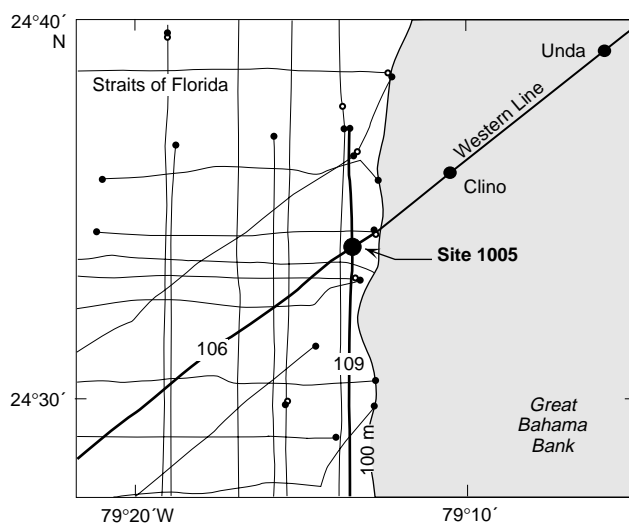


Figure 1. Location map of Site 1005. The site is located 30 shot points southwest of the crossing of seismic Lines 106 and 107. Seismic Line 106 retraced the Western Geophysical seismic line (Western Line) to provide a precise correlation between the cross-bank line and the high-resolution MCS lines of the grid in the Straits of Florida. The two drill sites, Unda and Clino, on the shallow top of the Great Bahama Bank were positioned on the Western Line.

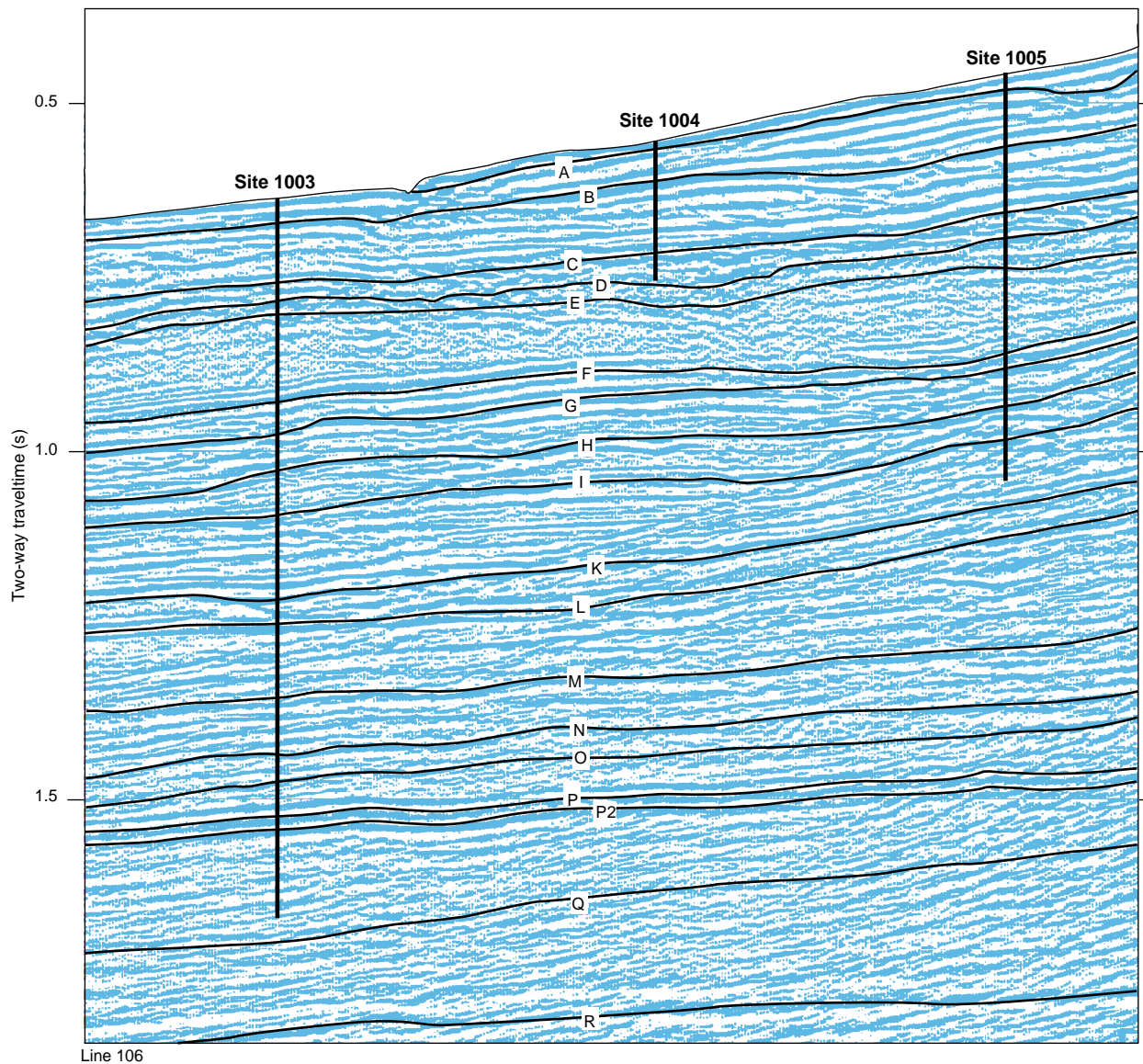


Figure 2. Portion of the high-resolution multichannel seismic Line 106 that retraced the cross-bank Western Line, with positions of Sites 1003, 1004, and 1005.

Site 1005 was positioned on the thick proximal bulge of several prograding sequences to document the facies in this portion of the carbonate sequences. This expanded section was intended to retrieve the sedimentary record of the high-frequency sea-level changes within lower-order seismic sequences. A logging suite was collected to provide a continuous record of the sedimentary succession, and a vertical seismic profile was made to allow an accurate time-depth conversion of the seismic reflections for a precise correlation of the cores to the seismic data. These data sets, in conjunction with quantitative shore-based analyses, can be used to study the problem of how high-frequency, sea-level changes produce sedimentary packages that eventually form seismic sequences.

The objectives of Site 1005 were to:

1. Retrieve a high-resolution record of climate and sea-level fluctuations for the Quaternary and Late Pliocene;
2. Determine the facies within the different systems tracts, especially the nature of the onlapping units that were interpreted as lowstand deposits;

3. Date precisely the sequence boundaries; and
4. Serve as a proximal site for determining fluid-flow using geothermal and geochemical profiles.

## OPERATIONS

### Hole 1005A

The ship was moved 0.9 nmi from the location of Hole 1004A to the GPS coordinates for Site 1005, and Hole 1005A was initiated at 2000 hr, 7 March. The water depth was determined to be 350.7 mbsl based on recovery of the mudline core. APC Cores 1H through 9H were cut from 0 to 67.5 mbsf with 101.3% recovery (Table 1). Cores 3H–9H were oriented with the Tensor tool. Adara heat flow measurements were deferred until Hole 1005B to determine the approximate depth of hard layers that might damage the tool. As at Sites 1003 and 1004, recovery was reduced by hard layers jamming in the throat of the bit. The core liner shattered on Cores 8H and 9H, prompting a change to the XCB coring system. XCB Cores 10X–53X were cut

Table 1. Site 1005 coring summary.

Core	Date (March 1996)	Time (UTC)	Depth (mbsf)	Length cored (m)	Length recovered (m)	Recovery (%)	Core	Date (March 1996)	Time (UTC)	Depth (mbsf)	Length cored (m)	Length recovered (m)	Recovery (%)
166-1005A-							166-1005B-						
1H	8	0225	0.0–2.5	2.50	2.46	98.4	1H	11	0520	0.0–9.5	9.50	9.92	104.0
2H	8	0330	2.5–12.0	9.50	9.78	103.0	2H	11	0545	9.5–13.5	4.00	0.28	7.0
3H	8	0425	12.0–16.0	4.00	3.55	88.7	3H	11	0655	13.5–23.0	9.50	9.75	102.0
4H	8	0525	16.0–25.5	9.50	9.46	99.6	4H	11	0740	23.0–32.5	9.50	9.17	96.5
5H	8	0550	25.5–35.0	9.50	10.00	105.2	5H	11	0830	32.5–42.0	9.50	9.80	103.0
6H	8	0625	35.0–44.5	9.50	9.84	103.0	6H	11	0925	42.0–48.0	6.00	0.00	0.0
7H	8	0650	44.5–52.0	7.50	7.48	99.7	7H	11	1330	48.0–51.0	3.00	2.61	87.0
8H	8	0735	52.0–61.5	9.50	9.34	98.3	8X	11	1525	51.0–52.0	1.00	1.00	100.0
9H	8	0800	61.5–67.5	6.00	6.48	108.0	9X	11	1635	52.0–61.7	9.70	6.92	71.3
10X	8	1005	67.5–72.0	4.50	3.75	83.3	Coring totals				61.7	49.45	80.1
11X	8	1035	72.0–81.6	9.60	4.95	51.5	166-1005C-						
12X	8	1150	81.6–91.2	9.60	7.54	78.5	1R	12	1120	386.6–395.9	9.3	2.24	24.1
13X	8	1250	91.2–100.4	9.20	5.26	57.2	2R	12	1210	395.9–405.2	9.3	2.21	23.7
14X	8	1350	100.4–109.9	9.50	0.36	3.8	3R	12	1300	405.2–414.5	9.3	2.32	24.9
15X	8	1525	109.9–119.4	9.50	0.15	1.6	4R	12	1350	414.5–424.0	9.5	1.81	19.0
16X	8	1720	119.4–128.7	9.30	4.81	51.7	5R	12	1445	424.0–433.4	9.4	2.20	23.4
17X	8	1755	128.7–138.0	9.30	0.25	2.7	6R	12	1545	433.4–442.4	9.0	2.84	31.5
18X	8	1830	138.0–147.3	9.30	1.25	13.4	7R	12	1655	442.4–451.4	9.0	2.68	29.8
19X	8	1905	147.3–156.6	9.30	4.03	43.3	8R	12	1745	451.4–460.7	9.3	2.09	22.5
20X	8	2040	156.6–166.0	9.40	7.69	81.8	9R	12	1835	460.7–470.0	9.3	2.02	21.7
21X	8	2120	166.0–175.2	9.20	0.14	1.5	10R	12	1955	470.0–479.3	9.3	3.86	41.5
22X	8	2200	175.2–184.6	9.40	4.17	44.3	11R	12	2045	479.3–488.6	9.3	2.09	22.5
23X	8	2340	184.6–194.0	9.40	1.82	19.3	12R	12	2155	488.6–497.6	9.0	3.50	38.9
24X	9	0010	194.0–203.3	9.30	0.59	6.3	13R	12	2300	497.6–506.9	9.3	2.88	30.9
25X	9	0040	203.3–212.3	9.00	0.00	0.0	14R	13	0015	506.9–516.3	9.4	3.46	36.8
26X	9	0125	212.3–221.3	9.00	1.16	12.9	15R	13	0510	516.3–525.3	9.0	4.02	44.6
27X	9	0150	221.3–230.3	9.00	0.00	0.0	16R	13	0620	525.3–534.3	9.0	2.54	28.2
28X	9	0205	230.3–239.8	9.50	0.00	0.0	17R	13	0730	534.3–543.8	9.5	1.80	18.9
29X	9	0245	239.8–249.3	9.50	0.17	1.8	18R	13	0905	543.8–553.3	9.5	3.07	32.3
30X	9	0300	249.3–258.7	9.40	5.77	61.4	19R	13	1040	553.3–562.7	9.4	1.15	12.2
31X	9	0325	258.7–268.1	9.40	6.56	69.8	20R	13	1245	562.7–571.7	9.0	4.37	48.5
32X	9	0510	268.1–274.0	5.90	0.00	0.0	21R	13	1355	571.7–580.7	9.0	3.44	38.2
33X	9	0820	274.0–280.3	6.30	0.00	0.0	22R	13	1445	580.7–589.7	9.0	1.89	21.0
34X	9	0845	280.3–286.6	6.30	2.63	41.7	23R	13	1545	589.7–599.0	9.3	2.74	29.4
35X	9	0910	286.6–296.1	9.50	4.23	44.5	24R	13	1755	599.0–608.0	9.0	4.23	47.0
36X	9	0940	296.1–305.7	9.60	3.65	38.0	25R	13	1940	608.0–617.5	9.5	4.43	46.6
37X	9	1005	305.7–314.6	8.90	0.75	8.4	26R	13	2110	617.5–627.0	9.5	4.58	48.2
38X	9	1040	314.6–324.2	9.60	1.54	16.0	27R	13	2230	627.0–636.0	9.0	0.49	5.4
39X	9	1155	324.2–333.7	9.50	0.38	4.0	28R	13	2335	636.0–645.4	9.4	3.47	36.9
40X	9	1225	333.7–343.1	9.40	0.20	2.1	29R	14	0100	645.4–654.4	9.0	2.82	31.3
41X	9	1320	343.1–351.9	8.80	0.31	3.5	30R	14	0210	654.4–663.4	9.0	3.88	43.1
42X	9	1400	351.9–360.9	9.00	2.94	32.6	31R	14	0320	663.4–672.4	9.0	4.99	55.4
43X	9	1440	360.9–370.4	9.50	0.68	7.2	32R	14	0435	672.4–682.0	9.6	4.77	49.7
44X	9	1530	370.4–379.7	9.30	0.62	6.7	33R	14	0630	682.0–691.0	9.0	5.58	62.0
45X	9	1630	379.7–389.2	9.50	0.00	0.0	34R	14	0810	691.0–700.0	9.0	6.64	73.8
46X	9	1720	389.2–398.2	9.00	0.06	0.7	Coring totals				313.4	107.10	34.2
47X	9	1810	398.2–407.6	9.40	1.60	17.0							
48X	9	1910	407.6–417.1	9.50	0.03	0.3							
49X	9	2215	417.1–426.5	9.40	0.00	0.0							
50X	9	2330	426.5–435.5	9.00	0.39	4.3							
51X	10	0025	435.5–444.5	9.00	0.05	0.6							
52X	10	0135	444.5–453.8	9.30	0.37	4.0							
Coring totals				462.40	149.58	32.3							

Note: An expanded version of this coring summary table that includes lengths and depths of sections, location of whole-round samples, and comments on sampling disturbance is included on CD-ROM in the back pocket of this volume.

from 67.5 to 462.4 mbsf with 20.6% recovery. The interval between Cores 14X–29X and 37X–53X, which contained soft, gassy sediments, with lithoclasts and occasional cemented layers, had only 12% average recovery despite minimal pump circulation rates. As a result of poor recovery, XCB coring was terminated at 462.4 mbsf. The pipe became stuck while cutting Core 38X when the hole apparently collapsed, stalling the rotary. The drill string was eventually worked free after circulation and rotation were re-established. Subsequently, the hole was back-reamed to 172 mbsf, and then reamed to the bottom. The WSTP was deployed after Cores 11X, 14X, 19X, and 22X. As a result of the unstable hole conditions, a precautionary short trip was made to 255.6 mbsf to condition the hole prior to logging.

Because of the previous difficulty logging Hole 1003C, we chose to log Hole 1005A rather than risk not obtaining any logging data if similar unstable hole conditions were encountered in Hole 1005C. The bit was pulled up to the logging depth at 103.8 mbsf. A DIT/sonic log was run to 445 mbsf, and an IPLT log was run to 434 mbsf. Finally, a VSP log was run to 409 mbsf (for additional details on logging operations and tools see “Downhole Logging” section, this chapter and the “Explanatory Notes” chapter, this volume). After running the VSP experiment in the open hole, the VSP tool would not re-enter the bit because the hydraulic clamping arm would not retract;

therefore, a Kinley crimper and cutter tools were dropped to clamp the line inside the BHA and then sever the wireline above the tool. The VSP tool was retrieved with only minor damage, and the pipe cleared the rotary at 2030 hr on 10 March.

### Hole 1005B

Coring at Hole 1005B was initiated 10 m to the south of Hole 1005A. The hole was spudded at 0011 hr on 11 March using the same APC BHA without the nonmagnetic drill collars. Hole 1005B was drilled primarily to obtain heat flow measurements and fluid samples. The water depth was determined to be 351.7 mbsl based on recovery of the mudline core. APC Cores 1H through 7H were cut from 0 to 51.0 mbsf with 81.4% recovery. Adara heat flow measurements were performed on Cores 3H through 7H. Core 7H was a partial stroke that threw slack in the coring line, entangling it on the heave compensator where the line subsequently parted. Core 7H was retrieved after the wireline was restrung. XCB Core 8X was taken from 51.0 to 52.0 mbsf to penetrate a hard layer, and XCB Core 9X was cut from 52.0 to 61.7 mbsf. A WSTP was deployed after Cores 8X and 9X. With the objectives of Hole 1005B achieved, the hole was terminated and the bit cleared the rotary table at 1305 hr on 11 March.

**Hole 1005C**

The ship was moved 20 m south of Hole 1005B, and Hole 1005C was initiated with a RCB BHA with a mechanical bit release (MBR) at 1750 hr on 11 March. The water depth was estimated to be 351.7 mbsf based on bit contact. A hole was drilled with a center bit to 386.6 mbsf. RCB Cores 1R–34R were cut from 386.6 to 700.0 mbsf with 34.1% recovery.

A conditioning trip for logs was made to 85.5 mbsf, and the bit was released using the MBR. The hole was filled with sepiolite mud, and the open drill string was positioned at 398.3 mbsf. The following suite of logs was run: (1) an IPLT log to 700.0 mbsf; (2) a DIT/sonic log to 693.0 mbsf; (3) a FMS log to 613 mbsf; and (4) a VSP log to 541 mbsf. After the hole was plugged with cement and gel mud, the pipe was pulled and secured for sea voyage at 0854 hr on 15 March.

**LITHOSTRATIGRAPHY**

**Lithologic Units**

Site 1005, located approximately 1.2 km from the margin of the present-day Great Bahama Bank, is the most proximal of the sites drilled during Leg 166. Although some differences exist, the sediments found at Site 1005 are similar to those found at Site 1003, and most of the units identified at Site 1003 are traceable to Site 1005. Therefore, the units at this site largely follow the subdivisions made for the sediments of Site 1003.

The sedimentary succession at Site 1005 consists of unlithified to partially lithified wackestones that intercalate with a few coarser grained intervals consisting of packstones and grainstones (Fig. 3). The sediments consist of a mixture of aragonite mud, platform-derived biota, and pelagic components. The sediments contain between

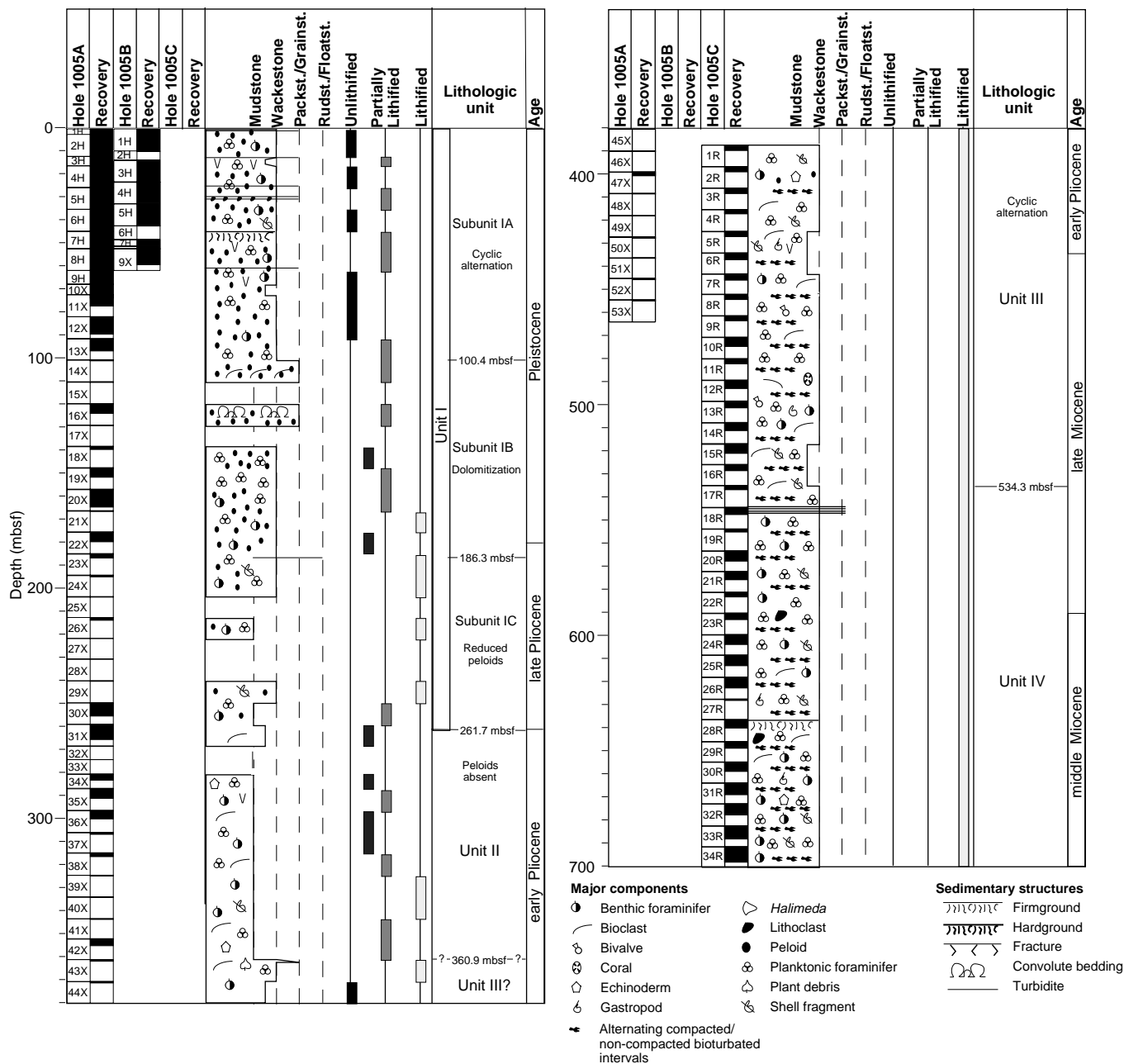


Figure 3. Synthesis of dominant textures and components of the sedimentary succession at Site 1005.

72 and 99 wt% carbonate. The XRD analyses showed that the carbonates consist of aragonite, high- and low-magnesium calcite, and dolomite (see "Inorganic Geochemistry" section, this chapter).

The degree of lithification of the sediments varies throughout Site 1005. Unlithified to partially lithified sediments dominate in Unit I, whereas in Unit II, most sediments are lithified. Unlithified sediments are encountered once again in Cores 166-1005A-44X and 50X (Unit III). From 380 mbsf (Unit III) downcore, only lithified sediments are present.

## Description of Lithostratigraphic Units

### Lithologic Unit I

Intervals: 166-1005A-1H through 31X-2; 166-1005B-1H through 9H  
Age: Pleistocene to late Pliocene  
Depth: 0–261.7 mbsf, Hole 1005A; 0–61.7 mbsf, Hole 1005B

Lithologic Unit I was divided into three lithologic subunits on the basis of sedimentological (VCD descriptions) and compositional (smear-slide analyses) differences (Fig. 4). The upper part of Unit I consists mostly of unlithified to partially lithified peloidal wackestones. The components present in the silt- and sand-sized fraction are predominantly peloids and benthic foraminifers. Other minor components include *Halimeda*, coral debris, echinoderm spines, bivalve fragments, gastropods, planktonic foraminifers, and plant debris. The matrix contains varying amounts of aragonite needles (2%–40%), nannofossils (up to 40%), and micrite (up to 45%).

Although only a few distinct turbidite layers occur, the presence of stringers and burrows filled with coarse-grained infill may indicate the obliteration of thin turbidites by bioturbation. Figure 5 gives an overview of the turbidites and the stringers (former turbidites?) found in the upper 14 cores of Hole 1005A. The abundance of turbidites gradually increases toward the top of the sedimentary sequence. In addition, the turbidite abundance is higher in intervals with increased aragonite content (as indicated by the high color reflectance values and XRD data). Distinct variations in the input of pellets and aragonite needles were used to subdivide this unit (Fig. 4).

### Lithologic Subunit IA

Intervals: 166-1005A-1H through 13X-CC, 20 cm; 166-1005B-1H through 9H  
Age: Pleistocene  
Depth: 0–100.4 mbsf, Hole 1005A; 0–61.7 mbsf, Hole 1005B

This subunit consists primarily of unlithified to partially lithified peloidal mudstones to wackestones with occasional packstones to grainstones. The major grains in the silt- to sand-sized fraction are peloids, bioclasts, planktonic and benthic foraminifers, with minor shell fragments, echinoderm spines, gastropods, pteropods, coral debris, and *Halimeda*. The matrix contains varying amounts of aragonite

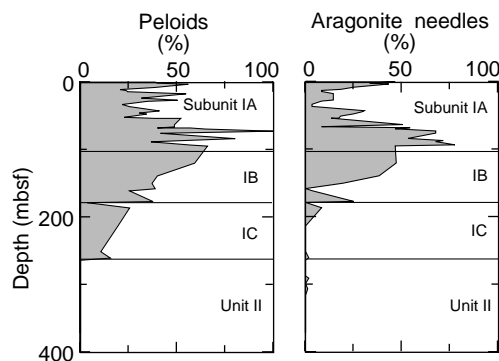


Figure 4. Percent abundance of peloids and aragonite needles in sediments of Hole 1005A (visual estimation in smear slides).

needles (up to 25%), nannofossils (maximum of 35%), and micrite (maximum of 55%) (Fig. 5). The sediments have a mottled appearance as result of intensive bioturbation. The intensity of the burrowing decreases downhole. Although burrow morphology is invariant, four distinct types of burrow fill occur: (1) concentration of black grains; (2) greenish infill; (3) clayey, more compacted, brown-colored infill; and (4) distinct white, grain-supported infill. The light gray/yellow intervals lack this specific burrowing.

The middle and lower parts of this subunit show a succession of gradual color changes (Fig. 4). Six cycles are present within the interval between Sections 166-1005A-4H-1 and 9H-5, and another three occur between Sections 166-1005A-12X-3 and 13X-CC. In the upper cycles, the sediments vary from coarse-grained gray wackestones that contain up to 30% nannofossils (coccoliths) and minor aragonite needles (less than 2%), to very fine-grained white wackestones with 5% nannofossils and up to 20% aragonite needles. The white aragonite-rich sediments also contain distinct burrows. The lower three cycles occur within a sequence of peloidal wackestones and are characterized by varying inputs of aragonite needles and planktonic foraminifers. The white-colored sediments contain up to 50% aragonite needles and 5% planktonic foraminifers. The black/gray sediments incorporate a maximum of 30% aragonite needles and up to 10% planktonic foraminifers.

A well-preserved, 0.2- to 0.4-cm, large bivalve *Glycymeris* sp. (both valves are still bound together; Fig. 6) and 1-mm-sized gastropods occur in the interval between Section 166-1005A-5H-5 (31.5 mbsf) and Section 166-1005A-6H-4 (41.00 mbsf), and between Section 166-1005B-5H-1 (32.5 mbsf) and Section 166-1005B-7H-1 (49.23 mbsf). These intervals have similar thicknesses and form good correlation horizons between Holes 1005A and 1005B.

At Site 1005, the boundary between Subunits IA and IB is defined at the top of a series of partially lithified to lithified bioclastic packstones, whereas the base of a nannofossil ooze defines this boundary in Site 1003. The onset of distinct color cycles in Section 166-1005A-9H-CC occurs at the same level.

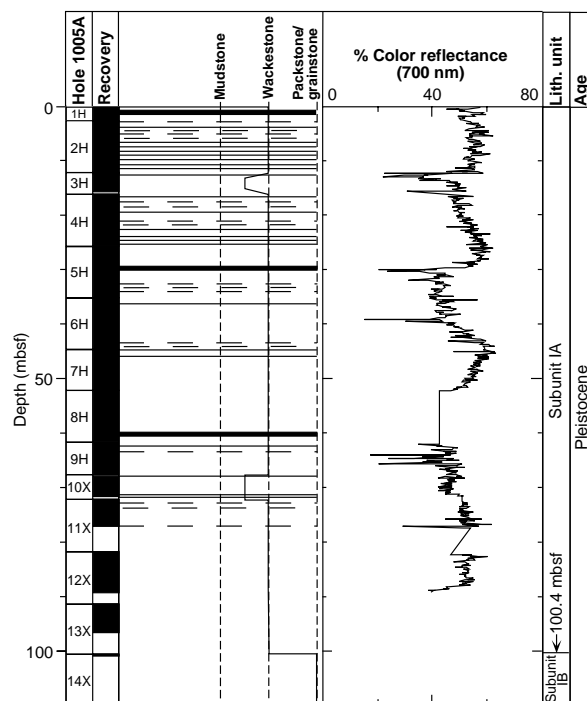


Figure 5. Abundance of turbidites present in the upper 100 m of Hole 1005A. The concentrations of turbidites (black line) and stringers presumed to be remnants of turbidites (dashed lines) fall preferentially in intervals that are characterized by high color reflectance in the 700-nm range. An additional visible trend is the general increase of turbidites toward the top of the hole.

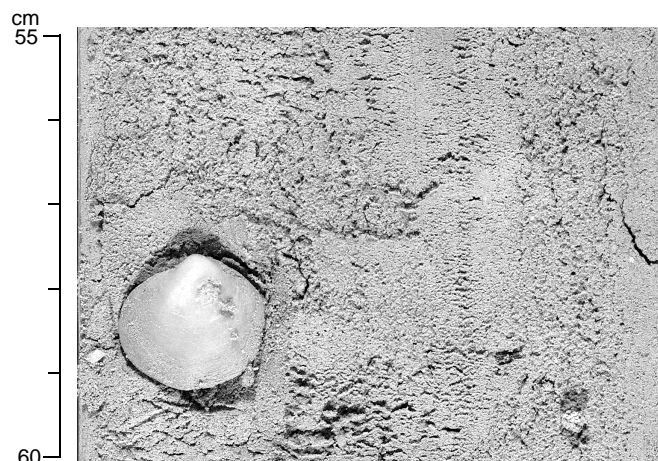


Figure 6. Detail of the *Glycymeris* interval 166-1005A-5H-7, 55–60 cm. Note that both valves are still bound together.

#### Lithologic Subunit IB

Interval: 166-1005A-14X through 23X-CC, 18 cm  
Age: Pleistocene to late Pliocene  
Depth: 100.4–186.3 mbsf

Macroscopically, the sediments in this subunit do not differ that much from the overlying Subunit IA and consist mainly of unlithified to partially lithified peloidal wackestones. The top of this unit is formed by an interval with peloidal to bioclastic packstones to grainstones, and foraminiferal wackestones (Cores 166-1005A-14X through 19X). The rest of this subunit has a rather monotonous appearance, and its sediments are slightly bioturbated. The size of the grains in the wackestones varies from coarse silt to fine sand. The main components found in these grain-size fractions are peloids, shell fragments, echinoderm spines, planktonic foraminifers, and gastropods.

The sediments are slightly to moderately dolomitized from the top of Core 166-1005A-16X downhole. Below Section 166-1005A-18X-CC (139.00 mbsf), the inorganic carbon and the weight percent carbonate starts to vary from 87.5 to 96 wt% (see “Inorganic Geochemistry” section, this chapter), and unlithified to partially lithified foraminifer wackestones occur. Distorted bedding structures, interpreted as convolute bedding, are present in Section 166-1005A-16X-CC (114.67 mbsf). A major transition occurs at the base of this subunit. Centimeter-scale alternations between layers with variable amounts of siliceous material (siliceous spicules, diatoms, and radiolarians) give way to white, structureless unconsolidated sediments, and partially lithified biowackestones.

The top of an interval containing bioclasts and lithoclasts in Section 166-1005A-23X-CC, 18 cm, (interpreted as a breccia) marks the upper boundary of Subunit IC. At the same level, the input of peloids is reduced from 10% to 15% to <5% in smear-slide analysis. A color change from light gray to white to grayish pale yellow also marks this boundary. It is preceded by a diminishing amount of aragonite needles, which may be a diagenetic effect.

#### Lithologic Subunit IC

Interval: 166-1005A-23X-CC, 18 cm, through 31X-2  
Age: late Pliocene  
Depth: 186.3–261.7 mbsf

The sediments in this poorly recovered subunit consist almost completely of partially lithified mudstones that are slightly dolomitized. The main sand- to silt-sized constituents are planktonic and benthic foraminifers, bivalve fragments, and unidentifiable bioclasts. As a result of the poor recovery and drilling disturbances, few sedi-

mentary structures were observed. The sediments of this subunit seem to be characterized by millimeter-scale laminations of clay-rich laminae and more silt-rich intervals. The clay-rich laminae contain minor percentages of diatoms as well as radiolarians. The silt-rich intervals are relatively enriched in planktonic and benthic foraminifers and pellets.

Thin-section analysis of a level with clasts in Section 166-1005A-23X-CC, 16–21 cm, near the upper boundary of this subunit shows that *Halimeda*, red algae, bivalve fragments, coral, and peloids are present. In addition, lithoclasts are found that exhibit a “clotted structure.” Such a structure is typical of intrareef depositional environments (Reid, 1987). The isopachous, fibrous, high-magnesium calcite cement found in the thin section are also characteristic of reef to fore-reef environments.

The complete disappearance of pellets and aragonite needles marks the boundary between Subunit IC and Unit II and coincides with the late Pliocene to early Pliocene boundary.

#### Lithologic Unit II

Interval: 166-1005A-31X-3 through 43X-1  
Age: early Pliocene  
Depth: 261.7–360.9 mbsf

The sediments present in this unit are primarily partially lithified mudstones, with some wackestones at the top and mud to wackestones at the bottom. The grains are predominantly planktonic foraminifers, with minor benthic foraminifers, lithoclasts, and unidentifiable bioclasts. Thin-section analysis shows the predominance of planktonic foraminifers in these sediments. The color varies from light yellow to light gray.

The carbonate contents for Cores 166-1005A-31X through 34X range from 96 to 98 wt%. The entire unit is partially dolomitized. Other diagenetic features observed were the micritization of the sediments in combination with partial dissolution and replacement/recrystallization of the individual grains.

The boundary between Units II and III is marked by the abrupt appearance of repetitive alternations of various sorts of biowackestones.

#### Lithologic Unit III

Intervals: 166-1005A-43X-1 through 51X-CC; 166-1005C-1R through 16R  
Age: early Pliocene to late Miocene  
Depth: 360.9–534.30 mbsf

At first view, Unit III and the underlying Unit IV are made up of a monotonous succession of partially dolomitized foraminifer wackestones. However, variations in the thicknesses of the dominating lithologies and the occurrence of some turbidite layers made subdivision possible (Fig. 7). At Site 1003, where a series of turbidites are deposited in the top interval, the sedimentological contrasts between the two units were more distinct.

The sedimentary cycles that characterize Unit III consist of two main lithologies that alternate on a decimeter scale. The first lithology consists of gray to light gray, well-cemented biowackestones with several generations of burrows. The diameter of the burrows varies from 5 to 25 mm. The sediments are fine-grained and contain planktonic and benthic foraminifers, shell fragments (preserved as molds), and bioclasts; in addition, they have a low moldic porosity. The second lithology is characterized by compacted burrows (flattened in vertical direction), a gray to olive gray color, less cementation, and high moldic porosity. In these intervals, the very fine silt- to silt-sized planktonic and benthic foraminifers present are partly infilled with cement. The cycles display differences in the degree of cementation, in the distribution of moldic porosity, and in the degree of compaction of the individual burrows. The boundaries between the litholo-

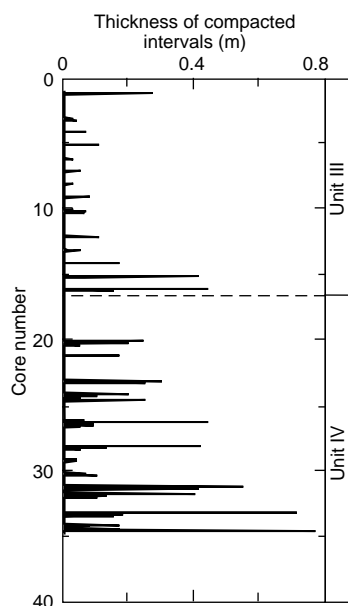


Figure 7. Thickness variations of the compacted burrow intervals throughout Unit III and IV plotted vs. core number, and the individual intervals that could be measured. Note the decrease in interval thickness toward the top of Unit IV and once again toward the top of Unit III.

gies are generally sharp, but occasionally they can be very gradual. Slight variations in the thicknesses of both lithologies also occur with depth. Thickness variations in the compacted intervals was one of the primary criteria used to separate Unit III from Unit IV. The maximum thickness of the compacted intervals in Unit III is 44 cm, whereas the maximum thickness of this interval in Unit IV is nearly 80 cm. The thickness of the noncompactd intervals is relatively constant throughout Units III and IV.

Fractures filled with celestite are present at the base of Unit III (Cores 166-1005C-14R and 17R). Veins filled with native sulfur were found at the top of Core 166-1005A-47X. The lowermost layers found in this unit consist of a series of foraminifer wackestones to mudstones.

#### Lithologic Unit IV

Interval: 166-1005C-17R through 34R-CC, 21 cm  
Age: late to middle Miocene  
Depth: 534.30–700.00 mbsf

Two features mark the upper boundary of Unit IV: (1) the presence of a series of gradational, fining-upward beds that are also heavily bioturbated and (2) a dramatic decrease in the thickness of the poorly cemented and compacted intervals from 44 to 21 cm (Fig. 7).

Unit IV consists of a monotonous series of foraminifer wackestones with the same cyclic variations described in Unit III, but the sediments are locally heavily dolomitized.

One of the cycles was studied in detail sedimentologically and petrophysically (Fig. 8). This cycle displays the various stages of compaction that are present in the succession (Figs. 9–11). Color reflectance decreases to 10% (at 700 nm) in the intervals that show compactional deformation of the individual burrows (compacted burrow intervals: Fig. 11) and reaches values up to 34% in the cemented intervals with noncompactd burrows. The compressional-wave velocities are relatively low (2 km/s) in the compacted intervals and high (up to 5 km/s) in the cemented intervals, with a gradational transition between these two types. Low natural gamma values (6 cps) are present in the cemented parts, whereas high values (up to 16 cps) occur in the compacted parts. Magnetic susceptibility is highest in the

intervals with high natural gamma values. The  $\text{CaCO}_3$  content of the cemented intervals reaches nearly 100% in Sample 166-1005C-33R-3, 41–42 cm. The poorly cemented and compacted intervals contain between 84 and 89 wt%  $\text{CaCO}_3$ . These intervals show relatively high TOC values (between 2.63 and 1.74 wt%). The highest value was measured in the most compacted part of the cycle at 683.53 mbsf (Sample 166-1005C-33R-2, 14–15 cm).

This relatively monotonous sedimentary succession displays variations in the level of dolomitization. Other diagenetic features include veins filled with celestite, and a large mass of elemental sulfur was found at the top of interval 166-1005C-33R-1, 0–8 cm (Fig. 12).

#### Interpretation

The sedimentary succession of Site 1005 is divided into four major units that can be separated into three large depositional packages on the basis of the type of sedimentary cycles recognized. These packages are related directly to changes in platform-to-basin morphologies, sea level, and ocean circulation patterns.

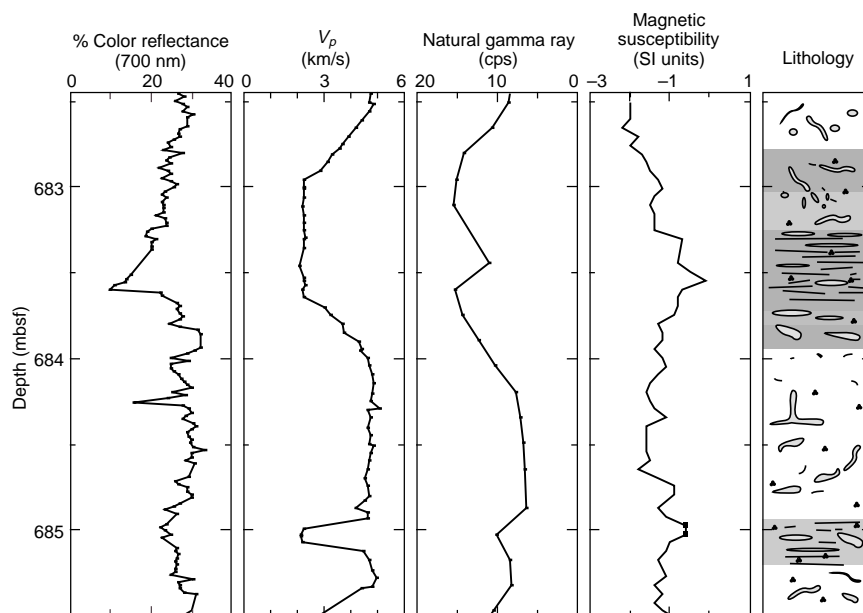
Depositional package 1 consists of Subunit IA. It shows clear sedimentation cycles with distinct variations in color that correspond to variations in sediment composition and burrowing type. High color reflectance corresponds with a high input of aragonite needles, a reduced input of nannofossils, and a slight increase in peloid abundance. Therefore, these depositional cycles have all the characteristics of periplatform aragonite cycles that record times of platform flooding and exposure and that are found in the basins and on the slopes surrounding the Bahamas Banks (Droxler et al., 1988; Reymer et al., 1988; Grammer and Ginsburg, 1992; Grammer et al., 1993). In this subunit, turbidite frequency coincides with intervals of increased aragonite percentage (Fig. 5). This result is in good agreement with the principle of highstand shedding that is characteristic of flat-topped platforms (Droxler and Schlager, 1985; Schlager et al., 1994).

Depositional package 2 includes Subunits IB and IC and Unit II. This package does not show any clear, visible cyclicity and can be seen as an intermediate stage between the upper and lower packages. Depositional package 2 displays an overall coarsening-upward trend. Sediment composition shows a stepwise, uphole increase in the dominance of platform-derived material, mainly peloids and aragonite needles, thus reflecting an increase of platform-derived input to Site 1005 resulting from platform progradation. The change in sediment composition from skeletal dominated toward peloidal dominated sedimentation probably resulted from the transformation of a Miocene carbonate ramp to the present-day, flat-topped platform (Eberli and Ginsburg, 1989) and probably a coeval change in climate.

The third depositional package, consisting of Units III and IV, shows a clear cyclicity of decimeter-scale alternations between cemented and compacted intervals (Figs. 9–11). The minor variations recorded were fluctuations in the thicknesses of the compacted intervals (flattened burrows). These intervals are soft (poorly cemented?), and their recovery may be suppressed in comparison with the well-cemented intervals. Higher carbonate values in the cemented intervals suggest an increased input of platform-derived carbonate during these intervals, whereas the compacted intervals result from normal pelagic sedimentation. The higher abundance of planktonic foraminifers in the compacted intervals supports this interpretation. The cycles in depositional package 3 are interpreted as platform input cycles. They correspond to either platform flooding and exposure or to gradual progradation/retrogradation of the facies belts along the carbonate ramp. The short-term cycles (up to 3 m thickness) are bundled into two large-scale cycles that coincide roughly with Units III and IV (Fig. 7). Units III and IV can be subdivided further into three medium-scale cycles (with thicknesses between 40 and 60 m). Whether or not this cycle-stacking pattern relates to different orders of sea-level changes is unclear at present.

When comparing the Miocene sedimentation cycles and the Pleistocene interglacial/glacial input cycles, it is clear that the ramp mor-

Figure 8. Detail of a sedimentary cycle as present in Core 166-1005C-33R. An increase in grayness in combination with the burrow orientation indicates the degree of compaction of the sediment (white, uncompacted; dark gray, compacted). Shown are the color reflectance (700 nm), the compressional-wave velocity ( $V_p$ ), the natural gamma ray (cps), and the magnetic susceptibility (SI units). Color reflectance decreases in the intervals in which bioturbation shows compactional deformation of the individual burrows (flattened burrow intervals) and is relatively high in the cemented and uncompacted intervals. Note the striking contrasts in  $V_p$  between the aforementioned interval types. Natural gamma ray is relatively low in the cemented parts and shows high values in the flattened burrow intervals. As expected, magnetic susceptibility is highest in the intervals with high natural gamma-ray values.



phology in the Miocene produced more symmetric cycles in response to sea-level variations. Another difference is that during the Miocene, more noncarbonate material was transported to Site 1005. This was probably caused by changes in ocean circulation and clay input during the lowstands, whereas during highstands neritic input from the platform prevailed. A third difference is that in the Miocene the platform neritic production zone was situated at greater distance and thus had less impact on the sedimentary environment at Site 1005.

In summary, differences between Pleistocene to Miocene depositional cycles likely result from changes in platform morphology (i.e., ramp vs. flat-topped platform) and the response of the platform to sea-level variations. In addition, variations in sea level ocean circulation and changes in climate seem to have played a significant role by controlling the input of noncarbonate material.

## BIOSTRATIGRAPHY

Site 1005 is the most proximal to the platform of the sites drilled on the upper slope adjacent to the Great Bahama Bank. The abundance and preservation of calcareous microfossils vary with the lithologic facies at Hole 1005A. The upper Pleistocene sediments (Cores 166-1005A-1H through 14X) contain abundant, well-preserved planktonic and benthic foraminifers and nannofossils. The lower Pleistocene section (Cores 166-1005A-15X through 23X) yields sparse to common calcareous fossils with poor preservation in general and was subdivided using nannofossil biohorizons. The shift from well- to poorly preserved assemblages coincides with the change from unaltered to partially dolomitized carbonate (see "Lithostratigraphy" section, this chapter).

The Pliocene/Pleistocene boundary is placed between Samples 166-1005A-23X-CC and 24X-CC at 190.49 mbsf. Although poor recovery and preservation of the calcareous fossils made zonal assignment and dating difficult below Core 166-1005A-23X, the fauna and flora present indicate a late Pliocene age (1.72–3.0 Ma) for the interval from Cores 166-1005A-24X through 29X. There was no recovery of sediments in Cores 166-1005A-27X and 28X. The planktonic foraminiferal assemblage in Sample 166-1005A-29X-CC is assigned to planktonic foraminiferal Zone N20 (3.2–3.5 Ma). The lower/upper Pliocene boundary is placed between Cores 166-1005A-29X and 166-1005A-30X on the basis of the boundary between nannofossil Zones NN14–15/16–18.

The lower part of Hole 1005A (Cores 166-1005A-30X through 42X) is assigned to the combined planktonic foraminiferal Zone N17–19 and nannofossil Zone NN14–15. Zonal assignment below Core 166-1005A-42X becomes difficult again as extreme dilution by platform material and diagenesis hindered identification of marker species; lower Pliocene–uppermost Miocene planktonic foraminifers and nannofossils are rare and poorly preserved. The contact between the lower Pliocene and upper Miocene is difficult to place. An unconformity was found at the top of nannofossil Zone NN10. This unconformity may span the Miocene/Pliocene boundary. However, at Site 1007, Messinian sediments were found above a similar unconformity. The faunal assemblages below this unconformity (Samples 166-1005C-5R-2, 55–57 cm, through 34R-3, 38–40 cm) are early late to late middle Miocene in age. Floral and faunal assemblages in this interval are poorly preserved, although moderately to well-preserved faunas were found in the distinct layers that contain small amounts of clay (see "Lithostratigraphy" section, this chapter).

Benthic foraminiferal assemblages indicate an upper bathyal paleodepth for Site 1005. There are diverse, abundant platform-derived benthic foraminifers in much of the Pleistocene section, none in the upper Pliocene section, and minor shallow-water taxa in the Miocene to lower Pliocene sections.

## Calcareous Nannofossils

Calcareous nannofossils from Site 1005 show excellent preservation in the uppermost Pleistocene and moderate to poor preservation below. The first occurrence of *Emiliania huxleyi*, which defines the base of Zone NN21, was found between Samples 166-1005A-3H-CC and 4H-CC. Below Sample 166-1005A-3H-CC, preservation of calcareous nannofossils is poor as a result of overgrowth. The last occurrence of *Pseudoemiliania lacunosa* corresponds to the upper limit of Zone NN19 (0.41 Ma) and was detected between Samples 166-1005A-9H-CC and 10X-CC. Samples 166-1005A-10X-CC through 23X-CC, which are correlated to Zone NN19, are characterized by the presence of *P. lacunosa*, *Gephyrocapsa caribbeanica*, and *Gephyrocapsa oceanica*. In this interval, the first occurrence of *Gephyrocapsa parallela* (just above the Jaramillo Event; 0.95 Ma) is recognized between Samples 166-1005A-16X-CC and 17X-CC. The concurrent range of *G. parallela* and *Reticulofenestra asanoi* is between 0.85 and 0.95 Ma. Because *R. asanoi* was not found in these samples, this level must be younger than 0.85 Ma. Large-form *Gephyrocapsa*

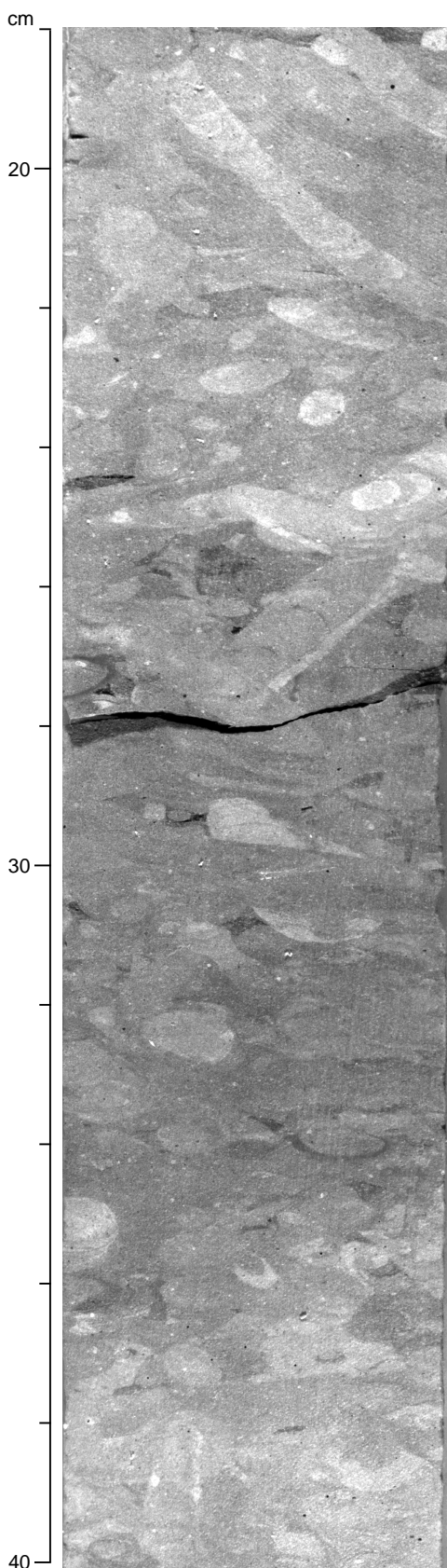


Figure 9. Well-cemented and uncompacted interval 166-1005C-20R-2, 18–40 cm. Several generations of burrows are visible, each with its typical color and diameter. Well-developed *Zoophycos*-type burrows are present at the top of the picture.

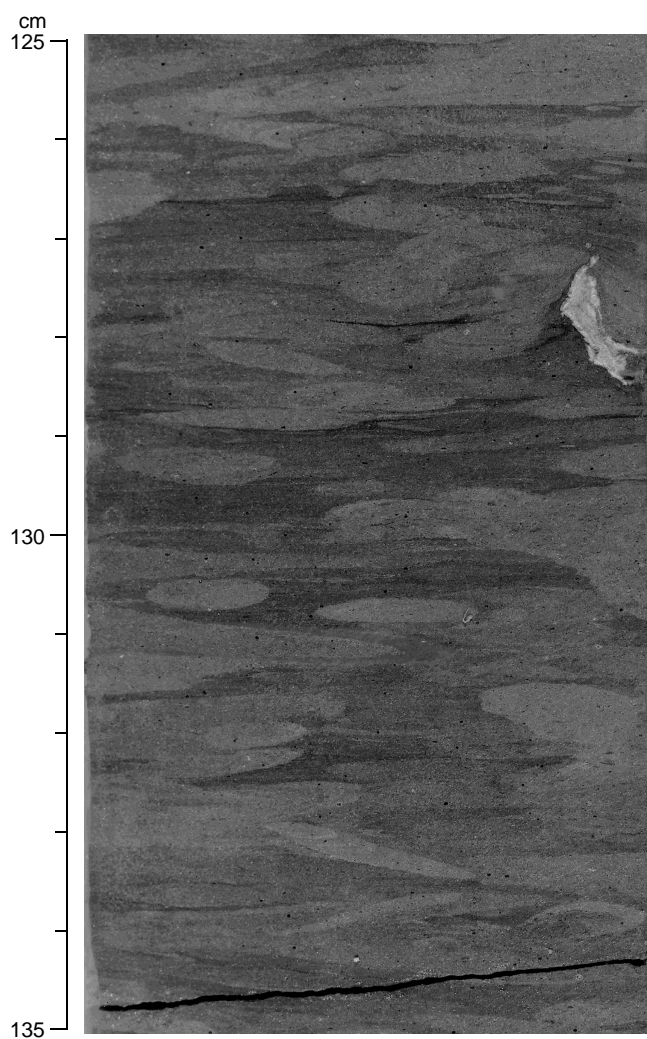


Figure 10. Moderately compacted interval 166-1005C-33R-1, 125–135 cm. The burrows are flattened in a vertical sense and tend to form parallel laminations. *Zoophycos*-type burrows still can be recognized and are present at the top of the photograph. A comparison with the same type of burrows shown in Figure 8 illustrates the severity of the deformation.

spp. (>6  $\mu\text{m}$ ; 1.20–1.44 Ma) was found in Sample 166-1005A-22X-CC.

The Pliocene/Pleistocene boundary is placed between Samples 166-1005A-23X-CC and 24X-CC on the basis of the first occurrence of *G. caribbeanica*, which is traceable to just above the Pliocene/Pleistocene. Samples 166-1005A-24X-CC through 29X-CC are characterized by the presence of *P. lacunosa* and the absence of discoasters. Samples 166-1005A-30X-CC through 42X-CC contain the lower Pliocene marker species *Sphenolithus abies*, *Discoaster asymmetricus*, and *Discoaster surculus*. Therefore, Samples 166-1005A-24X-CC through 29X-CC are assigned to the upper Pliocene Zone NN16–18, whereas Samples 166-1005A-30X-CC through 42X-CC are assigned to lower Pliocene Zone NN14–15. Below this interval, calcareous nannofossils are rare to barren with no marker species.

The assemblages from Hole 1005B are similar to those of Hole 1005A. Samples 166-1005B-1H-CC and 2H-CC contain *E. huxleyi* and are assigned to the uppermost Pleistocene Zone NN21. The interval between Samples 166-1005B-3H-CC and 9X-CC is assigned to Pleistocene Zone NN20.

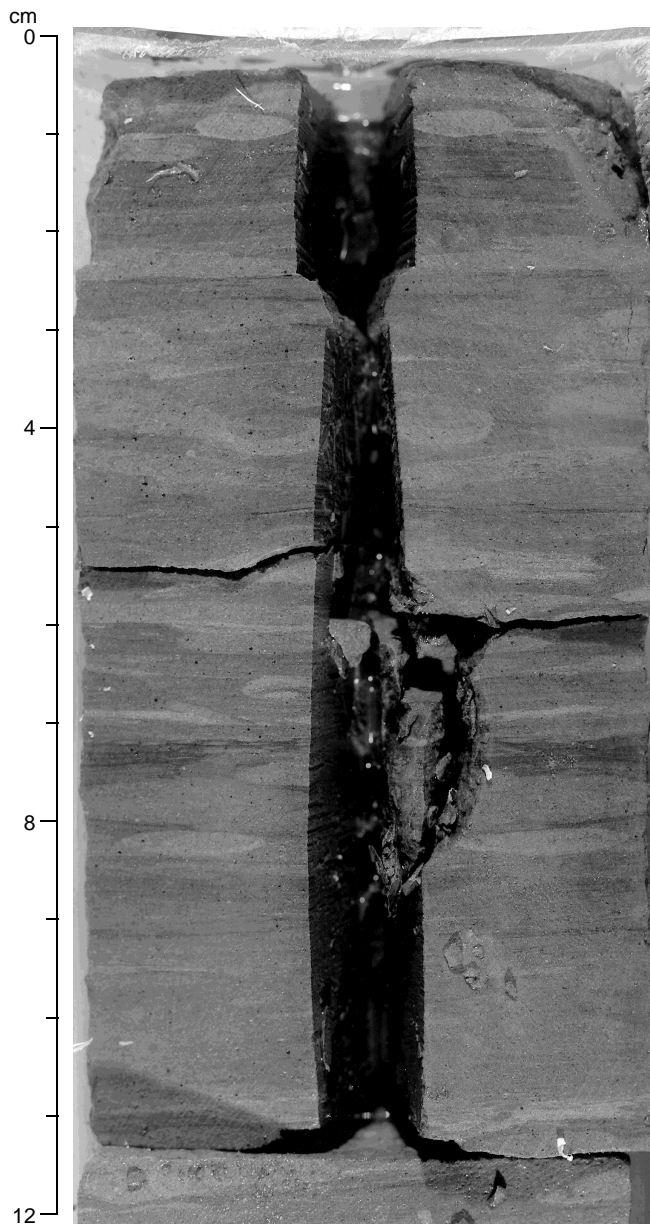


Figure 11. Photograph showing the end phase of the compaction that is present in the succession recovered at Site 1005 (Section 166-1005C-33R-2, at 0–12 cm). The deformation tends to form parallel-laminated intervals.

A total of 27 samples from Hole 1005C were examined. Samples 166-1005C-6R-2, 55–57 cm, through 12R-2, 5–7 cm, are characterized by the occurrences of early late Miocene age marker species, including *Discoaster neohamatus* and *Discoaster bellus*. As the large form of *Reticulofenestra pseudumbilicus* is also recognized in and below this interval, these samples correspond to the lower part of Zone NN10. The total range of *Discoaster hamatus*, which defines Zone NN9, is found between Samples 166-1005C-13R-2, 131–135 cm, and 21R-2, 97–99 cm. The first occurrence of *Catinaster coalitus* marks the NN7/8 boundary and is recognized in Sample 166-1005C-23R-1, 84–88 cm. *Cyclicargolithus floridanus*, which defines the base of Zone NN7 (13.2 Ma), was not found in this hole. *Coccolithus miopelagicus*, which last appears at the NN7/8 boundary, is present in Sample 166-1005C-24R-2, 52–54 cm, and down to the bottom of Hole 1005C. On the basis of these results, Sample 166-1005C-23R-

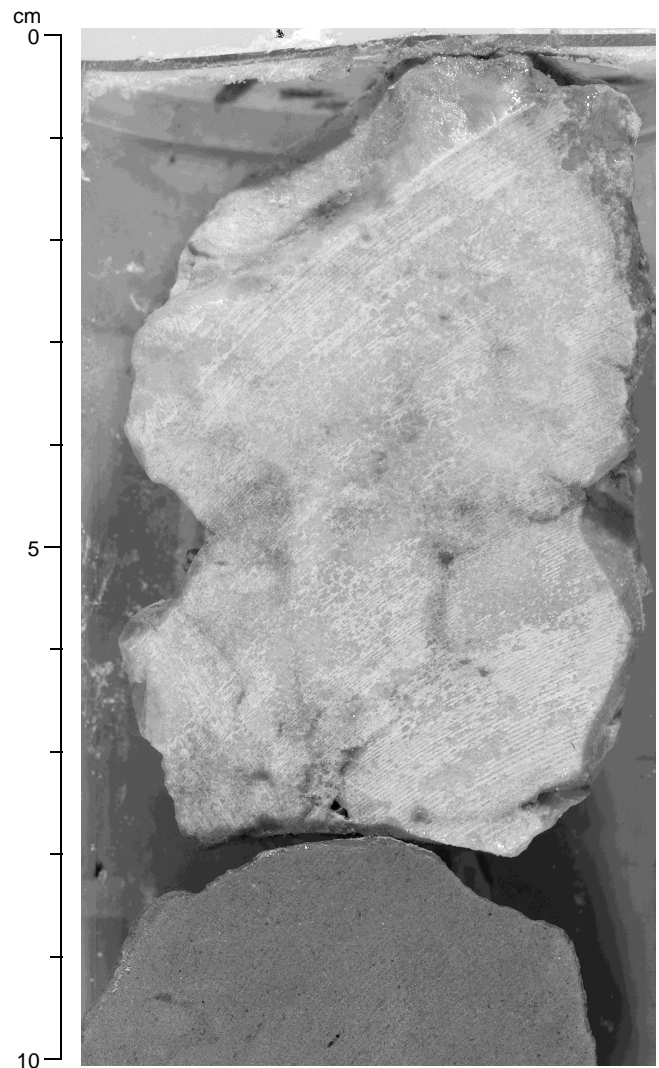


Figure 12. Interval 166-1005C-33R-1, 0–10 cm, containing native sulfur within dolomitized foraminifer wackestone.

1, 84–88 cm, is assigned to uppermost middle Miocene Zone NN8, and the interval below this sample corresponds to middle Miocene Zone NN7.

### Planktonic Foraminifers

Most of the core-catcher samples in Hole 1005A were examined for planktonic foraminifers. The upper Pleistocene section (Cores 166-1005A-1H through 14X) contains abundant, well-preserved foraminifers, whereas the lower Pleistocene (Cores 166-1005A-15X-CC through 23X-CC) generally yields sparse to common, poorly preserved specimens. *Globorotalia truncatulinoides* is present throughout both intervals, indicating the extent of Zone N22 from the top of the borehole to the depth between Samples 166-1005A-23X-CC and 24X-CC. The absence of *G. truncatulinoides* in Sample 166-1005A-24X-CC indicates that this level is in Zone N21. There was no sediment recovery in Core 166-1005A-25X, and Sample 166-1005A-26X-1, 62–64 cm, contains an abundant, moderately preserved late Pliocene age fauna including *Globorotalia tosaensis*, *Globorotalia exilis*, and *Globorotalia pertenuis*. The absence of *Dendoglobigerina altispira* and the presence of *G. pertenuis* indicate that the age of this sample is between 2.6 and 3.0 Ma (Zone N21). There was no sedi-

ment recovery in Cores 166-1005A-27X and 28X, but a late Pliocene age fauna was found in Cores 166-1005A-29X and 30X. The absence of *G. tosaensis* and *Globorotalia margaritae* indicate that this interval correlates to Zone N20 (3.2–3.55 Ma).

Planktonic foraminifers are common to abundant and moderately preserved in the interval from Cores 166-1005A-31X through 41X, although in some samples only few foraminifers were found. Early Pliocene age planktonic foraminiferal assemblages, and in particular the presence of *G. margaritae*, indicate that this section corresponds to Zone N19. The severe decline in preservation and abundance of planktonic foraminifers in the lower Pliocene–uppermost Miocene sediments necessitated discrete sampling from clay-rich layers within the cores because they contain better preserved foraminifers. Samples 166-1005A-42X-CC through 53X-CC contain rare to common planktonic foraminifers that are poorly preserved, making age assignment difficult. Although the early Pliocene fauna is similar to the late Miocene fauna, it should contain the delicate species *G. margaritae* and rare *Globorotalia tumida* (the indicator of lower Pliocene Zone N19). Both species are absent in the interval from Samples 166-1005A-42X-CC through 53X-CC. *Globigerinoides conglobatus*, a proxy for the first appearance of *G. tumida*, was found down through Sample 166-1005A-48X-CC at a depth of 415 mbsf. However, the first appearance datum of *G. conglobatus* is slightly older than *G. tumida*, occurring in the uppermost upper Miocene (Messinian). Therefore, it is possible that uppermost Messinian sediments are in and above Core 166-1005A-48X.

The first occurrences of *G. conglobatus* (6.2 Ma) and *Globorotalia cibaoensis* (7.7 Ma) at the same level in Sample 166-1005A-48X-CC indicate an unconformity at approximately 415 mbsf.

Below Core 166-1005A-48X, planktonic foraminiferal assemblages contain *Globorotalia languaensis*, *Globorotalia merotumida*, and *Neogloboquadrina continuosa*, placing this interval in upper Miocene Zone N16. Planktonic foraminiferal Zone N17 appears to be missing. The base of the upper Miocene, Zone N16, is indicated by the first appearance of *Neogloboquadrina acostaensis* between Samples 166-1005C-21R-2, 97–99 cm, and 23R-1, 84–88 cm (582 mbsf).

The uppermost middle Miocene Zone N15 is represented only by Sample 166-1005C-23R-1, 84–88 cm. The last appearance of *Globorotalia mayeri* (11.4 Ma) was found in Sample 166-1005C-24R-2, 52–54 cm, and places the top of Zone N14 at 596 mbsf. The base of Zone N14 (11.8 Ma) is placed at 651 mbsf between Samples 166-1005C-29R-1, 65–67 cm, and 30R-3, 18–20 cm, as indicated by the first appearance of *Globigerina nepenthes*. The last appearance of the *Fohsella* species marks the upper limit of Zone N12 between Samples 166-1005C-31X-CC and 32R-1, 100–102 cm (670 mbsf). The bottom of Hole 1005C (700 mbsf) is still within the middle Miocene planktonic foraminiferal Zone N12.

### Benthic Foraminifers

The Pleistocene section at Hole 1005A yields benthic foraminiferal faunas that contain *Cibicidoides incrassatus* (~100–600 m),

*Planulina foveolata* (~100–500 m), *Planulina ariminensis* (~100–800 m), and *Sigmoilopsis schlumbergeri* (>200 m) (van Morkhoven et al., 1986), indicating a paleodepth of ~200–500 m (within the upper bathyal zone). Other common taxa typical of the upper bathyal assemblages in this section are similar to those found at Sites 1003 and 1004 (see “Biostratigraphy” section, “Site 1003” chapter, this volume). The Pleistocene section also contains platform-derived shallow-water taxa similar to Sites 1003 and 1004 (see “Biostratigraphy” section, “Site 1003” chapter, this volume), but with a minor increase in diversity and abundance. Preservation was excellent in core-catcher samples examined from nannofossil Zones NN20–21, but was variable in Zone NN19 with a concomitant decrease in shallow-water taxa.

Benthic foraminifers are rare and preservation is poor in the upper Pliocene section at Site 1005. There are neither depth-diagnostic species nor platform-derived taxa in this section. Similarly, the upper Pliocene section at Site 1004 contains upper bathyal faunas with poor to moderate preservation and no platform-derived species. The coeval section at Site 1003 contains reworked deep-water Eocene species.

The Miocene–lower Pliocene section at Site 1005 yields upper bathyal benthic foraminiferal faunas including *Cibicidoides compressus* (~200–1000 m), *Cibicidoides incrassatus* (~100–600 m), *Hanzawaia mantaensis* (~200–1000 m), *P. ariminensis* (~100–800 m), *Planulina mexicana* (~100–800 m), and *Rectuvigerina striata* (~200–1000 m) with minor amounts of shallow-water taxa (*Amphistegina lessonii*, *Asterigerina carinata*, and *Elphidium* spp.). Core-catcher samples examined from this interval generally yielded depauperate benthic foraminiferal faunas, whereas samples from within the darker sediments taken from within the cores yielded well-preserved, diverse faunas.

### Sedimentation Rates

A 700-m-thick Holocene to upper middle Miocene section was recovered at Site 1005. Site 1005 is the shallowest and most proximal to the platform of the sites drilled on the slope transect west of the Great Bahama Bank. Variations in the sedimentation rates at this site most likely have been influenced by platform development and reflect the export of bank-derived material to the upper slope. The sedimentation rates for Site 1005 were established from the biostratigraphy of calcareous nannofossils and planktonic foraminifers. There is a good agreement between the nannofossil and planktonic foraminiferal biostratigraphic events (Tables 2, 3; Fig. 13).

The Pleistocene section yielded an excellent nannofossil biochronology spanning the last 1.72 m.y. The sedimentation rate is high (15 cm/k.y.) above the last occurrence of large *Gephyrocapsa* spp. (1.2 Ma). The late Pliocene–early Pleistocene (3.5–1.2 Ma) sedimentation rate was ~2 cm/k.y., much lower than the late Pleistocene sedimentation rate. This rate is characteristic of normal pelagic carbonate sedimentation with little to no addition of platform-derived material. The higher sedimentation rate in the later Pleistocene resulted from

Table 2. Calcareous nannofossil bioevents.

Event	Age (Ma)	Interval (cm)	Depth* (mbsf)
B <i>E. huxleyi</i> (NN20/21)	0.25	1005A-3H-CC to 1005B-3H-CC	19.26
T <i>P. lacunosa</i> (NN19/20)	0.41	1005A-9H-CC to 1005A-10X-CC	69.60
T <i>R. asanoi</i>	0.85	1005A-16X-CC to 1005A-17X-CC	126.56
T <i>Gephyrocapsa</i> spp. (large)	1.20	1005A-21X-CC to 1005A-22X-CC	172.74
B <i>Gephyrocapsa</i> spp. (large)	1.44	1005A-22X-CC to 1005A-23X-CC	182.88
B <i>G. caribbeanica</i> (NN18/19)	1.72	1005A-23X-CC to 1005A-24X-CC	190.49
T <i>R. pseudoumbilicus</i> (NN15/16)	3.66	1005A-29X-CC to 1005A-30X-CC	247.45
B <i>D. loeblichii</i>	8.7	1005A-50X-CC to 1005C-6R-2, 55–57	431.16
T <i>D. hamatus</i> (NN9/10)	9.40	1005C-12R-2, 5–7, to 1005C-13R-2, 131–135	495.27
B <i>D. hamatus</i> (NN8/9)	10.7	1005C-21R-2, 97–99, to 1005C-23R-1, 84–88	582.36
B <i>C. coalitus</i> (NN7/8)	11.3	1005C-23R-1, 84–88, to 1005C-24R-2, 52–54	595.78

Notes: B = base, T = top. \* = average depth for the interval; for actual interval depth, see coring summary on CD-ROM. Average depth was used for constructing Figure 13.

**Table 3. Planktonic foraminiferal bioevents.**

Event	Age (Ma)	Interval (cm)	Depth* (mbsf)
<i>T. G. obliquus</i>	1.3	1005A-22X-CC to 1005A-23X-CC	182.90
<i>B. G. truncatulinooides</i>	2.0	1005A-23X-CC to 1005A-24X-CC	190.51
<i>T. G. peruenis</i>	2.6	1005A-24X-CC to 1005A-26X-1, 0-2	203.45
<i>T. D. altispira</i>	3.09	1005A-26X-1, 0-2, to 1005A-29X-CC	226.72
<i>T. Sphaeroidinellopsis</i> spp.	3.12	1005A-26X-1, 0-2, to 1005A-29X-CC	226.72
<i>T. G. margaritae</i> (N19/20)	3.58	1005A-30X-CC to 1005A-31X-CC	260.17
<i>T. G. nepenthes</i>	4.18	1005A-31X-CC to 1005A-34X-CC	274.10
<i>B. G. conglobatus</i>	6.2	1005A-48X-CC to 1005C-5R-1, 33-36	415.98
<i>B. N. acostaensis</i> (N15/16)	10.9	1005C-21R-2, 97-99, to 1005C-23R-1, 84-88	582.36
<i>T. G. mayeri</i> (N14/15)	11.4	1005C-23R-1, 84-88, to 1005C-24R-2, 52-54	595.78
<i>B. G. nepenthes</i> (N13/14)	11.8	1005C-29R-1, 65-67, to 1005C-31R-CC	651.82
<i>T. Fohsella</i> spp. (N12/13)	11.9	1005C-31R-CC to 1005C-32R-1, 100-102	670.90

Notes: B= base, T = top. \* = average depth for the interval; for actual interval depth, see coring summary on CD-ROM. Average depth was used for constructing Figure 13.

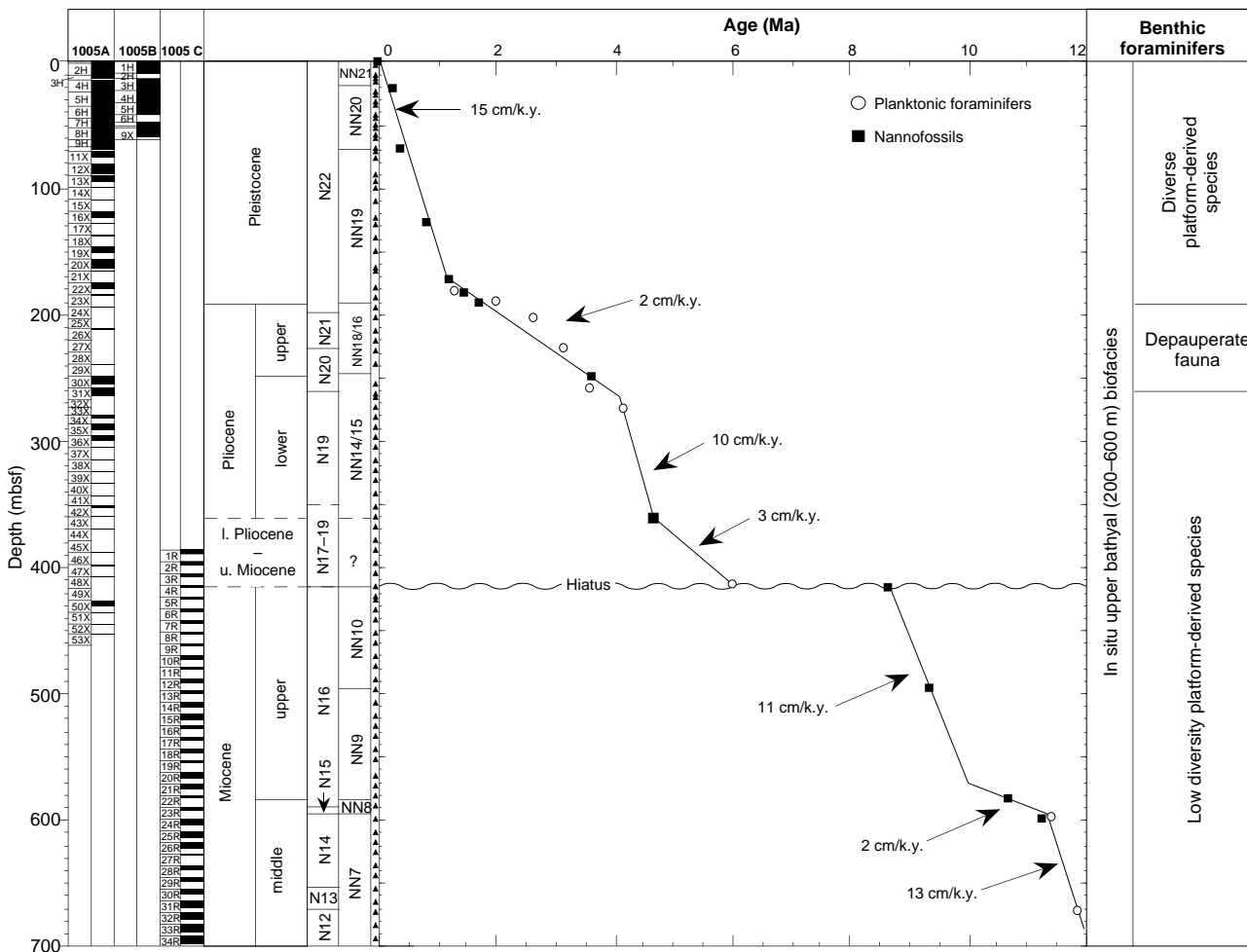


Figure 13. Calcareous nannofossil and planktonic foraminiferal zonation and benthic foraminiferal faunal changes for Site 1005. Recovery for each hole is adjacent to the cores. Solid triangles mark the position of samples examined for stratigraphy and benthic foraminiferal faunas. The age-depth plot is based on the biohorizons in Table 2.

increased influence of platform-derived material (aragonite needles, pellets, etc.) at about 1.2 Ma, shortly after a sharp increase in peloids that occurred at ~1.7 Ma (Subunits IB/IC boundary, see “Lithostratigraphy” section, this chapter). Higher sedimentation rates occurred in the late Pleistocene at Sites 1003 and 1004, although they were earlier at Site 1004.

The most conspicuous change in the sedimentation rate curve occurs at the level of the hiatus. The first useful biohorizon above the boundary is the first occurrence of *G. conglobatus* (6.2 Ma). Its low-

est occurrence at Site 1005 probably does not represent a true first appearance, and it is not known how much lower Pliocene section is missing. Another possibility is that some uppermost Miocene sediments lie on top of the unconformity. However, the minimal estimated early Pliocene sedimentation rate is at least 7 cm/k.y. (up to 10 cm/k.y., if we take into account the first occurrence of *Ceratolithus rugosus* at 4.7 Ma), indicating that the leeward side of the Great Bahama Bank received high amounts of platform material during this period. The hiatus spanned most parts of planktonic foraminiferal Zone N17

and probably resulted from current activity, as there is little to no pelagic sedimentation recorded or large-scale slope erosion associated with a lower sea-level stand.

An expanded section of lower upper Miocene sediments was drilled below the hiatus. The high sedimentation rate (11 cm/k.y.) probably reflects another period of platform shedding, consisting of very fine carbonate mud (see “Lithostratigraphy” section, this chapter) to the upper slope during nannofossil Zones NN9 and NN10. There was minimal input from platform production during nannofossil Zone NN8.

Sedimentation rates are high in the lowest part of the hole, which spans the planktonic foraminiferal Zones N12–N14 and nannofossil Zone NN7. The high sedimentation rate (13 cm/k.y.) indicates that there was late middle Miocene platform production on the Great Bahama Bank. In general, the changes in sedimentation rate observed at Site 1005 are similar to those found at Site 1003. The long-term pattern of alternating high and low sedimentation rates contrasts periods of bank flooding, concomitant shedding to the slope, and expansion of the sequences on the upper slope with periods of exposed banks, a “carbonate factory” shutdown, and largely pelagic sedimentation. The two largest sea-level falls straddled the middle/late Miocene and early/late Pliocene boundaries (Haq et al., 1987) and are clearly expressed in the sedimentation rates at Site 1003 and 1005, implying that they are global in origin (= third-order cycles of Haq et al., 1987).

## PALEOMAGNETISM

Shipboard paleomagnetic measurements were conducted at Holes 1005A, 1005B, and 1005C. As a result of the uncertainty in polarity, unrecovered intervals, and limitations in reliability of directional data from the shipboard cryogenic magnetometer, correlation to the geomagnetic polarity time scale (GPTS) was severely limited. Only one tentative reversal boundary could be correlated in the shallow part of Hole 1005A. In the upper portion of the Hole 1005A, archive-half cores were analyzed at 20-cm intervals at NRM and at 5-mT, and 15-mT AF demagnetization level in the pass-through cryogenic magnetometer. As a result of weaker intensities with depth and measurement problems associated with lower intensities (see following discussion), Holes 1005B and 1005C were not analyzed for magnetostratigraphic purposes. As with Sites 1003 and 1004, the reliability of the inclination and declination data was suspect as a result of what we interpreted as an axial bias in the cryogenic magnetometer. This axial bias showed very strong  $x$ -axis values relative to the other two axes, which gave a persistent northern declination (radial remagnetization problem?) and suspect inclination values when the sample was below a certain intensity level (see “Explanatory Notes” chapter, this volume). The intensity threshold for reliable directional data was judged to be about 1.0 to 1.2 mA/m. These values were assessed by reversing numerous split-core sections in the cryogenic magnetometer and noting at what intensity level the sign of the inclination value changed, and at what intensity level the declination values deviated from north. We also noted that inclination angle and remanence intensity (especially at the NRM level) change in phase with each other, which also may be an indication of some bias problem with the magnetometer.

The magnetic intensities of Holes 1005A and 1005B ranged from about 10 mA/m to about 1.0 mA/m at the NRM level (Fig. 14). After AF demagnetization at 15 mT, intensity values remained at about 1 mA/m (Fig. 14). Split-core measurements in Holes 1005B and 1005C failed to have sufficient intensities to overcome the axial bias problem discussed above. The low magnetic intensities throughout most of the core, the generally diamagnetic character of the whole-core susceptibility measurements, and several saturation isothermal remanent magnetization (SIRM) acquisition tests (Fig. 15) suggest that the remanence is carried by single-domain magnetite.

Directional data collected from the cryogenic magnetometer at Site 1005 should be viewed with caution, given the aforementioned

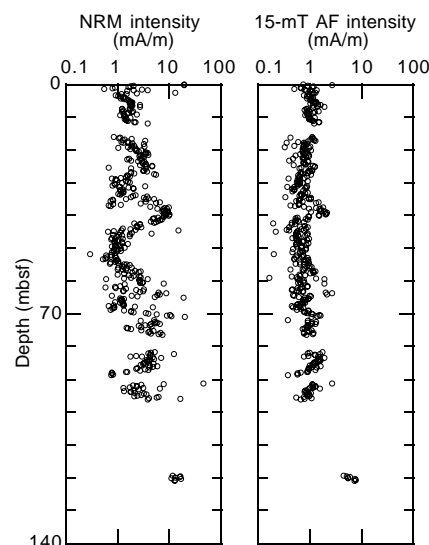


Figure 14. Remanence intensity at the NRM level and after the 15-mT AF demagnetization step in split cores from Hole 1005A.

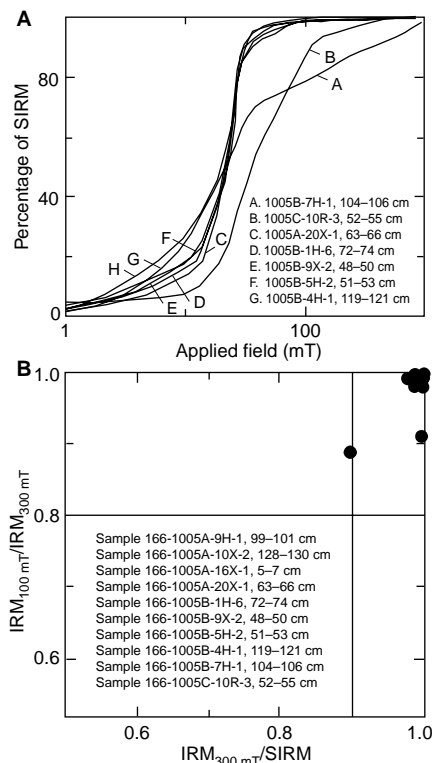


Figure 15. **A.** Isothermal remanent magnetization acquisition curves for several samples from Site 1005, representing differing lithologies and degree of cementation. Most of the samples show acquisition patterns similar to that of single-domain magnetite. Several samples (A and B) show slightly higher saturation levels, which may indicate either partial oxidation to maghemite or perhaps a component other than fine-grained magnetite. **B.** Comparison of ratios from the IRM acquisition data. The upper right portion of the plot is used to define a single-domain magnetite mineralogy. The Site 1005 data suggest remanence is mainly carried by fine-grained magnetite.

problems. The scattered NRM data show a better grouping around 30° after AF demagnetization at 15 mT (Fig. 16). The inclination angles that do not group near 30° after 15-mT AF demagnetization probably need additional demagnetization to give directional information. The upper 95 mbsf showed normal polarity, based on the inclination angle. Below an interval of low recovery (95–119 mbsf), inclination angles in a small interval of indurated sediment from about 119 to 125 mbsf showed a reverse polarity after 15-mT AF demagnetization (Fig. 16).

Magnetostratigraphically, only one reversal datum could be tentatively constrained in Hole 1005A. This is based on the indication of reverse polarity at about 119 mbsf and the overlying normal polarities. However, the reversal can only be constrained to lie somewhere between 95 and 119 mbsf because of a zone of no recovery.

The only possible correlation from the upper part of Hole 1005A is the Brunhes/Matuyama reversal boundary (at 0.78 Ma). The Brunhes/Matuyama is tentatively placed somewhere between 95 and 120 mbsf in the unrecovered interval. Therefore, the predominantly normal polarities above this boundary (95 mbsf) are correlated to the Brunhes Chron, with an age less than 0.78 Ma. The top of the *Reticulofenestra asanoi* datum (LAD 0.85 Ma) at about 125 m (Sample 166-1005A-16X-CC) supports positioning of the Brunhes/Matuyama in the unrecovered interval between 119 and 95 mbsf.

A discontinuous magnetic susceptibility record for the three holes at Site 1005 was generated by whole-core MST measurements (Fig. 17, corrected for spikes at core boundaries). Susceptibility was diamagnetic (negative) for the most part, which is characteristic of carbonate-dominated sediments (Shipboard Scientific Party, 1991). A proposed fine-grained magnetite remanence carrier is consistent with these diamagnetic susceptibility results, as susceptibility is grain-size dependent in magnetite (Maher, 1988) and often does not show positive susceptibilities with a carbonate sediment matrix. In the APC sections of Holes 1005A and 1005B, the diamagnetism varies in a cyclical fashion (Fig. 18) and may provide a method of correlation between the two holes, pending calibration with discrete samples. Downcore, several positive susceptibility spikes are prominent in Hole 1005A, especially between 100 and 200 mbsf. Examination of

the susceptibility data and the cores in this interval seem to suggest at least partial contamination related to XCB coring. Many of the positive susceptibility peaks were only single points and can be correlated tentatively with zones of inflow from drilling operations. In Hole 1005C, a similar, generally diamagnetic susceptibility was encountered; it also contained single-point spikes, although a few had slightly positive susceptibility. Cyclicity in Hole 1005C was not as well developed as in the lower part of Site 1003. Susceptibilities were usually in the 0 to -2 SI unit range.

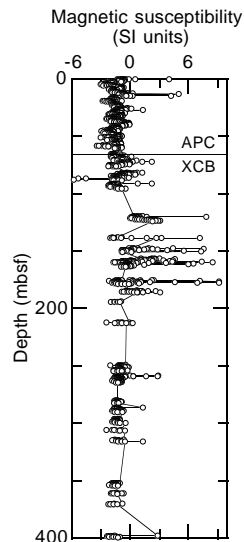


Figure 17. Whole-core magnetic susceptibility data from the MST at Hole 1005A. Susceptibility is mostly diamagnetic because of the high carbonate content. Positive susceptibilities encountered below 60 mbsf are partially attributed to XCB-coring disturbances, although several discrete samples between 156 and 158 mbsf showed positive susceptibilities and strong NRM intensities (~5 mA/m).

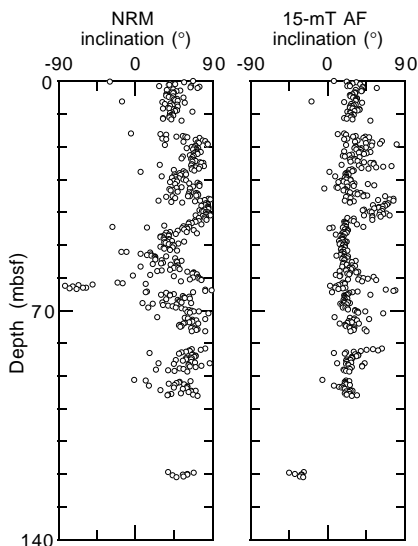


Figure 16. Inclination data from the shipboard cryogenic magnetometer in split cores from Hole 1005A. Inclination angles after 15-mT AF demagnetization show only one reversal in the lower part of the plot (at about 120 mbsf in the core). This interval has limited recovery that limits more refined placement of the reversal boundary (Brunhes/Matuyama?). See text for further discussion of the directional data and measurement problems encountered at this site.

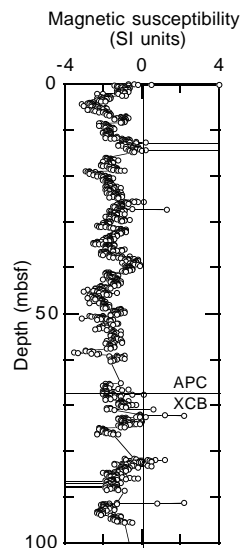


Figure 18. Magnetic susceptibilities for the top 100 m of Hole 1005A. A cyclical pattern in diamagnetism was present in the upper, unconsolidated portion of the hole. These variations in diamagnetism are also present in several of the other sites cored during Leg 166 and may correlate with lithologic cycles of platform sediment input.

## COMPOSITE DEPTH

### Composite Section

Holes 1005A and 1005B were evaluated for continuity of drilling in the upper 65 mbsf. High-resolution magnetic susceptibility, natural gamma, and GRAPE data were collected on whole cores at 5- to 15-cm intervals using the multisensor track (MST), and percent color reflectance was measured on split cores at 10-cm intervals. These records were used to construct a composite depth scale (meters composite depth, or, mcd) (Fig. 19), by first aligning significant events in the records and then depth-shifting the cores to achieve the maximum correlation coefficient over that interval (Table 4). Some of the deviation between Holes 1005A and 1005B is a result of stretching and compression related to coring. Because the cores were moved up and down rather than compressed or expanded to align the features, not all of the variation within a core can be perfectly aligned by adding a constant offset to each core. The correlation was improved by integrating correlations made on the different data sets, and biostratigraphic and lithostratigraphic events provided age control.

Correlations were made using magnetic susceptibility and color reflectance. There is good agreement between the magnetic susceptibility, percent color reflectance, and natural gamma data in those intervals where recovery was sufficient to make correlations (Fig. 19). The large amplitude variation in the color reflectance data is particularly useful for correlations. Variations in color are related to changes in aragonite content (see "Lithostratigraphy" section, this chapter). The color reflectance data were calibrated to the percent aragonite measured by XRD (see "Inorganic Geochemistry" section, this chap-

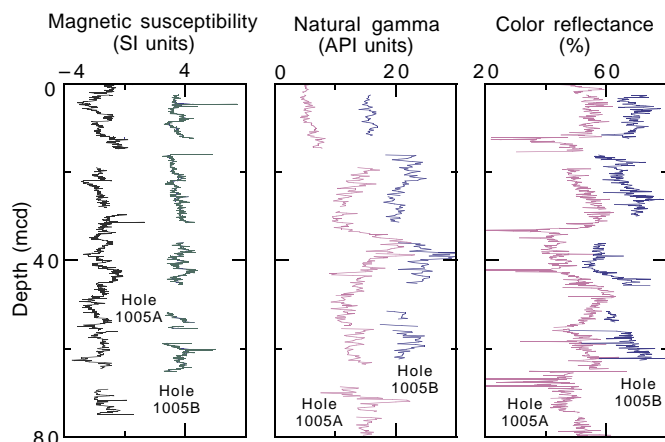


Figure 19. Magnetic susceptibility, natural gamma ray, and percent color reflectance data (700 nm) from Holes 1005A and 1005B plotted on the mcd scale. The data are offset for clarity.

Table 4. The offset of Hole 1005B, relative to Hole 1005A.

Core	1005A		1005B	
	Depth (mbsf)	Offset	Depth (mbsf)	Offset
1	0.00	0.00	0.00	2.55
2	2.50	0.00	9.50	2.55
3	12.00	0.00	13.50	2.55
4	16.00	3.05	23.00	2.55
5	25.50	3.40	32.50	3.50
6	35.00	3.40	42.00	3.50
7	44.50	3.40	48.00	3.85
8	52.00	3.40	51.00	3.85
9	61.50	3.40	52.00	6.65

Note: Add the offset to the depth (mbsf) to determine the meters composite depth (mcd).

ter) at Site 1004 (see "Lithostratigraphy" section, "Site 1004" chapter, this volume) wherein high aragonite content correlates to high percent reflectance.

The low recovery at this site limits correlations from hole to hole because the overlap of sedimentary events between the holes is not always present. For example, a large decrease in the color reflectance data at approximately 12 mcd in Core 166-1005A-3H (Fig. 19) is not present in Hole 1005B. This requires the correlation to be made on the basis of less significant events such as the peak in the base of the color reflectance data of Cores 166-1005A-2H and 1005B-1H (Fig. 19). A composite spliced record was not created for this site because of the inherent uncertainty in the correlations.

## ORGANIC GEOCHEMISTRY

At Site 1005, the shipboard organic geochemistry program included determinations of inorganic carbon, total carbon, total nitrogen, total sulfur, and Rock-Eval pyrolysis, in addition to safety monitoring for hydrocarbon gases. The analytical procedures are described in the "Explanatory Notes" chapter (this volume).

### Volatile Hydrocarbons and Hydrogen Sulfide

At Site 1005, low methane ( $C_1$ ) concentrations (2–4 ppm) were observed between 0 and 42.5 mbsf. Below this depth, methane showed a steady increase from 13 to 2403 ppm at 87.6 mbsf (Table 5 on CD-ROM; Fig. 20). The highest methane concentrations (>10,000 ppm) were observed below 148.8 mbsf. Ethane ( $C_2$ ) was first detected at 42.5 mbsf (Table 5 on CD-ROM). The  $C_1/C_2$  increased from less than 100 in the topmost part of the section to greater than 3000 at 194 mbsf. Below 324.2 mbsf, the  $C_1/C_2$  gradually decreased to a low value of 14 at the base of the hole (Fig. 20).

Propane ( $C_3$ ) was detected at 58.0 mbsf at Site 1005. Below 66.7 mbsf, trace levels (0.2–8 ppm) of isobutane, *n*-butane, isopentane, and *n*-pentane (Table 5 on CD-ROM) were also found. An increase in heavy-weight hydrocarbons (19 ppm) at 675.4 mbsf was also observed. The concentration of hydrogen sulfide ( $H_2S$ ) increased sharply between 66.7 mbsf (917 ppm) and 69.0 mbsf (2233 ppm). Below 315.4 mbsf, concentrations of  $H_2S$  decreased below detection limit (300 ppm) (Fig. 20).

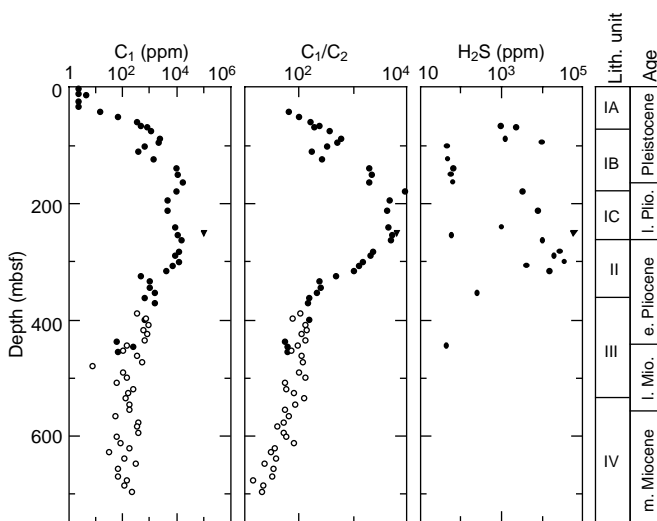


Figure 20. Methane concentration ( $C_1$ ), methane/ethane ( $C_1/C_2$ ) ratios, and hydrogen sulfide ( $H_2S$ ) of headspace gases (circles) and vacutainer gases (triangles) at Site 1005. Hole 1005A = solid circles, Hole 1005B = open circles.

### Inorganic and Organic Carbon, Total Sulfur, and Total Nitrogen

Carbonate data for Site 1005 are presented in Figure 21 and in Table 6 on CD-ROM. Carbonate content varied from 91 to 103.5 wt% (Fig. 21). Carbonate concentrations greater than 100 wt% result from the high dolomite content in these samples (>75 wt%; see "Inorganic Geochemistry" section, this chapter), which causes a 5–10 wt% over-estimation of carbonate concentrations (see "Explanatory Notes" chapter, this volume).

Eleven samples at Site 1005 with low carbonate content were selected for total carbon, total sulfur, and total nitrogen analysis. Total organic carbon (TOC) at Site 1005 varied from 0.11 to 2.63 wt% (Fig. 21). High concentrations (>1.0 wt%) were observed in lithologic Subunit IB and Units III and IV. In lithologic Subunit IB, the high TOC content is confined to an interval dominated by calcareous nanofossils and peloids. In lithologic Units III and IV, the organic-rich layers are confined to dark-colored, carbonate-poor intervals (see "Lithostratigraphy" section, this chapter). Total sulfur (TS) concentrations at Site 1005 were low (0.0–0.4 wt%) (Table 6 on CD-ROM). Total nitrogen (TN) ranged from 0.00 to 0.15 wt% (Table 6 on CD-ROM).

### Characterization and Maturity of Organic Matter

Five samples with TOC values greater than 0.5 wt% from lithologic Subunits IA and IB were characterized by Rock-Eval pyrolysis. The results are reported in Table 7 on CD-ROM.  $T_{max}$  values range from 414° to 436°C at Site 1005. Highest  $T_{max}$  values (436°C) are observed in the topmost part of the section (42.9 mbsf). The hydrogen index (HI) varied between 64 and 579 mg HC/g TOC.

### Discussion

The high  $C_1/C_2$  (>1000) observed below 138.8 mbsf at Site 1005 indicates that a significant amount of biogenic methane is produced in the sediment. The low  $C_1/C_2$  in the upper part of the hole (above 138.8 mbsf) is probably a result of preferential loss of  $C_1$  by either diffusion or selective microbiological  $C_1$  consumption (Claypool and Kvenvolden, 1983). The contribution of biologically produced meth-

ane apparently becomes less significant below 324.2 mbsf where the  $C_1/C_2$  is low (<250).

The high  $H_2S$  concentrations observed below 66.7 mbsf coincide with a sharp decrease in sulfate concentrations (see "Inorganic Geochemistry" section, this chapter). High rates of microbiological activity within the sulfate reduction zone (50–100 mbsf) and the deeper methanogenesis zone (100–300 mbsf) at Site 1005 account for the high concentrations. The high microbiological activity in the two zones might be related to the TOC-enriched interval observed in the lower part of lithologic Subunit IB (139.15–162.99 mbsf). The organic matter in lithologic Subunit IB is characterized by high HI values (405–579 mg HC/g TOC), that suggest a marine origin. Organic matter from the topmost part of lithologic Subunits IB and IA has lower HI (6–261 mg HC/g TOC), indicating a mixed marine and terrestrial or an oxidized marine origin. The organic matter in this interval also has a relatively high  $T_{max}$  value (430°–436°C), which could be the result of oxidation rather than thermal maturity.

One interval (80–140 mbsf) showed lower  $H_2S$  concentrations (<100 ppm) in the headspace samples. In this interval, lower methane concentrations and lower  $C_1/C_2$  were also observed. The presence of trace levels of higher weight hydrocarbons in the headspace gases below 74.3 mbsf indicates that some thermogenic gas may also partially contribute to the total gas composition at Site 1005.

### INORGANIC GEOCHEMISTRY

Inorganic chemical analyses were conducted on 40 interstitial water samples squeezed from whole-round samples at a frequency of one every other section in the first three cores and one per core thereafter. Analytical methods are detailed in the "Inorganic Geochemistry" section of the "Explanatory Notes" chapter (this volume).

The mineralogy of the carbonate fraction of the sediments at Site 1005 was quantified by X-ray diffraction (XRD) on 165 samples selected at frequencies ranging from one per section to one per core (Fig. 22). All carbonate mineralogy data were adjusted to include the weight percent noncarbonate fraction as determined by coulometric analysis of total carbonate (see "Organic Geochemistry" section, this chapter).

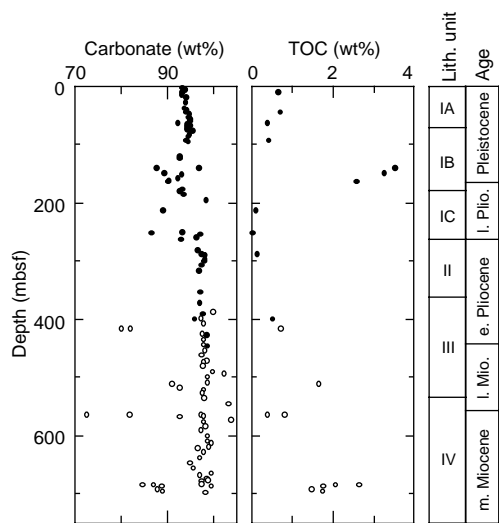


Figure 21. Concentration of carbonate and total organic carbon (TOC) at Site 1005. Hole 1005A = solid circles, Hole 1005C = open circles. Carbonate contents over 100 wt% are an artifact of the determination procedure (see "Explanatory Notes" chapter, this volume).

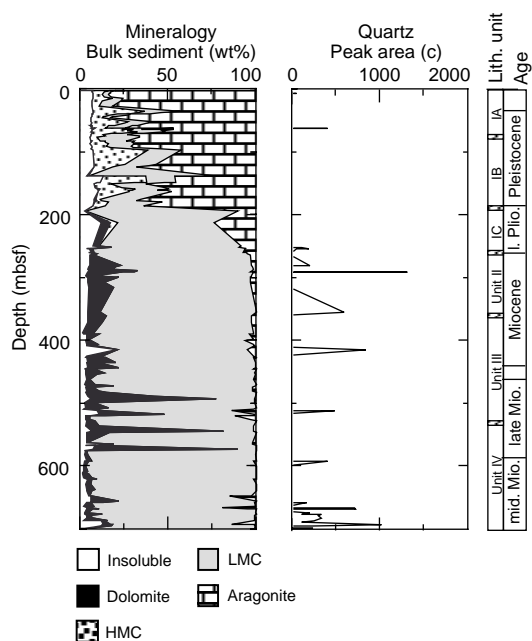


Figure 22. Quantitative X-ray mineralogy of sediments from Site 1005.

## Interstitial Waters

### Salinity, Chloride, Sodium, and Potassium

At Site 1005, the salinity and chloride ( $\text{Cl}^-$ ) increase from normal seawater values at the seafloor to approximately 1.6 times normal seawater at the base of the hole (700 mbsf) (Fig. 23; Table 8). The major characteristics of the  $\text{Cl}^-$  concentration may be summarized as follows: (1) no measurable change in the shallow portion of the sediments (0 to 45 mbsf); (2) a sharp increase beginning at 45 mbsf with a peak of 796 mM at 120 mbsf, followed by a decrease to 742 mM at 174 mbsf; and (3) a steady increase with a slope 0.5 mM/m below 180 mbsf to the base of the hole. The sodium ( $\text{Na}^+$ ) concentrations are conservative with respect to  $\text{Cl}^-$  to a depth of 400 mbsf, showing no change from normal seawater ratios within the analytical precision (see "Explanatory Notes" chapter, this volume). Below 400 mbsf, the  $\text{Na}^+/\text{Cl}^-$  decreases from normal seawater ratios (0.85) to about 0.82. The ratio of potassium ( $\text{K}^+$ ) to  $\text{Cl}^-$  initially increases in the upper 400 mbsf, but shows a decrease similar to that of  $\text{Na}^+/\text{Cl}^-$  below 400 mbsf.

### Alkalinity, Sulfate, Ammonium, and Phosphate

The titration alkalinity, sulfate ( $\text{SO}_4^{2-}$ ), and ammonium ( $\text{NH}_4^+$ ) concentrations at Site 1005 change significantly at 45 mbsf from normal seawater values (Fig. 23). Alkalinity and  $\text{NH}_4^+$  increase to broad

maxima of 65 and 16 mM, respectively, at a depth of 200–250 mbsf, and then decrease to 10 and 4 mM at 400 mbsf, remaining near these concentrations to the base of the hole. There is a noticeable anomaly in the profile between 120 and 174 mbsf, where alkalinity and  $\text{NH}_4^+$  decrease by several millimoles. The distribution of  $\text{SO}_4^{2-}$  mirrors the alkalinity profile at the expected 2:1 ratio in the upper 540 mbsf, but deviates from this trend in the lowest portion of the core. The  $\text{SO}_4^{2-}$  concentration is completely depleted by a depth of 75 mbsf, increases within the anomaly zone to 11 mM, then returns to 0 below 200 mbsf. Below 400 mbsf,  $\text{SO}_4^{2-}$  increases to 34 mM at 540 mbsf, followed by an abrupt decrease to 25 mM at 580 mbsf, that is maintained to the base of the hole with the exception of the last sample, which shows a concentration of 16 mM. Phosphate ( $\text{HPO}_4^{2-}$ ) concentrations range from 1 to 10  $\mu\text{M}$ , showing a much smaller increase and suggesting active removal of  $\text{HPO}_4^{2-}$  from pore waters (see "Inorganic Geochemistry" section, "Site 1004" chapter, this volume).

### Calcium, Magnesium, Strontium, and Lithium

The concentrations of calcium ( $\text{Ca}^{2+}$ ) and magnesium ( $\text{Mg}^{2+}$ ) decrease sharply below 45 mbsf from normal bottom-water concentrations of 10.9 and 56.8 mM, respectively (Fig. 23). This decrease is punctuated between 120 and 174 mbsf, where the concentrations of both  $\text{Ca}^{2+}$  and  $\text{Mg}^{2+}$  increase to 10 and 55 mM, respectively. Below

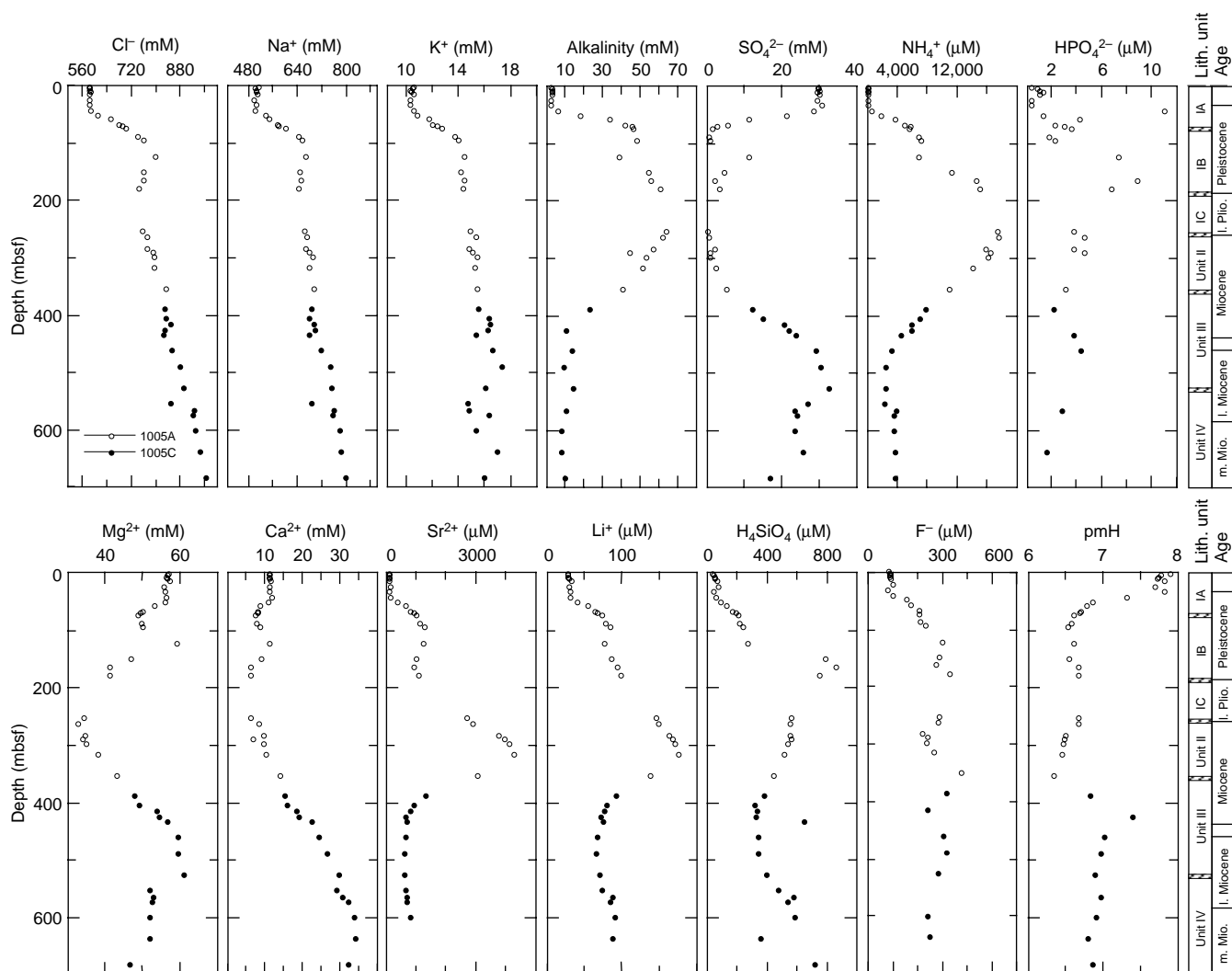


Figure 23. Depth profiles of interstitial water constituents at Site 1005.

Table 8. Composition of interstitial waters from Site 1005.

Core, section, interval (cm)	Depth (mbsf)	pmH	pH	Alk (mM)	Sal	Cl <sup>-</sup> (mM)	Na <sup>+</sup> (mM)	Mg <sup>2+</sup> (mM)	Ca <sup>2+</sup> (mM)	SO <sub>4</sub> <sup>2-</sup> (mM)	HPO <sub>4</sub> <sup>2-</sup> (μM)	NH <sub>4</sub> <sup>+</sup> (μM)	H <sub>4</sub> SiO <sub>4</sub> (μM)	K <sup>+</sup> (mM)	Li <sup>+</sup> (μM)	Sr <sup>+</sup> (μM)	F <sup>-</sup> (μM)	Fe <sup>2+</sup> (μM)
166-1005A-																		
1H-1, 145-150	1.4	7.90	7.73	2.45	36.5	583	511	56.8	11.2	29.9	0.4	41	33	10.5	27	95	80	5
2H-1, 145-150	4.0	7.78	7.65	2.81	36.5	580	499	56.7	11.2	29.9	0.9	93	41	10.4	27	100	86	7
2H-3, 140-150	6.9	7.74	7.69	3.14	36.5	581	503	56.4	11.2	30.0	1.0	152	45	10.2	28	101	84	11
2H-5, 140-150	9.9	7.73	7.72	3.00	36.5	586	503	56.7	11.2	29.4	1.3	149	49	10.4	28	95	85	6
3H-1, 140-150	13.4	7.81	7.64	2.59	36.5	583	510	57.1	11.5	29.9	1.0	91	62	10.5	32	101	88	6
4H-5, 140-150	23.4	7.69	7.67	2.58	36.5	580	495	55.8	11.3	29.6	0.4	66	70	10.2	29	122	98	6
5H-5, 140-150	32.9	7.81	7.60	2.55	36.5	580	503	56.1	11.2	30.7	0.4	53	37	10.3	30	100	75	4
6H-5, 140-150	42.4	7.32	7.72	5.84	37.0	586	502	56.4	11.8	28.4	11.0	581	54	10.6	30	139	98	19
7H-4, 140-150	50.4	6.86	7.90	17.76	38.0	607	534	55.8	10.8	21.1	1.3	1,771	87	10.8	40	380	154	3
8H-4, 140-150	57.9	6.78	8.00	33.43	40.0	650	546	53.1	8.6	11.2	4.3	3,731	125	11.8	54	633	169	1
9H-5, 135-150	68.0	6.70	8.00	41.68	42.0	679	572	50.0	8.1	5.5	2.3	4,963	168	12.0	64	809	203	0
10X-1, 135-150	68.8	6.68	7.95	45.77	42.0	690	579	49.2	8.0	2.6	3.0	5,761	189	12.3	66	910	206	4
11X-1, 135-150	73.4	6.61	7.97	46.25	44.0	702	600	48.7	7.3	1.4	3.6	5,593	202	12.7	74	1,023	204	3
12X-4, 135-150	87.4	6.58	7.97		45.0	739	645	49.8	7.6	0.5	1.8	6,909	215	13.7	78	1,105	209	1
13X-2, 135-150	94.0	6.53	7.89	48.39	46.0	758	654	50.0	8.5	0.9	2.3	7,091	237	13.9	83	1,286	230	5
16X-2, 135-150	122.2	6.61	6.75	38.51	49.5	796	668	59.0	11.2	11.2	7.4	6,797	271	14.4	76	1,231	297	8
19X-2, 135-150	150.2	6.54	6.72	54.10	46.5	760	645	46.9	8.8	4.6	12.2	11,316	784	14.2	86	1,006	283	3
20X-5, 135-150	164.0	6.66	6.84	55.41	46.5	759	652	41.3	6.2	2.1	8.9	14,535	856	14.5	94	932	272	2
22X-2, 135-150	178.0	6.66	8.07	60.46	46.0	742	645	41.1	6.1	3.1	6.8	15,028	748	14.4	99	1,097	327	3
30X-3, 135-150	253.6	6.66	6.83	63.96	46.0	756	664	34.1	6.0	0.3	3.8	17,435	555	14.9	145	2,710	283	1
31X-3, 135-150	263.0	6.66	6.71	61.86	46.5	772	669	32.6	8.2	0.4	4.7	17,609	552	15.3	149	2,908	279	4
34X-2, 135-150	283.2	6.49	7.93	57.09	48.0	771	664	34.5	9.7	2.1	3.8	15,869	549	14.8	163	3,767	215	2
35X-2, 135-150	289.4	6.48	8.08	44.29	48.0	790	677	34.0	6.9	0.7	4.7	16,362	556	15.0	167	3,948	237	4
36X-2, 135-150	299.0	6.46	7.89	53.30	48.5	793	688	35.0	9.5	0.9		16,072	531	15.5	171	4,098	236	6
38X-1, 135-150	316.0	6.44	6.58	51.34	48.5	795	678	38.2	10.3	2.5		14,129	511	15.2	175	4,253	265	6
42X-1, 135-150	353.2	6.34	6.7	40.36	50.0	831	693	43.1	14.0	5.3	3.1	10,852	440	15.4	138	3,064	373	9
166-1005C-																		
1R-1, 140-150	388.0	6.83	7.00	22.98	50.0	827	685	47.9	15.3	12.1	2.2	7,756	379	15.5	92	1,308	313	
3R-1, 0-8	405.2				50.0	830	678	49.0	15.8	15.0		7,016	317	16.3	80	930		
4R-2, 0-7	416.0				52.0	846	693	53.8	18.3	20.5		5,943	329	16.4	76	806	238	
5R-2, 0-8	425.5	7.39	7.79	10.41	52.0	826	695	54.3	19.1	21.8		5,943	322	16.2	71	631		
6R-1, 0-4	433.4				52.0	823	676	56.5	22.6	23.7	3.7	4,537	646	15.4	75	707		
9R-1, 0-10	460.7	7.02	7.05	13.34	52.0	850	716	59.5	24.3	29.1	4.4	3,279	340	16.6	67	643	300	
12R-2, 0-10	490.0	6.97	7.13	9.10	54.0	878	749	59.5	26.7	30.3		2,428	335	17.3	65	626	314	
16R-2, 0-10	526.8	6.88	6.80	13.88	56.0	891	751	60.9	29.8	32.5		2,502	396	16.0	71	592	281	
19R-1, 0-5	553.3				50.0	846	685	51.8	29.0	26.8		2,206	467	14.7	73	637		
20R-2, 124-124	564.9	6.97	7.00	10.14	56.0	925	758	52.8	30.7	23.6	2.8	3,908	575	14.8	88	708		
21R-1, 145-150	573.2				56.0	922	756	52.6	32.3	24.2		3,464	533	16.3	84	700		
24R-2, 50-58	601.0	6.90	7.03	7.81	56.0	929	777	51.9	33.7	23.5		3,501	578	15.3	91	797		
28R-1, 102-111	637.0	6.80	6.91	8.16	57.0	944	782	51.9	34.1	25.7	1.6	3,760	357	17.0	88		238	
33R-2, 0-11	683.4	6.86	7.12	9.72	57.0	962	799	46.4	32.4	16.9		3,686	713	15.9			248	

174 mbsf, the  $\text{Ca}^{2+}$  concentration begins a steady increase, reaching a value near 35 mM at the base of the hole. Over the same interval, the  $\text{Mg}^{2+}$  concentration decreases to 35 mM at 300 mbsf, increases to 60.9 mM at 527 mbsf, and then abruptly shifts to 52 mM down to the base of the hole. Dissolved strontium ( $\text{Sr}^{2+}$ ) increases sharply below 45 mbsf from seawater concentrations (0.094 mM), shows a decrease within the anomaly zone, and then reaches a high of 4.2 mM at 312 mbsf. Below 312 mbsf,  $\text{Sr}^{2+}$  sharply decreases back to 0.6 mM, and this concentration is maintained to the base of the hole. The dissolved lithium ( $\text{Li}^+$ ) concentrations generally track the  $\text{Sr}^{2+}$  profiles.

### Silica, Fluoride, pmH, and Iron

Silica concentrations ( $\text{H}_4\text{SiO}_4$ ) increase significantly below 45 mbsf to a high of 856  $\mu\text{M}$  at 164 mbsf (Fig. 23). Farther downcore, silica decreases gradually to 400  $\mu\text{M}$ , with two notable spikes at 433 and 683 mbsf. Fluoride ( $\text{F}^-$ ) also increases sharply below 45 mbsf to a maximum value of 327  $\mu\text{M}$  at a depth of 178 mbsf. The value of pmH remains above 7.6 down to a depth of 45 mbsf, below which it declines sharply through the sulfate-reduction zone to values near 6.6. Below this depth, pmH remains below 6.5 to a depth of 400 mbsf, after which it sharply increases to 6.9, which is maintained to the base of the hole. Iron ( $\text{Fe}^{2+}$ ) concentrations are generally very low at Site 1005. With the exception of one sample at 42 mbsf, all iron concentrations are less than 8  $\mu\text{M}$  and show no particular trends downcore.

### Interpretation of Pore-Water Chemistry

As observed at Sites 1003 and 1004, pore-water chemistry profiles at Site 1005 are heavily influenced by the presence of a deep-seated saline fluid rich in  $\text{Na}^+$ ,  $\text{Cl}^-$ ,  $\text{K}^+$ ,  $\text{SO}_4^{2-}$ , and  $\text{Mg}^{2+}$ . Although many of these ions show some degree of nonconservative behavior, the distribution of  $\text{Cl}^-$  is interpreted to be a result of conservative diffusional mixing with this deeper saline fluid. Small amounts of lateral fluid flow between lithologic boundaries are evident at Site 1005, particularly in the upper 200 mbsf (see following discussion). The most likely origin of the deeper saline fluid is from subsurface dissolution of evaporite minerals, such as halite ( $\text{NaCl}$ ). Triassic to Early Jurassic age sediments underlying the Bahamas/Florida region are thought to contain evaporites (Sheridan, 1974).

The increase in  $\text{K}^+/\text{Cl}^-$  in the upper 400 mbsf (fluid Zones 2 and 3) is interpreted to be the result of ion-exchange reactions involving organic-rich (1–4 wt%) sediments (see “Organic Geochemistry” section, this chapter) (Mackin and Aller, 1984). Below 527 mbsf, the relative decreases in  $\text{K}^+/\text{Cl}^-$  and  $\text{Na}^+/\text{Cl}^-$  (not shown) are probably caused by clay mineral diagenesis. For example, the conversion of

kaolinite ( $\text{Al}_2\text{Si}_2\text{O}_5(\text{OH})_4$ ) to montmorillonite ( $[\text{Na}_{0.2}\text{K}_{0.1}\text{Mg}_{0.1}\text{Mg}_{0.8}]\text{Mg}_{0.66}\text{Al}_{3.34}\text{Si}_{10.8}\text{O}_{20}(\text{OH})_4$ ) will remove varying amounts of  $\text{Mg}^{2+}$ ,  $\text{K}^+$ , and  $\text{Na}^+$  from pore fluids (Loughnan, 1969). Substantial quantities of clay minerals (>2%) occur in the sediments at Site 1005 below 500 mbsf, roughly coinciding with small decreases in the normalized  $\text{Na}^+$  and  $\text{K}^+$  concentrations (see “Downhole Logging” section, this chapter).

The major changes reflected in the alkalinity,  $\text{SO}_4^{2-}$ ,  $\text{NH}_4^+$ ,  $\text{HPO}_4^{2-}$  and pmH profiles are interpreted to be caused by the microbial consumption and oxidation of primary organic matter (see “Inorganic Geochemistry” section, “Site 1004” chapter, for more detailed discussion). Rates of organic matter remineralization are highest between 45 and 200 mbsf, where the availability of labile organic material is high (see “Organic Geochemistry” section, this chapter). The high amounts of sulfide, methane, alkalinity, and  $\text{NH}_4^+$  measured between 45 and 300 mbsf at Site 1005 suggest that the more proximal position of this site favors the accumulation of greater amounts of organic material. This material was probably trapped in sediments during rapid Pliocene–Pleistocene platform shedding events (see “Biostratigraphy” section, this chapter).

The oxidation of organic material provides ideal conditions (low pmH, high alkalinity) capable of driving early carbonate alteration reactions in these shallow sediments. In the Pleistocene interval (45–200 mbsf), changes in the  $\text{Ca}^{2+}$  and  $\text{Mg}^{2+}$  concentration are interpreted to be caused by alteration of metastable aragonite and high-magnesium (HMC) to dolomite and low-magnesium calcite (LMC). The absence of  $\text{SO}_4^{2-}$ , high alkalinity, and high  $\text{Mg}^{2+}/\text{Ca}^{2+}$  ratios may provide a favorable geochemical environment for dolomite formation (e.g., Baker and Kastner, 1981; Katz and Mathews, 1977) (Fig. 24). Below 280 mbsf, the  $\text{Mg}^{2+}/\text{Ca}^{2+}$  gradually decreases to 1.5 at the base of the hole. Changes in the  $\text{Mg}^{2+}/\text{Ca}^{2+}$  in the lowest portions of the hole (below 500 mbsf) are probably caused by continued addition of  $\text{Ca}^{2+}$  to pore waters from moderate aragonite dissolution and the loss of  $\text{Mg}^{2+}$  to clay mineral diagenetic reactions discussed previously.

The  $\text{Sr}^{2+}$  concentration measured in the pore fluids is controlled by the dissolution and alteration of metastable aragonite and the precipitation of celestite ( $\text{SrSO}_4$ ) (Baker and Bloomer, 1988; Swart and Guzikowski, 1988). The measured ion molar product of  $\text{SrSO}_4$  is plotted in Figure 24. Pore fluids are undersaturated with respect to  $\text{SrSO}_4$  between 0 and 400 mbsf and saturated below 400 mbsf, where abundant celestite cements were found in the cores. The plotted  $\text{Sr}^{2+}/\text{Ca}^{2+}$  downcore (Fig. 22) shows how aragonite dissolution and celestite solubility influence the  $\text{Sr}^{2+}$  and  $\text{Ca}^{2+}$  concentrations. In the upper zone, the  $\text{Sr}^{2+}/\text{Ca}^{2+}$  increases during alteration of aragonite to calcite and dolomite in the absence of appreciable concentrations of  $\text{SO}_4^{2-}$ . In the lower zone, however, while moderate dissolution of

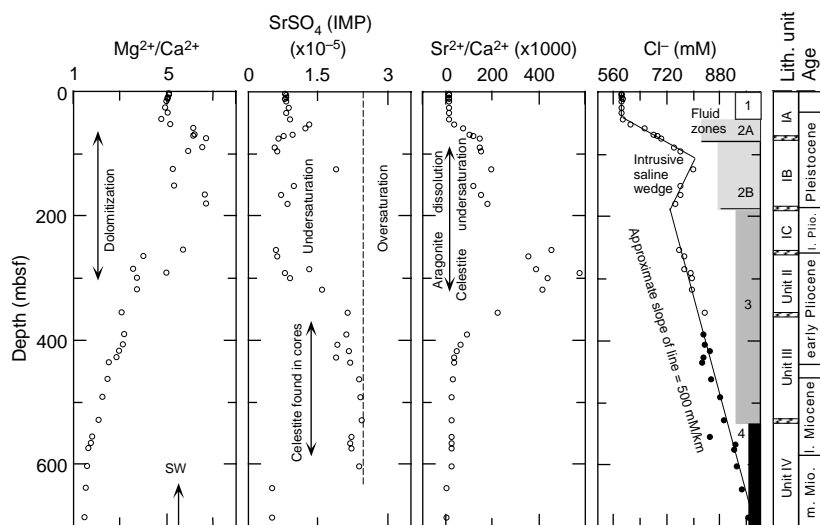


Figure 24. Depth profiles of selected interstitial water constituents at Site 1005. The plot of the  $\text{SrSO}_4$  ion molar product (IMP) shows regions of celestite saturation. See the text for an explanation of the four fluid zones distinguished at Site 1005.

aragonite continues to add  $\text{Ca}^{2+}$  and  $\text{Sr}^{2+}$  to the pore fluids, the presence of sulfate causes most of this added  $\text{Sr}^{2+}$  to precipitate out as celestite.

At Site 1005, fluid flow is hypothesized to explain the large anomalies in pore-water profiles within the upper 200 mbsf. Four distinct zones were identified (Fig. 24). These zones roughly correspond to the lithologic sequence boundaries, though limited vertical exchange and diffusion in these lithologic boundaries obscure some of the relationships. Zone 1 extends from the seafloor to lithified layers located just below 45 mbsf (see "Lithostratigraphy" section, this chapter). Zone 2 contains a large chloride anomaly and is divided into two sub-zones on the basis of changes in  $\text{Ca}^{2+}$ ,  $\text{Mg}^{2+}$ ,  $\text{SO}_4^{2-}$ , and  $\text{Sr}^{2+}$ , as well as trace elements. The division between the two subzones corresponds to the lithologic division between Subunits IA and IB (see "Lithostratigraphy" section, this chapter). The lower boundary of zone 2B is located at the Pliocene/Pleistocene boundary (187 mbsf). Zone 3 extends to 540 mbsf, corresponding to the boundary between lithologic Units III and IV. Zone 4 extends below this boundary to the base of the hole.

Zone 1 contains no gradients in any of the dissolved species measured. It is interpreted to be an interval with enhanced seawater flushing that prevents diffusional gradients from developing between the overlying seawater and underlying saline fluid. A similar interval was described at Sites 1003 and 1004 (see "Inorganic Geochemistry" section, "Site 1003" and "Site 1004" chapters, this volume). Zone 2 is marked by a sharp change in all the major and minor pore-water constituents, including a large increase in  $\text{Cl}^-$ . Zone 2 is interpreted to contain an intrusion of saline, sulfate-rich water derived from farther upslope on the platform margin. An alternative explanation is that bottom water of lower  $\text{Cl}^-$  concentration is penetrating into the sediment below 187 mbsf, causing the  $\text{Cl}^-$  in zone 2 to appear anomalously high. High rates of microbial sulfate reduction within Subzone 2A reduce  $\text{SO}_4^{2-}$  to zero. Lower amounts of microbial activity within Subzone 2B allow a shift in the opposite direction for sulfate and alkalinity, giving them a distinctly anomalous appearance. The profiles of  $\text{Ca}^{2+}$ ,  $\text{Mg}^{2+}$ , and  $\text{Sr}^{2+}$  also reflect distinct anomalies within Subzone 2B.

The  $\text{Cl}^-$  gradient changes below zone 2 are less dramatic, displaying a steady-state distribution to the base of the hole. Other constituents, however, continue to show considerable change in the lower two units. For example,  $\text{SO}_4^{2-}$  reappears again below 300 mbsf, increasing to 31 mM at the base of zone 3 before dropping again within zone 4 (see also  $\text{Ca}^{2+}$ ,  $\text{Mg}^{2+}$ , and  $\text{H}_2\text{SiO}_4$ ). At this time, it is not known to what degree shifts in these elements are influenced by (1) diagenetic controls within each of the lithologic units, and (2) the movement of fluid within these boundaries.

### Mineralogy

Quantitative XRD analysis of the bulk sediments at Site 1005 shows distinctive changes in mineralogy downcore (Table 9 on CD-ROM; Fig. 22). The abundance of aragonite in the upper 180 mbsf averages 65%, with pronounced cycles observed in its distribution as reported at Site 1004 (see "Inorganic Geochemistry" section, "Site 1004" chapter, this volume). Below 180 mbsf, there is an abrupt drop in the aragonite abundance to less than 7%, with several peaks up to 15% at depths of 400, 510, and 660 mbsf (Fig. 22). The 180-mbsf boundary between these two sections coincides with the Pliocene/Pleistocene boundary (see "Lithostratigraphy" and "Biostratigraphy" sections, this chapter).

In the upper 180 mbsf, the abundance of HMC shows a marked increase of up to 40% between the aragonite cycles. The HMC maxima appear to coincide with firmgrounds and hardgrounds formed during periods of nondeposition (see "Physical Properties" and "Lithostratigraphy" sections, this chapter). The abundance of HMC in these intervals is interpreted to reflect the increased role of marine

seafloor cementation during lowstand sea-level events. The abundance of HMC also drops significantly below 180 mbsf, and it disappears completely below 240 mbsf.

Dolomite was first detected at 120 mbsf, and it occurs in trace amounts to 180 mbsf. Below this depth, dolomite content averages 5%–15%, with distinctive spikes of up to 70 wt% at 280, 485, 510, 540, 570, and 650 mbsf. These dolomite spikes roughly coincide with the presence of gamma-ray peaks (see "Downhole Logging" section, this chapter) and are interpreted to represent dolomitization of these hardground surfaces during early burial (Melim et al., 1997). The similarity between the cyclic aragonite/HMC distribution in the upper 180 mbsf and the dolomite/aragonite distribution between 480 and 700 mbsf further supports this interpretation and suggests that much of this early dolomitization may be limited to metastable HMC cement layers.

Quartz abundance is low throughout the cores, increasing slightly below 600 mbsf with a coincident increase in clay mineral abundance. In contrast to Site 1003, no chert intervals were encountered at this site. Elemental sulfur concretions were observed at several deeper intervals in the cores (below 400 mbsf). In general, the sulfur is limited to fracture-filling zones and forms only a small fraction 10% of the total sediment (see "Lithostratigraphy" section, this chapter). Other diagenetic cements include large amounts of celestite found below 400 mbsf, as both fracture-filling veins and replacement cements (see "Lithostratigraphy" section, this chapter).

## PHYSICAL PROPERTIES

Measurements of physical properties at Site 1005 were made on whole cores using the MST, on split cores using the DSV, and on discrete samples for index properties. Thermal conductivity was measured only on unconsolidated whole-round cores. The vertical spacing of the MST measurements was maintained at 15 cm for the NGR and 5 cm for GRAPE density, velocity, and magnetic susceptibility. DSV velocity, however, was measured only in the shallow section down to 52 mbsf, where the core maintained contact with the liner. In the unconsolidated cores, three discrete velocities per section were measured with the DSV. Consolidated sediments were measured using the frame transducers at a frequency averaging five measurements per section. Shear strength data were collected at an average of three measurements per section to a depth of 100 mbsf.

The following descriptions focus on the downhole variation in petrophysical properties and their correlation with lithostratigraphy. At the end of this section, downhole trends in thermal conductivity are described. Variations in the magnetic susceptibility are discussed within the "Paleomagnetism" section (this chapter).

### Index Properties, GRAPE Density, and *P*-Wave Velocity

Tables 10 through 15 on CD-ROM summarize the index properties, GRAPE density, discrete velocity measurements, and NGR for Site 1005. Figures 25 and 26 show the combined results of the petrophysical measurements for the entire Site 1005 and for the upper interval to 100 mbsf, respectively. Site 1005 was subdivided into three petrophysical units based on the characteristics of the downhole patterns in the various physical properties.

Petrophysical Unit I (0–180 mbsf) coincides with the lithologic Subunits IA and IB (Pleistocene), which consist of burrowed, unlithified to partially lithified wackestone with rare packstone layers. It is characterized by an overall low velocity that can be subdivided into several intervals (Subunits Ia through If). Each of these intervals shows a gradual downcore decrease in velocity followed by an abrupt increase across the boundary below (Fig. 26). In each subunit, sonic velocity is higher near the top (1.6 km/s) and decreases to approximately 1.5 km/s near the base. Abrupt downcore shifts to higher

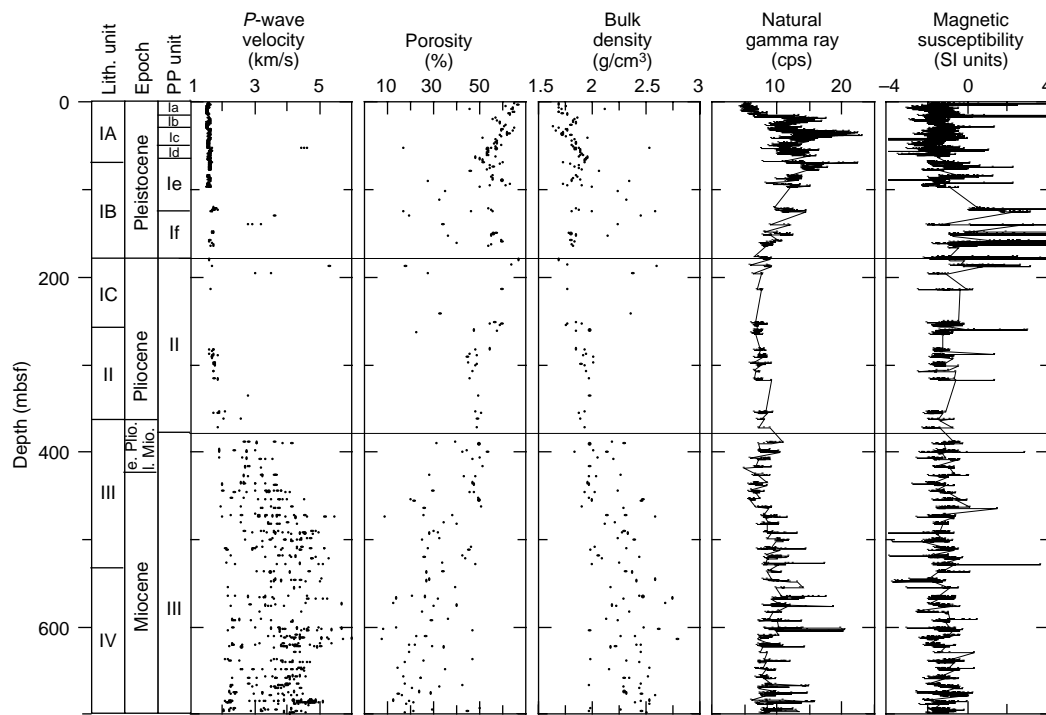


Figure 25. Combined plot of *P*-wave velocity from discrete measurements using the DSV and velocity frame, porosity, bulk density measured on discrete samples, NGR, and magnetic susceptibility from Hole 1005A. Lithologic and petrophysical units are indicated along with age.

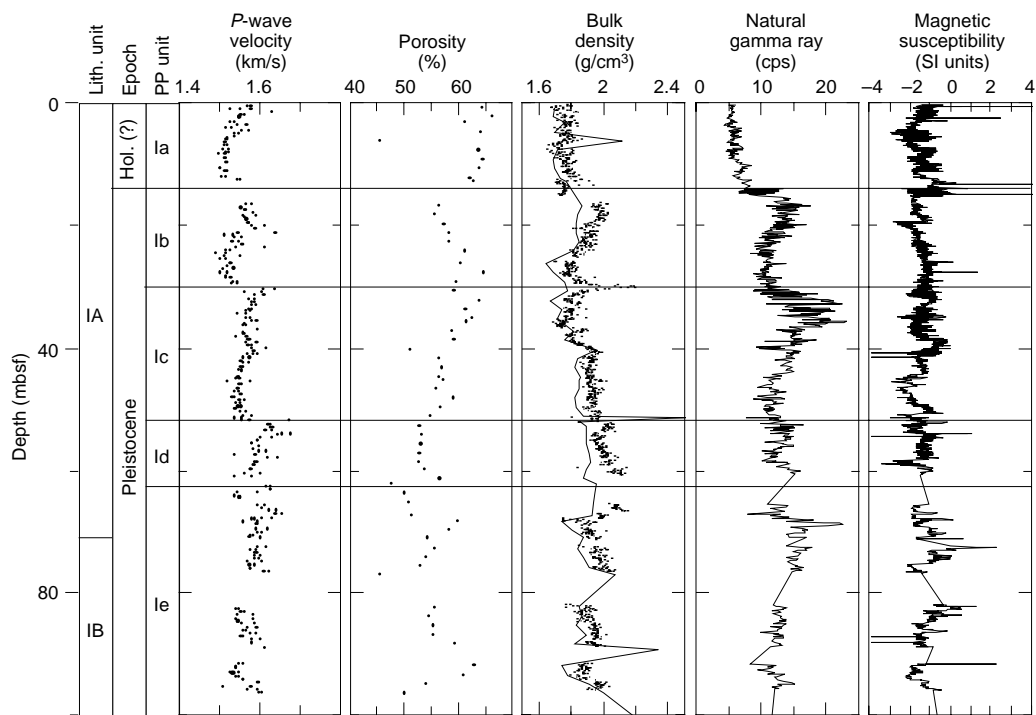


Figure 26. Summary of *P*-wave velocity from discrete measurements using the DSV and velocity frame, porosity, bulk density measured using the GRAPE (points) and discrete samples (line), NGR, and magnetic susceptibility for the shallow interval to 100 mbsf. Lithologic and petrophysical units are indicated along with age. GRAPE density values were corrected for the mass-attenuation effect of water in high-porosity sediments (see “Explanatory Notes” chapter, this volume).

values in  $V_p$  occur at 14, 30, 52, 63, and 126 mbsf to form interval boundaries (Fig. 27). Two subunits are characterized by exceptionally high velocities near the top. The boundary between petrophysical Subunit Ic and Subunit Id (52 mbsf) is marked by a thin, highly cemented layer (only recovered in Hole 1004B, see “Lithostratigraphy” section, this chapter) that has velocities greater than 5 km/s (Fig. 25). Velocities near the top of Subunit If (126 mbsf) have values of up to 3.5 km/s. It is possible that similar high-velocity layers cap the other petrophysical subunits but that they were not recovered nor detected by the sonic log because pipe remained in the hole to a depth of 100 mbsf during logging. The gradual downcore decrease in velocity within each subunit correlates well with the aragonite content (Fig. 27), which may be related to the input of shallow-water-derived aragonitic sediment (see “Lithostratigraphy” section, this chapter). In addition, the tops of the subunits coincide with a relatively high gamma-ray intensity. The maximum values for natural gamma ray, however, are located several meters below the top of a subunit (e.g., petrophysical Subunits Ib, Ic, and If; Figs. 25, 26). A similar correlation was also observed at previous sites (e.g., Site 1004). This coincidence of upcore-increasing velocities with increasing aragonite content and gamma ray strongly suggests that these subunits represent depositional sequences. The velocity increase as well as the high NGR values may be related to submarine cementation resulting from extended exposure times at the seafloor at periods of reduced sediment deposition.

Bulk density shows a gradual downcore increase from 1.6 to approximately 1.9 g/cm<sup>3</sup> near the bottom of petrophysical Unit I. The variations in bulk density generally follow the velocity trend. Subunit Id is an exception, as bulk density increases downcore with decreasing velocity.

The boundary between petrophysical Units I and II coincides with the change from lithologic Subunit IB to Subunit IC, a downcore transition from partially lithified to lithified wackestone at the Pleistocene/Pliocene boundary. Petrophysical Unit II (180–380 mbsf) forms most of the Pliocene section. Low recovery in this interval prohibits a detailed evaluation of the physical properties distribution. Overall, both velocity and bulk density show a subtle, but gradual downcore increase from 1.7 to 1.9 km/s and 1.8 to 1.9 g/cm<sup>3</sup>, respectively. The sonic log (Fig. 28), however, displays less variation in velocity than observed in petrophysical Units I and III. With the exception of one high-velocity layer at 260 mbsf (up to 3 km/s), the lower part of the unit shows low velocities (less than 2.2 km/s). The boundary with underlying petrophysical Unit III is located approximately 20 m above the transition from lithologic Unit I to Unit II, characterized by a change from wackestone to packstone.

Petrophysical Unit III (380–700 mbsf) encompasses most of the Miocene section and is characterized by a gradual downcore increase in velocity and bulk density, a decrease in porosity, and an overall increase in the range of these parameters. Near the top of the unit, velocity ranges from 1.9 to 3.0 km/s, whereas downcore this range increases to values between 2.0 and 5.0 km/s. In a similar manner, bulk density changes from 1.9–2.2 to 2.0–2.7 g/cm<sup>3</sup> and porosity from 30%–50% to 10%–45%. Petrophysical Unit III consists of thin-bedded alternations of dark and light layers consisting of variably cemented mudstone to wackestone (see “Lithostratigraphy” section, this chapter). Similar to Site 1003, these alternations have a strong signature in physical properties. The light-colored layers are characterized by high velocity, high density, lower porosity, and, in general, lower gamma-ray intensity, whereas the dark beds show opposite characteristics. This relationship is demonstrated by high-resolution measurements of velocity, density, gamma ray, and color intensity within a 3-m interval (Fig. 8).

**Logging Data vs. Discrete Measurements**

Several logging tools were run in Holes 1005A and 1005C (see “Downhole Logging” section, this chapter). These logging data com-

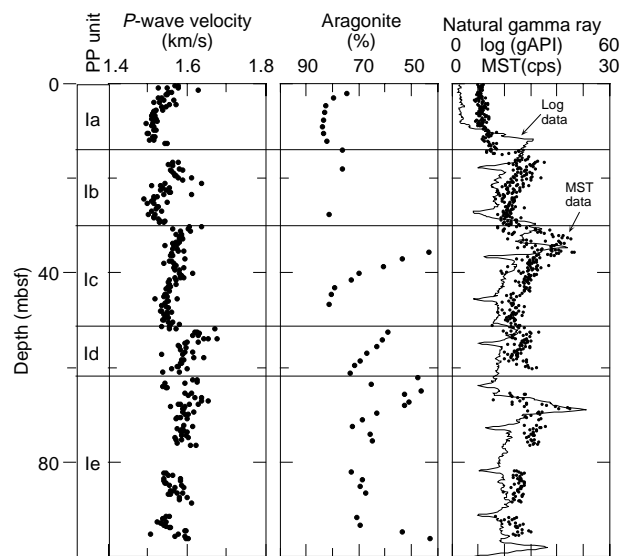


Figure 27. Combined plot of sonic velocity from the DSV, aragonite content from XRD measurements, and natural gamma ray from the MST and well log (measured through pipe). Note the low gamma-ray kicks caused by the pipe joints and local vertical offset between the log gamma ray and MST measurements caused by incomplete recovery. See text for discussion.

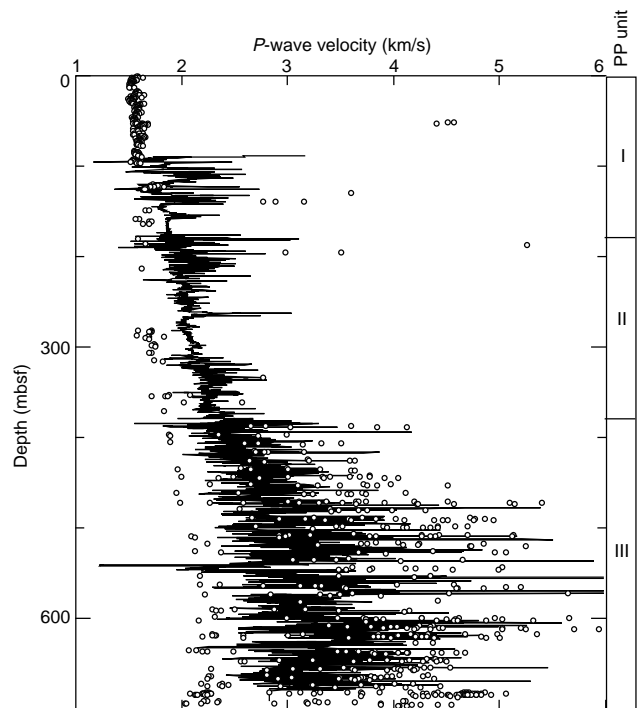


Figure 28. Combined plot of discrete  $P$ -wave velocity measurements from the DSV (points) and sonic velocity from well logs in Hole 1005C (line). See text for discussion.

plement the onboard physical property measurements as they provide a continuous record of the downhole variation in physical properties. An overlay of the sonic log data with DSV measurements shows good agreement, despite their different frequencies, confining pressures, and sampling intervals (Fig. 28). The offset of the sonic velocity baseline below 200 mbsf is probably a result of the higher in situ

confining pressure of the logged borehole wall. In the uppermost 100 m at Site 1005, where drill pipe remained in the hole, the high-resolution DSV data can be used to complete this missing shallow section of the sonic log. For correlation of other discrete measurements with the equivalent logs (NGR, porosity, and density), see Figures 32 and 33 in the “Downhole Logging” section of this chapter.

### Shear Strength

Shear strength measurements were made in the unconsolidated sediments down to 100 mbsf. Values from shear strength measurements are shown in Table 16 on CD-ROM. Shear strength values can reach values over 60 kPa (Fig. 29). Although the range of shear strength increases downhole, the lower values remain the same, indicating the presence of sediments with low shear strength throughout the upper 100 mbsf. The boundaries between the petrophysical Subunits Ia–Ie can be recognized by lower shear strength values than those of the sediments within the subunits, resulting in a subtle undulating downhole trend in shear strength.

The  $S_u/P_o'$  at Site 1005 shows a similar trend to that at Sites 1003 and 1004, with higher values at the surface and decreased values below (Fig. 29).

### Thermal Conductivity

A total of 54 thermal conductivity measurements were made on sediments from 0 to 200 mbsf at Hole 1005A. Results are shown in Table 17 on CD-ROM and Figure 30. The average and the standard deviation of all conductivity measurements at this site are 1.07 and 0.07 W/(m·K), respectively. The number of measurements from 100 through 200 mbsf is limited as a result of poor core recovery.

Some of the subunits within petrophysical Unit I show distinct conductivity patterns. Subunit Ic is characterized by an upward decrease of thermal conductivity from 1.2 W/(m·K) at the base to 0.95 W/(m·K) at the top, whereas Subunit Ib shows an inverse trend, with conductivities increasing downward. The other subunits show no clear correlation between depth and conductivity.

## DOWNHOLE LOGGING

### Logging Operations

Downhole logging at this site was performed in two stages. The upper part of the sequence was logged in Hole 1005A, and the lower part in Hole 1005C (Fig. 31). After coring operations ended in Hole 1005A, seawater and sepiolite mud were pumped into the hole, and a wiper trip was performed to ream the borehole irregularities and remove any remaining cuttings from the hole. We deployed two logging tool strings, the induction-sonic and integrated porosity-lithology tool (IPLT), and performed a vertical seismic profile (VSP) experiment, making nine check-shot stations with the well seismic tool (WST) (Fig. 31).

In Hole 1005A, the first tool string began collecting data at 445 mbsf near the bottom of the hole, and successive tool deployments reached slightly shallower depths, probably as a result of minor borehole infill (about 10–20 m) during the course of logging operations. Hole 1005C reached a total depth of 700 mbsf, and open-hole logging was performed in the lower section between 400 and 700 mbsf, providing an interval of overlapping data with Hole 1005A of about 40 m. In this hole, we successfully acquired data from the IPLT, induction-sonic and Formation MicroScanner (FMS) strings and performed six check-shot stations with the WST (Fig. 31). The first two tool strings reached the bottom of the hole, but the FMS and WST tools were prevented from reaching total depth by borehole bridges at 613 and 540 mbsf, respectively.

Site 1005 is the first ODP site logged using the new tool string comprising natural gamma-ray spectrometry/accelerator porosity

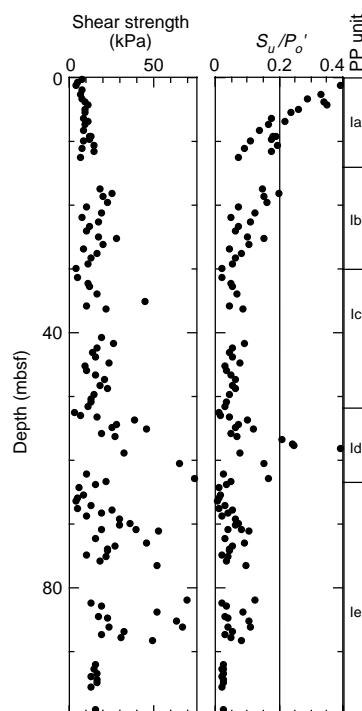


Figure 29. Shear strength and  $S_u/P_o'$  ratios calculated from shear strength and overburden stress for cores from Hole 1005A.

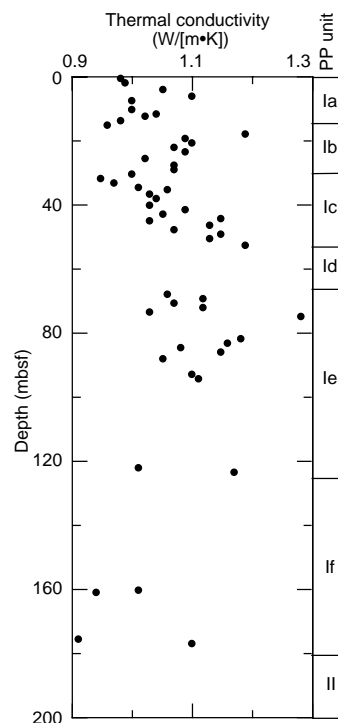


Figure 30. Thermal conductivity for Hole 1005A plotted with the petrophysical units.

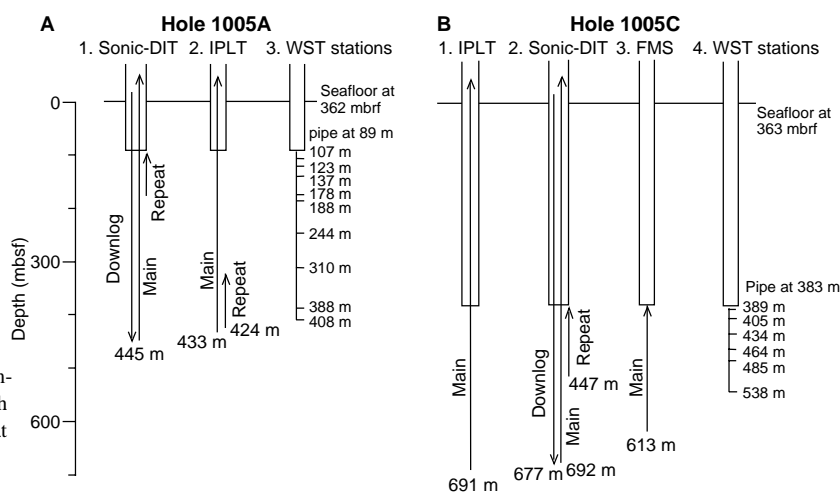


Figure 31. Summary of the logging runs at Site 1005. The temperature logging tool was included on the first two runs of both holes. The logging speeds were sonic-DIT at 300 m/hr, IPLT at 350 m/hr, and FMS 550 at m/hr. See “Explanatory Notes” chapter (this volume) for description of the tool strings.

sonde/hostile-environment litho-density sonde (HNGS/APS/HLDS), which represents a major improvement in gamma-ray and neutron logging techniques to evaluate formation properties (see “Explanatory Notes” chapter).

### Data Quality

Logging data quality can be severely affected by the quality of the borehole. Hole 1005A was enlarged by washout of the softer sediment to a diameter beyond the maximum extent of the HLDS caliper (16.5 in, 42 cm), resulting in a large uncertainty in the density log in these intervals (Fig. 32). Resistivity and velocity logs tend to be less affected by borehole enlargement, as can be noted by the overall lack of correlation between these logs and the caliper curve (Fig. 32). Hole 1005C was less enlarged, and the caliper curve is punctuated by only a few washouts. In Hole 1005A, the short-spaced sonic logs (DT and DTL) gave very low velocity readings, probably a result of the enlarged borehole. Nevertheless, integration of the sonic logs compares well with the check-shot results, suggesting that these logs are good (see “Seismic Stratigraphy” section, this chapter).

The standoff measurement provided by the accelerator porosity sonde (APS) remained below 1 in (2.5 cm) throughout the logged interval in Holes 1005A and 1005C, indicating a good-quality porosity log. We suspect that eccentricization of the tool string also provided for a better gamma-ray log, which is less susceptible to local variations caused by changes in borehole size.

The borehole diameter changed significantly during the FMS logging run in Hole 1005C, but the resulting images are of good overall quality, with good pad contact maintained by the four pads except above 430 mbsf, where two or fewer pads maintained contact in the enlarged borehole.

The IPLT and induction-sonic logs were shifted from depths measured in meters below rig floor (mbrf) to mbsf for preliminary analysis and combined into a single data file. The gamma-ray logs usually provide a good indication of the seafloor depth, but at this site the upper 15 m or so of the sediment column displays little natural radioactivity (~5 cps, see “Physical Properties” section, this chapter) and corresponds to a pronounced shift in the logging gamma-ray readings in the drill pipe. The overlap section between Holes 1005A and 1005C indicates good correspondence between major logging data peaks and troughs, but shore-based processing is required for detailed correlation between the different logging runs.

### Preliminary Observations

The combined downhole measurements from Holes 1005A and 1005C provide geophysical and geochemical (U, K, Th) data covering the interval from 90 to 700 mbsf. As sediment recovery in this in-

terval was low, averaging about 30%, these logs can provide extremely valuable information about Site 1005 that can be correlated with the data obtained from the cores. Log-to-core correlation permits significant improvements of the interpretations on specific aspects of variations in the sedimentation patterns on the margin of the Great Bahama Bank from the middle Miocene to the present.

Figure 32 contains a compilation of all logged data plotted against depth in the section and related to core recovery, biostratigraphic age, lithologic units, and physical property laboratory data compiled from discrete samples and whole-core sections (Fig. 32). The compatibility of the discrete points with the data obtained from the total logged interval supports the integrity of the data sets. In particular, the extreme fluctuations in the values for discrete samples from the lower portion of the section are constrained by wide variability in the logged curves for the same interval.

Gamma-ray logs obtained from within the drill pipe are also available for the interval from 0 to 90 mbsf, which had approximately 100% recovery (Fig. 33). Corrected for the effect of the drill pipe on the intensity of the signal, these logs reveal in detail the same cyclic variability as observed in the MST data (see “Physical Properties” section, this chapter).

The strong cyclic nature of the data is the most notable feature recorded in all the logs, specifically from 700 to 385 mbsf (middle Miocene to lowermost lower Pliocene) and from 260 to 90 mbsf (upper Pliocene to Pleistocene) (Fig. 32). The intervening section from 385 to 260 mbsf (lower Pliocene) is marked by an apparent decrease of the intensity of the cycles, which is particularly reflected by the monotonous resistivity curve. The overall character of the cycles recorded in the lower and upper intervals is not equivalent. Between 260 and 90 mbsf (upper Pliocene–Pleistocene), intervals of sharp increases in gamma-ray intensity basically correlate with increased density, resistivity, and velocity and decreased porosity. This association of properties is characteristic for hardgrounds (Serra, 1986). We propose that sharp peaks in the interval from 260 to 90 mbsf probably indicate interruptions of neritic input leading to the formation of well-cemented intervals that might become hardgrounds during periods of reduced sedimentation. These harder layers alternate with less lithified, more porous sediments that represent periods of reduced neritic input.

Between 700 and 385 mbsf (Miocene), the peaks of increased gamma-ray intensity tend to be associated with intervals of decreased density, resistivity, and velocity, and increased porosity. A more detailed examination of the lower cycles in a selected interval from 630 to 590 mbsf reveals the tendency of the softer layers to be associated with increased gamma-ray intensity (Fig. 34). One notable exception within the illustrated interval is where two major gamma-ray peaks between 608 and 604 mbsf correlate with physical characteristics indicative of more indurated intervals. The data indicate that the Mio-

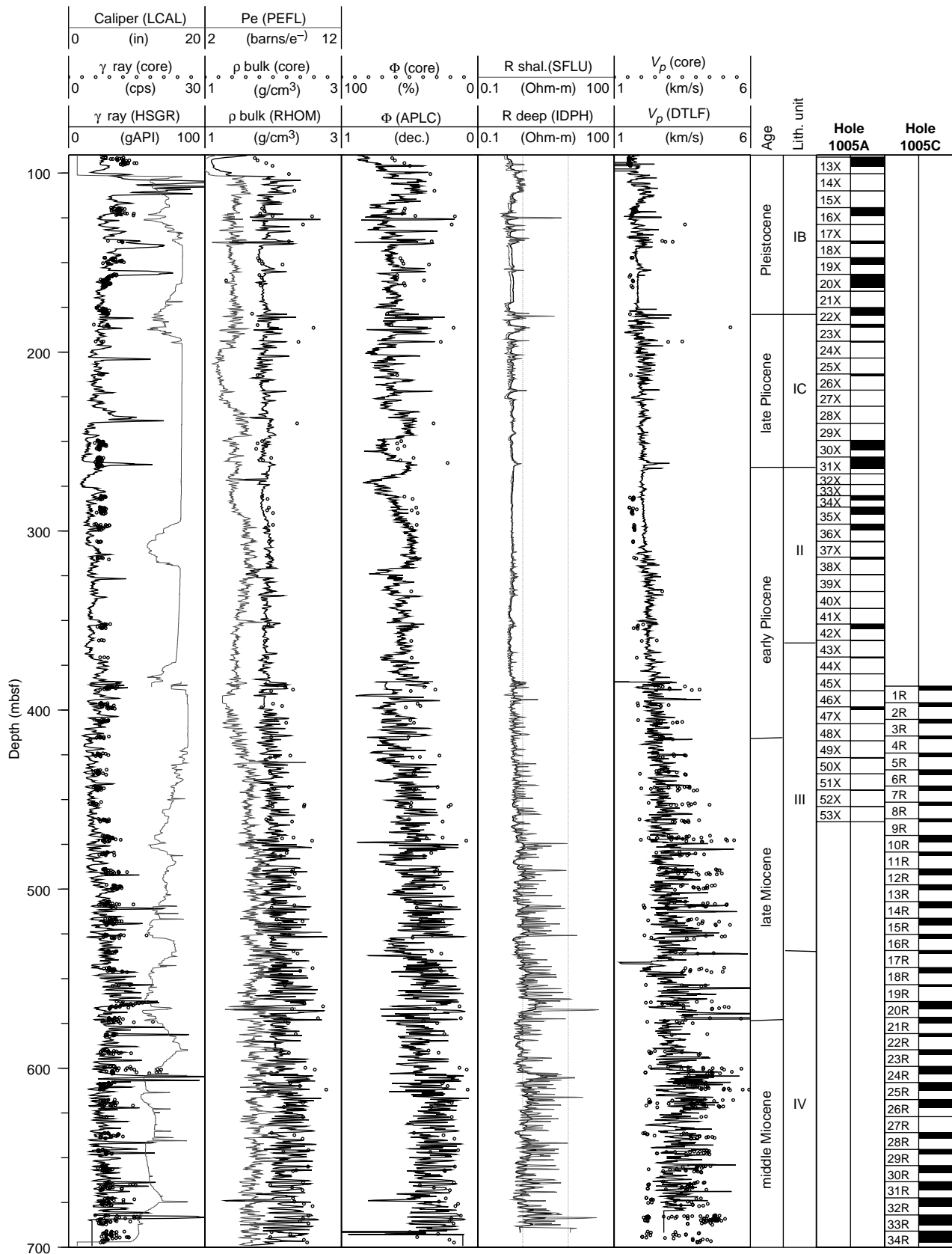


Figure 32. Summary of key geophysical logs acquired with the IPLT and induction-sonic logging strings. From left to right, columns are gamma ray and caliper, bulk-density ( $\rho$  bulk) and photoelectric index (Pe), porosity ( $\Phi$ ), shallow and deep resistivity (R), and sonic velocity ( $V_p$ ). The points represent core measurements from the MST (natural gamma ray) and index properties (bulk density, porosity, and velocity from the DSV instrument; see “Physical Properties” section, this chapter), age, lithologic units, and core recovery.

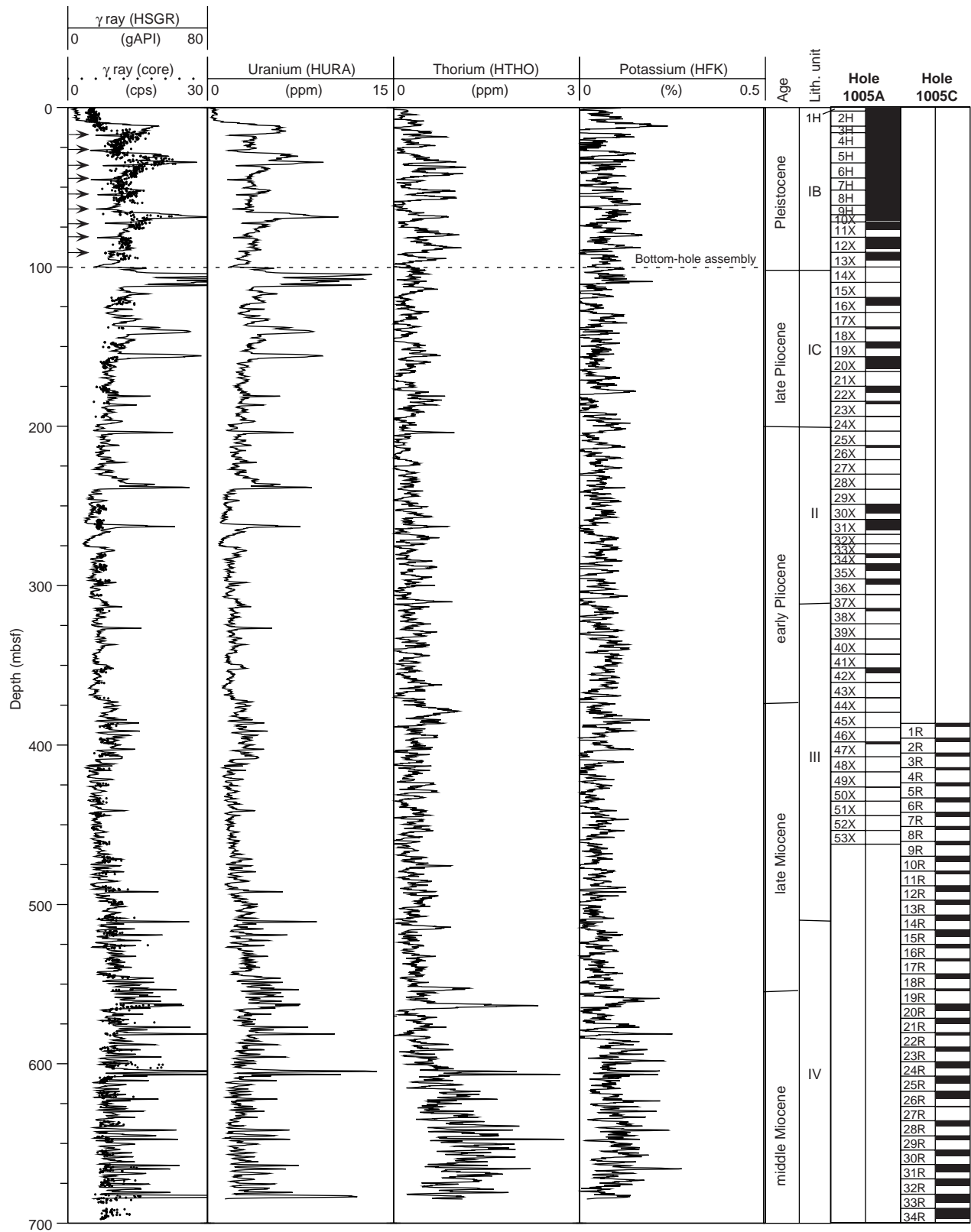


Figure 33. Spectral gamma-ray results using the HNGS tool. The curves between 0 and 90 mbsf were corrected for the attenuation of the gamma-ray spectra caused by measurement in the drill pipe following an empirical correction constant obtained by comparing logging runs in Holes 1005A and 1005C. Arrows indicate the position of the pipe joints. The points represent natural gamma-ray spectra of core measurements using the MST (see “Physical Properties” section, this chapter).

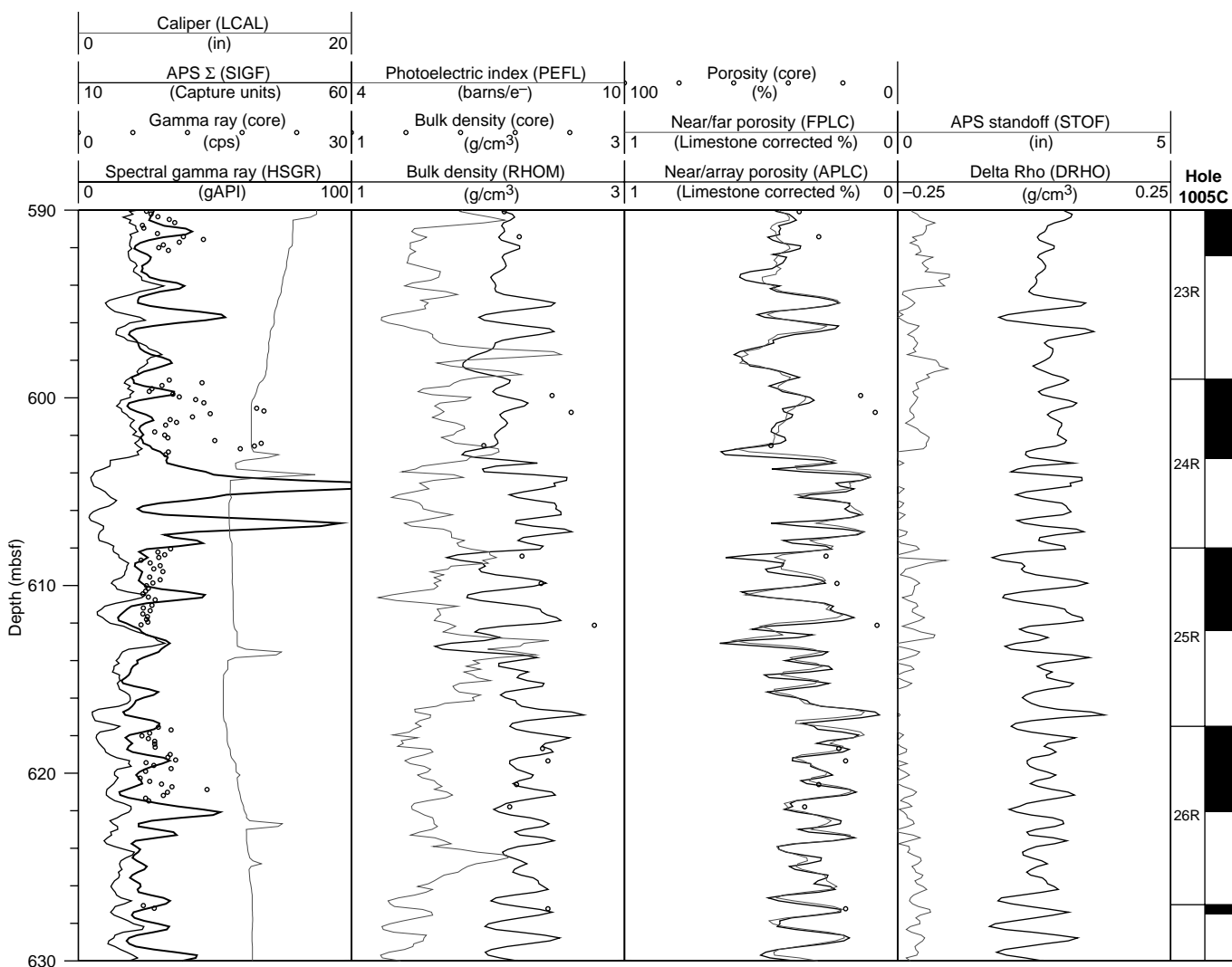


Figure 34. Detail of IPLT logging data within the middle Miocene (lithologic Unit IV) showing the nature of the bedding cycles. Cycles correspond to alternation between beds of high gamma ray, high porosity, and high capture cross-section (sigma) and beds of low porosity, high density, low gamma ray, and low sigma. These cycles are sporadically interrupted by more pronounced gamma-ray peaks, which are prominent and contrast with other gamma-ray peaks because of their very high U content (see Fig. 33) and low-porosity, high-density, and low sigma values.

cene sediments are also punctuated by alternating periods of reduced neritic input and increased neritic input leading to hardground formation.

FMS scans of the Miocene cycles reveal a distinctive alternation between more and less resistive layers (Fig. 35). The less resistive layers are basically characterized by increased gamma-ray activity. The FMS images show the presence of burrows throughout, but those of the less resistive layers appear flattened, indicating differential compaction. Lithologic descriptions of the cycles from this interval, as well as geochemical data, indicate that the intervals containing flattened burrows are darker and softer and are associated with increased clay and organic matter contents (see "Lithostratigraphy" and "Organic Geochemistry" sections, this chapter).

The HNGS logging can resolve the three most common components of naturally occurring radiation: uranium, thorium, and potassium (Fig. 33). An interval with relatively higher Th content occurs from the base of the section to about 600 mbsf, covering middle Miocene sedimentation period. This interval shows apparent cyclic increases or peaks of Th above the generally low background level.

Clay minerals contain relatively elevated Th concentrations, whereas Th is not associated with chemical sediments. Thus, the presence of Th in carbonate sequences is considered an important indicator of clay minerals (Serra, 1986). This explanation for a Th increase in clays is consistent with observations stated previously for the Miocene cycles. From 600 mbsf to the top of the logged section, the Th concentration decreases to a fairly constant low level, except for a few peaks (e.g., 570–550 mbsf).

The U content, however, displays a high degree of variability in the logged section. Between 600 and 500 mbsf, the U content appears higher than a baseline level. In the 200-m interval representing the upper Miocene to lower Pliocene, the U concentration remains relatively monotonous, indicating low levels between approximately 500 and 300 mbsf. Starting at about 300 mbsf, the U content tends to increase progressively up section. Superimposed upon this overall increasing pattern are sharp spikes of elevated U concentrations. As mentioned previously, these spikes correlate with the geophysical logs and are interpreted to be the expression of hardgrounds. Carbonates usually display a low gamma-ray signature, and the presence of

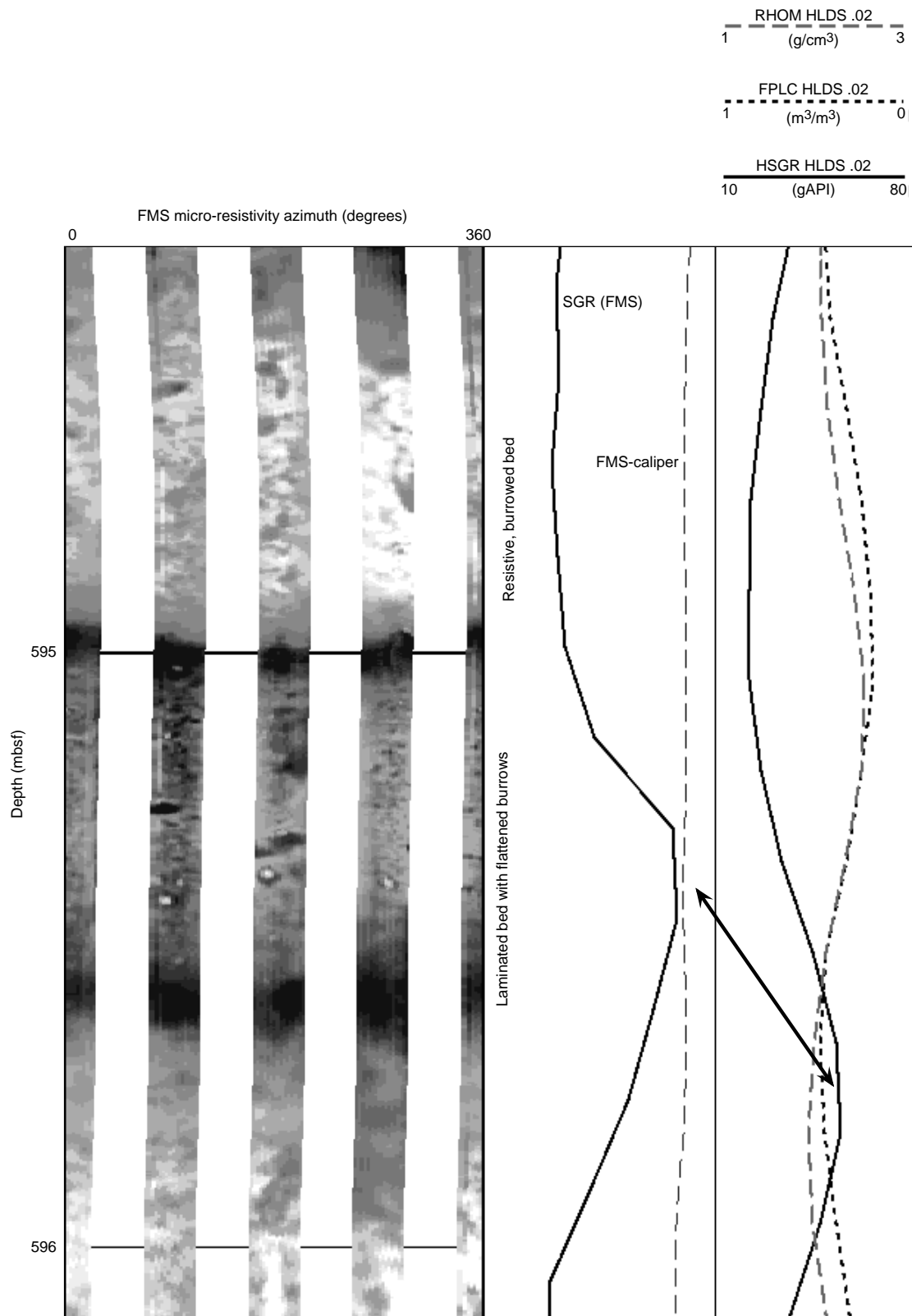


Figure 35. FMS image together with gamma-ray (SGR, line) and caliper (dashed line) logs from the FMS string (center track) and gamma-ray (HSGR), porosity (FPLC), and bulk density (RHOM) logs from the IPLT string (right track). The dark (conductive) bed displays faint laminations and flattened conductive features that are probably burrows. The resistive (low porosity, high bulk density) layer shows evidence for numerous burrows. The boundaries between adjacent layers are marked by an increase in conductivity. Logs between different runs were not depth matched aboard ship, and the arrow indicates correlation between the gamma-ray peaks observed in the different runs.

U is associated with organic matter in gamma-ray log interpretations (Serra, 1986). In nature, U, as uranyl cations ( $\text{UO}_2^{2+}$ ), is commonly complexed with carbonate or phosphate anions and becomes incorporated into carbonate and phosphate minerals. For this reason, it appears that the U spikes in the upper Pliocene–Pleistocene sediments may be associated with phosphate minerals precipitated within hardgrounds.

The general overall increase in the background U concentration above 300 mbsf, in conjunction with the spikes, however, requires a different interpretation: it is more likely related to an increase in the flux of aragonitic peloidal sediments derived from the carbonate banks. Lithologic Unit I is denoted by an abundance of peloids, as well as an associated increase in aragonite (see “Organic Geochemistry,” “Inorganic Geochemistry,” and “Lithostratigraphy” sections, this chapter). U is apparently not enriched in the aragonitic sediments at the time of deposition, as indicated by the near-zero reading in the youngest sediments of the uppermost 13 m of the section (Fig. 33). Thus, the enriched U signal probably represents a postdepositional or diagenetic phenomenon. Specifically, complexed uranyl cations carried by migrating fluids can precipitate as  $\text{UO}_2$  within the permeable sediments under reducing conditions. Intense microbial activity in the upper 300 m of the section promotes conditions ideal for this reaction to occur, as reflected by the enrichment in U seen in the gamma-ray logs.

The Lamont temperature logging tool (TLT) was incorporated into the logging tool strings for Holes 1005A and 1005C. Figure 36 shows temperature–depth profiles for two of these runs. The temperature data are not representative of thermal equilibrium with the environment because of disturbance during drilling operations associated with fluid circulation. However, these data indicate a lower geothermal gradient than normal ( $\sim 30^\circ\text{C}/\text{km}$ ). A change in the temperature gradient was observed at about 200 mbsf in both runs in Hole 1005A (Fig. 36). This change may be the result of sepiolite mud filling the hole to that level.

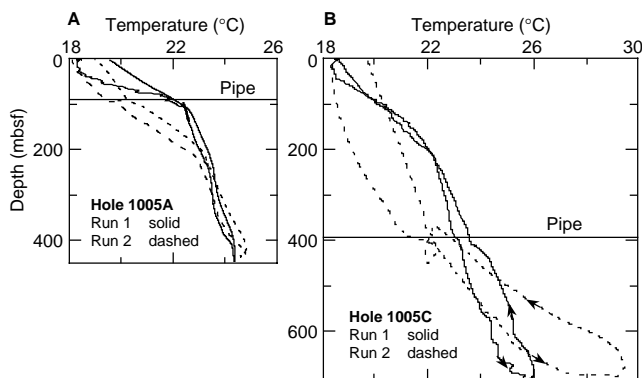


Figure 36. Temperature logs in (A) Hole 1005A and (B) Hole 1005C. Two borehole temperature runs were made in each hole, separated by about 6 hr.

## IN SITU TEMPERATURE MEASUREMENTS

### Introduction

Nine in situ temperature measurements were made at Site 1005 using two sets of Adara tools and one unit of downhole water sampler, temperature, and pressure probes (WSTP). Eight of the measurements were considered successful. One was probably made in the bottom-hole infill. The measurements and errors (Table 18) are described in the “In Situ Temperature Measurements” section of the “Explanatory Notes” and “Site 1003” chapters, this volume. The temperature at the seafloor ( $\sim 18.7^\circ\text{C}$ ) has been estimated from the mudline stops.

### Geothermal Profile

Figure 37 shows the geothermal profile obtained from the measurements. Similar to previous Leg 166 sites, the shallow portion of the geothermal profile is concave upward. Temperatures measured in the upper 32.5 mbsf show no increase or even a little decrease with depth. Below 48 mbsf, the measurements show a linear trend. As discussed in Site 1004, this type of profile suggests either a recent warming of the bottom water, a recent increase in the sedimentation rate, or a downward flow of the pore water. The sedimentation rate was greater at this site than at Site 1004, but unless a massive slumping occurred in recent years, which was not observed in the sedimentologic record (see “Lithostratigraphy” section, this chapter), changes in sedimentation alone could not explain the remarkable uniformity of the temperature of the top 30 m of the sedimentary column. Similar

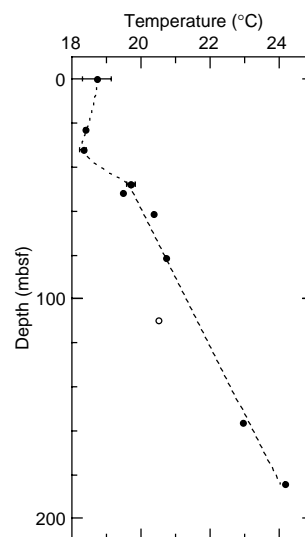


Figure 37. Geothermal profile at Site 1005. Solid circles represent the reliable temperature measurements, and open circles represent unreliable measurements.

Table 18. In situ bottom-hole sediment temperatures measured at Site 1005.

Core	Depth (mbsf)	Temperature ( $^\circ\text{C}$ )	Error ( $^\circ\text{C}$ )	Mudline ( $^\circ\text{C}$ )	Tool	Notes
166-1005B-						
3H	23.0	18.40	0.05	18.81	Adara18	
4H	32.5	18.32	0.10	18.54	Adara11	
6H	48.0	19.70	0.13	18.56	Adara18	
9X	52.0	19.47	0.01	18.55	WSTP201	
10X	61.7	20.36	0.01	18.69	WSTP201	
166-1005A-						
12X	81.6	20.72	0.01	18.66	WSTP201	
15X	109.9	20.49	0.01	18.06	WSTP201	Anomalous, poor recovery
20X	156.6	22.95	0.01	19.10	WSTP201	
23X	184.6	24.17	0.01	19.58	WSTP201	

to Site 1004, some type of water circulation in the sediments is possible.

### Heat Flow

The lower linear part (below 48 mbsf) of the geothermal profile at Site 1005 gives a geothermal gradient of 32.3°C/km. The average of the thermal conductivities measured in the upper 200 mbsf is 1.07 W/(m·K), yielding a heat flow value of 34.6 mW/m<sup>2</sup>. This heat flow value is at least 10% lower than values at Sites 1003 or 1004.

## SEISMIC STRATIGRAPHY

### Introduction

The Holocene to middle Miocene section drilled at Site 1005 comprises nine seismic sequences (*a–k*). The seismic facies of the individual sequences is similar to the ones observed at Site 1003 (see “Seismic Stratigraphy” section, “Site 1003” chapter, this volume). However, in this more proximal position on the upper slope, the prograding sequences are thicker, and downcutting unconformities are observed on three sequence boundaries (A, C, and E) (Fig. 38), indicating that this site experienced erosion during the formation of the sequence boundaries (Fig. 38).

### Time-Depth Conversion

Site 1005 is located upslope of Sites 1003 and 1004 at a distance of 1.15 km from the bank margin. Preliminary depth estimates for the seismic reflections at this site prior to drilling were made with the ve-

locity information from Sites 1003 and 1004. The downhole logging suite at this site included a vertical seismic profile (VSP), with several check-shots with the single-channel well seismic tool (WST), that provides an accurate time-depth conversion (Fig. 39). The VSP was shot using a 120-in<sup>3</sup> air gun that was located portside at an offset of 48.5 m from the hole. The gun was fired at a water depth of 6 m, with a hydrophone placed immediately below, to record the firing time of the air gun. Despite the partly enlarged borehole (see “Downhole Logging” section, this chapter), it was possible to place the VSP tool within Hole 1005A at 10 stations, down to 408 mbsf. A second check-shot survey in Hole 1005C resulted in an additional six stations to a maximum depth of 538 mbsf (Table 19). The traveltimes of the signal from the airgun to the total 16 stations were corrected for offset, water depth, gun depth, and two-way distance, so that a sub-bottom time-depth conversion could be established. The overlap of these two runs showed excellent agreement. Figure 39 displays the depth-traveltime curve along with the pre-drilling predictions, the integrated sonic log velocities, and the pre-cruise estimates. The prediction, based on core measured velocity data at Sites 1003 and 1004, lies very closely to the VSP data points. The largest deviation of +20 m occurs at a depth of 400 mbsf, while above and below the two curves are similar. This offset can be partly explained by (1) the thicker Pleistocene section at Site 1003, which places all pre-Pleistocene units deeper in the hole, and (2) the discrete steps chosen for the velocity prediction, compared to the closer spaced VSP stations. Interestingly, the integrated sonic data from the SDT tool (see “Explanatory Notes” chapter, this volume) produce higher velocities than the VSP, resulting in an error of up to –50 m in the deeper part of the site. The comparison of the VSP interval velocities with the sonic log velocities (Fig. 38) shows that in zones of variable lithologies, where

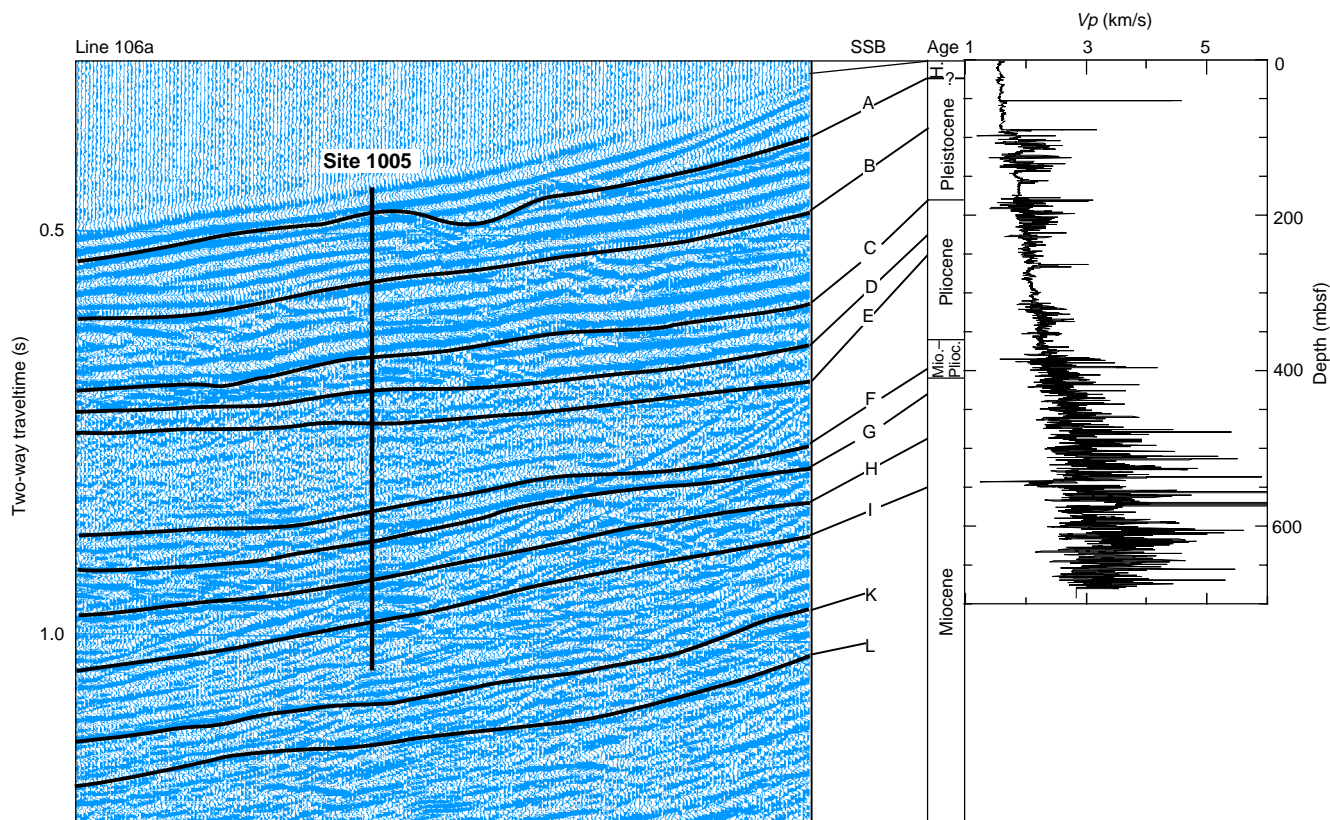


Figure 38. A portion of seismic Line 106a showing the location of Site 1005. The major sequence boundaries have been traced and converted to depth. Origin of seismic reflections can be identified in the displayed sonic log.

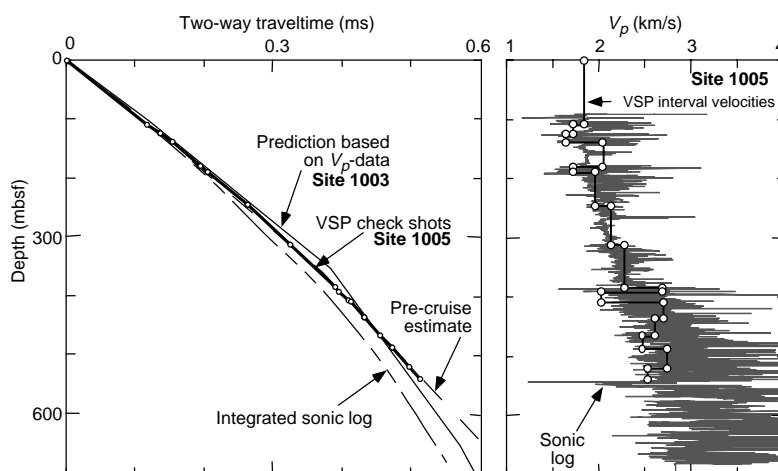


Figure 39. Left side: time-depth curves for Site 1005. VSP check shots are displayed in thick line, and stations are marked by open circles. The measured VSP values have been compared with the integrated sonic log, predictions based on nearby Site 1003 and pre-cruise estimates. Right side: the interval velocities derived from traveltimes between the 16 VSP stations are displayed overlying the sonic log velocities (for discussion see text).

Table 19. Check-shot stations of VSP survey in Holes 1005A and 1005C.

Check-shot station	Depth (mbsf)	TWT below seafloor (msbsf)	TWT below sea level (msbsl)
Seafloor	0	0	467.6
166-1005A-			
1	107	116.9	584.5
2	123	135.6	603.2
3	137	152.7	620.3
4	178	193	660.6
5	188	204.7	672.3
6	244	262	729.6
7	310	324.3	791.9
8	383	388.5	856.1
9	390	393.7	861.3
10	408	411.6	879.2
166-1005C-			
1	405	407.2	874.8
2	434	430.9	898.5
3	464	454	921.6
4	485	471	938.6
5	519	495.9	963.5
6	538	510.9	978.5

high- and low-velocity layers alternate (lower Pleistocene, upper Pliocene and Miocene sections), the integrated sonic log overestimates formation velocity. This might indicate that the thin-bedded alternations of lithologies with very different physical properties can decrease the average formation velocity. In more homogenous zones (lower Pliocene), the VSP interval velocities closely match the sonic log. The pre-cruise velocity estimate, based in the shallow zones on seismic stacking velocities, and in the deeper zones on expected lithologies and their known properties from the Bahamas Drilling Project, shows an excellent match with the VSP data. The continuation of those estimates at greater depths, however, are likely to result in a larger offset.

The comparison of these approaches shows that the different methods result in time-depth conversions with variable accuracy. Integrated sonic log velocities and estimates from seismic stacking velocity combined with regional data can result in a considerable offset, especially at greater depths, where velocity differences can add up. On the other hand, predictions based on discrete velocity measurements from cores in nearby sites seems to be a good method to produce reliable velocity downhole trends. However, the VSP survey provides the single most reliable method to precisely tie the seismic reflections to log and core data.

## Holocene-Pleistocene Sequences

During the Pleistocene and Holocene, the prograding sequences display steep inclined clinoform angles with a pronounced platform margin and downlapping wedges in the slope section. The first Sequence *a* is probably of Holocene age based on a nearby dated piston core that penetrated the same sequence (Wilber et al., 1990). It consists of peloidal wackestone with some coarser bioclasts. Its basal sequence boundary (SSB A) is placed at the reflection at 25 milliseconds below seafloor (msbsf [TWT]), which correlates to 20 m sediment thickness (Fig. 40). This depth might coincide in the cores with the first encountered hard layer at 15 mbsf, which resulted in a partial stroke of the APC core. The blackened, bored layer consisted of lithoclasts and cemented bioclasts. Its upper surface is characterized by a sharp downhole increase in natural gamma ray and velocity and by an abrupt decrease in aragonite content, all of which indicate longer exposure on the seafloor (Fig. 41). The underlying Sequence *b* is considerably thicker (75 m) than at Site 1003, where it was only 17 m thick. It consists of peloidal wackestones with layers of packstones and grainstones that are interpreted as turbidites (see "Lithostratigraphy" section, this chapter). SSB B at 100 msbsf (TWT) or 90 mbsf coincides with another black hard layer that was partially recovered in a limestone nodule overlain by a brownish packstone. The lithologic boundary between Subunits IA and IB was placed on top of the lower core where partially lithified bioclastic packstones start to form a cyclic sedimentation pattern. At SSB B, the mineralogy displays an abrupt increase in high-magnesium calcite (see "Inorganic Geochemistry" section, this chapter). The age of SSB B is calculated as 0.6 Ma based on sedimentation rates of the upper Pleistocene section. The oldest Pleistocene sequence, Sequence *c*, extends down to 200 msbsf (TWT) or 185 mbsf, which corresponds to the depth at which the sonic log images an abrupt increase of  $V_p$  from  $<2$  to  $>3$  km/s. Its lower boundary, SSB C, is dated as 1.6 Ma, which lies closely to the Pliocene/Pleistocene boundary and to an interval of low sedimentation (Table 20). Pieces of a breccia horizon that contain lithoclasts from the reef and fore-reef environment occur at this depth (Fig. 41) in Section 166-1005A-23X-CC (184.6–194 mbsf). The reduced sedimentation rate during the time of the platform erosion indicates that the platform was not producing sediment. Therefore, the platform was probably exposed at the time the sequence boundary was formed. This interpretation is supported by the sharp decrease of aragonite across SSB C, which also indicates the absence of newly produced platform sediment or the increased dissolution of metastable arago-

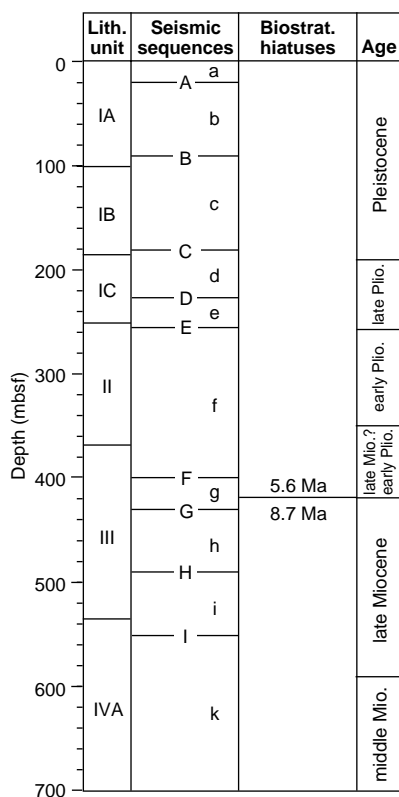


Figure 40. Correlation chart of lithologic units, sequence boundaries, and biostratigraphic ages.

nite due to the prolonged exposure to reactive waters close to the sea-floor.

### Pliocene Sequences

The two upper Pliocene sequences are relatively thin at Site 1005. Sequence *d* is 45 m thick and extends down to 240 mbsf (TWT) or 225 mbsf, whereas Sequence *e* is 30 m thick and has its basal SSB at 270 mbsf (TWT) or 255 mbsf. Both sequences fall into times of reduced sedimentation rates of approximately 2 cm/k.y., a normal pelagic sedimentation rate. The benthic fauna is depauperate in both sequences (see “Biostratigraphy” section, this chapter). Both characteristics give evidence of a reduced input of platform-derived sediment, probably as a result of platform exposure and a generally lower sea level throughout most of late Pliocene (see “Biostratigraphy” section, this chapter). Lithologically, these two sequences are also similar. They consist of partially lithified mudstones that are slightly dolomitized. Pelagic foraminifers are the dominant faunal element with pellets and aragonite needles as minor components. Laminated clay-rich intervals also contain diatoms and radiolarians. This sediment composition again indicates only minor platform-derived input. The sequence boundary between the two sequences falls into a zone with no recovery, but it correlates with a change of the log pattern. Velocity, porosity, and resistivity variations decrease across SSB D and gamma ray increases just below the boundary (see “Downhole Logging” section, this chapter). SSB E is also not expressed by a major sedimentologic change, but by a rather thin package of biowackestone within the unlithified mudstone. The logs, however, mark the boundary with sharp spikes in the gamma-ray signal, resistivity, and velocity logs. SSB E coincides biostratigraphically with the early/late Pliocene boundary and is dated as being approximately 3.6 Ma in age. The underlying lower Pliocene Sequence *f* is a thick unit that consists mostly of wackestones. The homogenous character of the sediment is also reflected in the relatively flat curves on the logs and

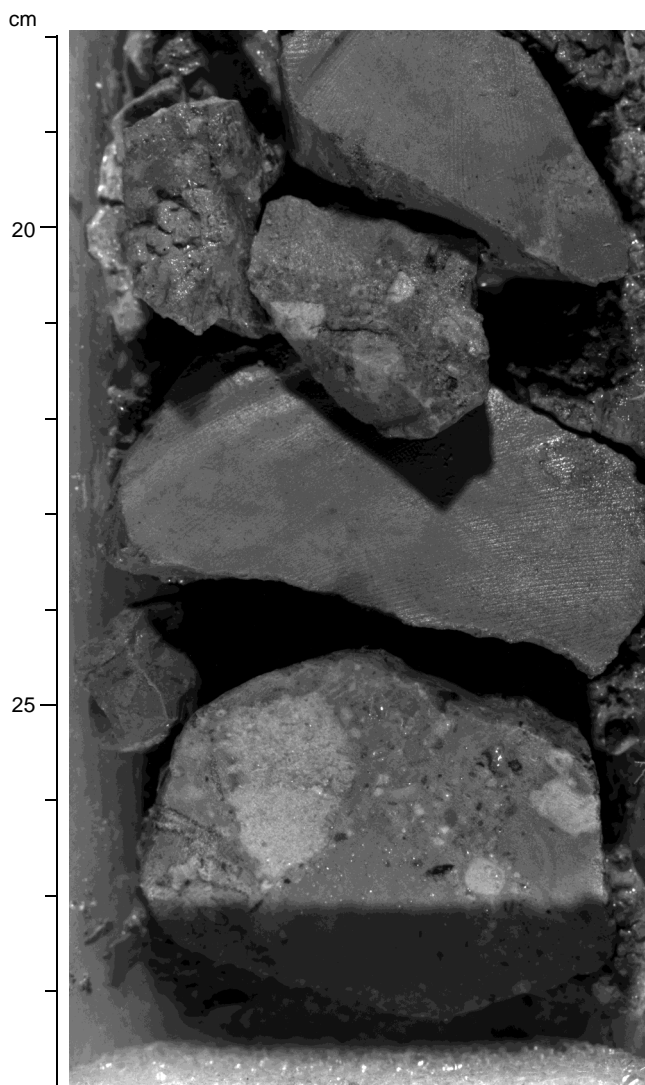


Figure 41. Core photograph of brecciated horizon, which correlates with SSB C at the Pliocene/Pleistocene boundary. The components in the breccia consist of platform-derived lithoclasts mostly from a reef and fore-reef environment. The well-cemented horizon is surrounded by partially lithified wackestones to mudstones (interval 166-1005A-23X-CC, 18–29 cm).

in the physical properties. The basal SSB F is placed at 400 mbsf (TWT) or 400 mbsf at a level that does not show a lithologic change. In the logs a major change occurs about 15 m higher where velocity, resistivity, density, and gamma-ray values increase. The age of boundary cannot be determined accurately because of the poor preservation of age diagnostic foraminifers. The age could be either latest Miocene or early Pliocene (see “Biostratigraphy” section, this chapter).

Considering the limits of resolution, all of the six SSBs (A–F) coincide in the logs with distinct changes in resistivity, porosity, and velocity. In particular, sonic velocity shows a rhythmic pattern at all of these horizons with a sudden uphole decrease across the SSB and a gradual upward increase toward the top of the sequence.

### Miocene Sequences

Four Miocene sequences (*g*, *h*, *i*, and *k*) were drilled at Site 1005, but the sequence boundary of Sequence *k* was not reached at TD of 700 mbsf (Figs. 38, 40).

**Table 20. Time-depth conversion and tentative age assignments of seismic sequence boundaries.**

Seismic sequence boundary	TWT below seafloor (msbsf)	Depth (msbsf)	Nannofossil zone	Foraminifer zone	Age	Age* (Ma)
A	25	20	NN21	N23	Holocene/Pleistocene	0.1
B	100	90	NN19	N22	Pleistocene	0.6
C	200	185	NN19	N22	Pleistocene/Pliocene	1.6
D	240	225	NN18/16	N20/21	late Pliocene	2.9
E	270	255	NN18/16	N19/18	early/late Pliocene	3.6
F	400	400	?	?	Messinian?	?
G	430	430	NN10	N16	late Miocene	6.2–8.8
H	475	485	NN9	N16	late Miocene	9.3
I	520	550	NN7	N14	middle Miocene	10.2

Note: \* = ages are preliminary and based on shipboard biostratigraphy (see “Biostratigraphy” section, “Explanatory Notes” chapter, this volume).

Sequence *g* is only 30 m thick. Its SSB is placed at 430 msbsf (TWT) or 430 mbsf, which correlates to the uppermost Miocene at 424 mbsf with a hiatus of at least 3 m.y. (8.8–6.2 Ma). In the cores, this hiatus is not evident, but the mineralogy records it in a large amount of insoluble residues at this interval. In the logging data, this SSB is recognized by an increase of variations in resistivity, porosity, and density. Sequence *h* is of late Miocene age and extends to a depth of 475 msbsf (TWT) or 485 mbsf. It comprises the middle part of lithologic Unit III, which consists of a monotonous succession of partially dolomitized wackestones. Based on the extrapolation of diagnostic age dates and the rate of the sedimentation, the age of SSB H is approximately 9.3 Ma. The underlying Sequence *i* has a lithologic content similar to Sequence *h*. The basal SSB I is placed at the reflection at 520 msbsf (TWT) or 550 mbsf, which lies close to the base of lithologic Unit III at 534.3 mbsf. This coincides with a mudstone interval, suggesting reduced platform input. In the logging data, it is manifested by a sharp decrease of porosity, velocity, resistivity, and density values. The boundary coincides with a thin zone of high dolomite content (45%) and an increased amount of insoluble residues. The age is biostratigraphically determined as 10.2 Ma. SSB I correlates in the logs of both Sites 1003 and 1005 to the upper boundary of a high-velocity package. At Site 1005, only the upper part of Sequence *k* was drilled. Lithologically, this sequence is also similar to Sequences *h* and *i*. All of these Miocene sequences display an absence of thick redeposited carbonates despite the fact that they are the most proximal site of the transect. Slight changes in mineralogy and composition, in particular the increase of clay layers, provide evidence that the sequence boundaries were formed during sea-level lowstands when platform-derived input was reduced.

## SUMMARY AND CONCLUSIONS

Site 1005, the most proximal site drilled during Leg 166, is positioned approximately 1150 m from the modern platform edge in 350 m of water depth. The thick, upper Neogene section at this site yielded the data that were needed to achieve the objectives of this site. For the sea-level objectives, the expanded Quaternary and upper Pliocene section provides the high-resolution record of climate and sea-level changes during this time period. Facies of eight seismic sequences were recovered that provide information about the lithologic content of the proximal portions of carbonates sequences in conjunction with the logging data. Foraminifer and nannofossil biostratigraphy yielded precise ages of the lithologic units and SSBs. Interstitial water chemistry together with in situ temperature measurements give additional evidence for fluid flow through the margin of GBB. A check-shot survey (VSP) was performed after logging that enables the correlation of the cores to the seismic data.

### Facies of the Upper Slope

A 700-m-thick Holocene to upper middle Miocene section was recovered at Site 1005. The sedimentary succession consists of a peri-

platform sediments with a carbonate content between 72% and 99%. The section is composed of unlithified to partially lithified wackestones and slightly coarser grained intervals consisting of packstones and grainstones. Compositional variations document pulses of bank-derived sediments that are reflected in increased sedimentation rates with intervals of more pelagic sediments. The sediments of Site 1005 document that the upper slope environment of the prograding margin of GBB is dominated by fine-grained sediments. The scarce occurrence of mass gravity flow deposits at this site, compared to Site 1003, indicate that these flows bypassed the upper slope and were deposited farther basinward, in spite of the fact that the slope angle at this site is only approximately 5°. The bypass nature of the slope within these relatively steep clinofolds is surprising, as bypass margins are generally not considered to be progradational (Schlager and Ginsburg, 1981). Obviously, fine-grained mudstones to wackestones can form thick bulges of prograding clinofolds without major contributions from gravity flow deposits.

The log data correlate well with the sedimentary succession and can be used to fill in gaps in low-recovery zones. The strong cyclic nature of the data is the most notable feature recorded in all the logs, specifically from 700 to 385 mbsf (middle Miocene–lowermost Pliocene) and from 260 to 90 mbsf (upper Pliocene–Pleistocene). The intervening section from 385 to 260 mbsf (lower Pliocene) is marked by an apparent diminution of the intensity of the cycles, as reflected in particular by the monotony of the resistivity curve. Between 260 and 90 mbsf, the sharp increases in gamma-ray intensity correlates with increased density, resistivity, velocity, and decreased porosity. This association is indicative of an increase in induration of sediment deposited during periods with a reduced sedimentation rate, which led to hardground formation. The logs clearly display that the sedimentation pattern was punctuated by periods of decreased sediment input marked by the formation of better cemented layers.

### Sedimentary Record of the Sea-Level Changes

In the sediments at Site 1005, sea-level changes are recorded in three different ways. Variations in the composition of the mudstones–wackestones give a record of a high-frequency cyclicality of platform shedding alternating with more pelagic sedimentation. Alternating high and low sedimentation rates reflect a long-term pattern of bank flooding with concomitant shedding to the slope, periods of exposed banks, a shutdown of shallow-water carbonate production, and largely pelagic sedimentation. The pulses of bank-derived material coincide with the prograding pulses that are seen on the seismic data as sequences, which, with their geometries, indicate base-level lowerings as a result of sea-level falls.

Cyclic sedimentation is best developed in the upper Pleistocene lithologic Subunit IA and in the Miocene Units III and IV. The upper Pleistocene cycles display the characteristics of periplatform aragonite cycles described from other deep-water areas adjacent to GBB (Droxler and Schlager, 1985; Reymer et al., 1988; Grammer and Ginsburg, 1992). In these cycles, an increase in aragonite content coincides with sea-level highstands (Droxler et al., 1988). Higher ara-

gonite content is reflected in higher color reflectance. Several thin turbidite beds are intercalated in these high aragonite intervals, documenting the highstand shedding of these turbidites. The cycles are also separated by a layer of cemented packstones and/or floatstones that indicate redeposition of platform material during sea-level lowstands.

The Miocene cycles display decimeter-thick alternations of gray to light gray well-cemented biowackestones and less-cemented gray to olive-gray wackestones with compacted burrows. The boundary between the two lithologies is generally sharp. The darker intervals carry a higher amount of pelagic foraminifers and some clay, whereas the lighter intervals have more neritic material. Again, the neritic input is taken as indication for platform flooding, such as sea-level highstands, whereas increased pelagic input and current-transported clay occurs during sea-level lowstands. We observed a trend of increasing thickness of the gray lithologies of the cycles within Unit IV, a sharp drop at the base of Unit IV, followed again by a gradual increase in Unit III. These changes are interpreted as two prograding pulses in these units during the middle and late Miocene.

Variations in sedimentation rates reflect the export of bank-derived material to the upper slope. The upper Pleistocene sedimentation rate is high (15 cm/k.y.), whereas it is reduced to approximately 2 cm/k.y. during the upper Pliocene and lower Pleistocene (3.5–1.2 Ma), which is characteristic of normal pelagic carbonate sedimentation. The lower Pliocene sedimentation rate was high (10 cm/k.y.). Obviously, the leeward side of GBB received high amounts of platform-derived material during this period. A hiatus that spans nannofossil Zone NN11 (5.6–8.6 Ma) was probably caused by the combination of large-scale slope erosion associated with lower sea levels and increased current activity during a period with little to no pelagic sedimentation. An expanded lower upper Miocene section was drilled below the hiatus. The high sedimentation rate of 11 cm/k.y. during nannofossil Zones NN9 and NN10 reflects another period of platform shedding. There is minimal input from the platform during nannofossil Zone NN8, but another high input occurred during the late middle Miocene, which yielded sedimentation rates of 13 cm/k.y. The sedimentation rates are in concert with long-term sea-level changes. The two largest known sea-level falls straddle the middle/upper Miocene and lower/upper Pliocene boundaries and are clearly expressed in the sedimentation rates at Site 1005.

The diversity and abundance of platform-derived benthic foraminifers provide an additional record of platform progradation and flooding events. In much of the Pleistocene section, there is a diverse and abundant benthic fauna, whereas only a depauperate assemblage is found in the upper Pliocene. In the lower Pliocene and the Miocene succession, a low-diversity shallow-water assemblage is diluted in the monotonous sediments.

Seismic sequences provide a third record of sea-level changes on the western GBB. Nine seismic sequences (*a–k*) were penetrated at Site 1005. Changes of rates in sedimentation coincide with SSBs. For example, SSB G coincides with a hiatus in the upper Miocene, and three other boundaries correlate to changes in sedimentation rates. There is also a good correlation of the SSBs with the changes in mineralogy. In the Pleistocene section, the sequence boundaries coincide with low contents in HMC and aragonite, which record reduced platform-derived sediment input. In the Pliocene and Miocene section, the boundaries are either associated with high amounts of insoluble residues or peaks of dolomite. The overall monotonous sediments do not yield dramatic facies changes at sequence boundaries. They generally correlate to mudstone intervals that contain a larger amount of nannofossil ooze, indicating reduced platform-derived input as a result of platform exposure.

Three Holocene–Pleistocene sequences can be distinguished on the seismic lines. Their sequence boundaries all coincide with cemented layers within unlithified to partially lithified strata. Blackened lithoclasts and cemented bioclasts from the platform top give evidence that these layers formed during sea-level lowstands. Their

composition is similar to Pleistocene–Holocene surfaces on the uppermost slope surrounding GBB above the Holocene onlapping wedge (Grammer et al., 1993). Sequence *a* probably comprises the Holocene onlapping wedge with its base at 15 mbsf. SSB A is approximately 0.1 Ma based on the extrapolation of the sedimentation rate given by age-diagnostic fossils. The underlying Sequence *b* is 75 m thick and its age is about 0.6 Ma. The third Pleistocene sequence, *c*, extends to a depth of 180 mbsf. Its basal SSB correlates with the sharp decrease of the rate of sedimentation at 1.8 Ma and lithologically with a breccia horizon. The two Pliocene sequences, Sequences *d* and *e*, are relatively thin units of partially lithified mudstones and wackestones that are slightly dolomitized. SSB D was not recovered in the core, but is clearly visible on the logs. The age assignment has some uncertainty; it is tentatively determined as 2.9 Ma. SSB E is lithologically expressed only by a thin package of biowackestone within mudstone, but again with a clear increase in the values of most parameters in the log data. It is dated as 3.6 Ma, which is the early/late Pliocene boundary. As at Site 1003, Sequence *f* is not datable as a result of the absence of age-diagnostic fossils. It could be either late Miocene or early Pliocene in age. The underlying Sequences (*g*, *h*, *i*, and *k*) are of Miocene age and correspond to lithologic Units III and IV, which consist of the cyclic alternation of cemented and compressed wackestones. Sequence *g* is only 30 m thick. Its SSB is placed at the seismic reflection at 430 mbsf, which coincides with the biostratigraphic hiatus at 424 mbsf. This hiatus lasted from 8.7 to 5.6 Ma (see “Biostratigraphy” section, this chapter). A hiatus of similar duration was also found farther downslope at Site 1003. In the shallow-water sites Unda and Clino, the hiatus is slightly smaller as more of the upper Miocene section is preserved. The next older SSB H coincides with the lithologic unit boundary III/IV, which is placed in a mudstone above a horizon with thin turbidites. This pelagic interval indicates reduced platform sedimentation and a sea-level lowstand. The age of this boundary is 9.4 Ma. Sequence *i* corresponds to the upper part of Unit IV and consists entirely of cyclic bioturbated wackestones. Lithologically, SSB I (11.3 Ma) at 600 mbsf, is not discernible in the core, but is well expressed on the gamma log with a sharp increase in the signal. The bottom 100 m of the core at Site 1005 corresponds to Sequence *m*. SSB M was not reached at TD. The biostratigraphic data from Site 1005 confirm the ages that were carried along seismic reflections from Site 1003 to Site 1005 (see Fig. 1, “Site 1003” chapter, this volume).

In summary, the sedimentary, mineralogical, geophysical, and stratigraphic data give the record of a sedimentary system characterized by variable input of platform-derived sediment that is most probably caused by changing sea level. These input fluctuations occur on several levels. A high-frequency cyclic alternation is seen in the sedimentary and the log data, whereas the sedimentation rates monitor the long-term changes. The seismic sequences reflect these long-term changes and in addition give the record on an intermediate scale. Site 1005 yielded abundant biostratigraphic markers that allow for the precise age dating of the sequence boundaries. For a test of the sequence stratigraphic concept, the most important result arising from drilling at this site is that the ages can be carried along the seismic reflection horizons to Site 1003, where they fall on the same stratigraphic level. This consistency documents that seismic reflections are also time lines and have a chronostratigraphic significance. In these carbonate slope sediments, sediment composition is largely controlled by the input of platform-derived sediment that is related to sea-level changes. Early diagenetic alteration is strongest during reduced sedimentation rates when the platform is exposed. Both facies and diagenesis are related to sea level that leaves its expression in physical properties and in the seismic sequences.

### Indications for Fluid Flow

The interstitial water chemistry at Site 1005 yielded interesting geochemical profiles that can be subdivided into four zones. As ob-

served at Sites 1003 and 1004, pore-water chemistry profiles over the upper 40 m display normal seawater concentrations of all constituents. This upper 40-m zone probably experiences pervasive flushing of seawater that prevents diffusional gradients from developing between the overlying seawater and the underlying more saline fluid. Zone 2 extends to a depth of 190 mbsf, and is characterized by a sharp change in the gradient of all major and minor pore-water constituents. The best evidence for active flow is given by the Cl<sup>-</sup> profile. The Cl<sup>-</sup> concentration displays a peak between 94 and 122 mbsf. The high salinity in this zone could be indicative of an intrusive saline wedge that is derived from the platform surface. Alternatively, the water below the wedge could represent a lateral intrusion of less saline bottom water into the sediments. High rates of microbial sulfate reduction within this zone reduce the sulfate concentration to zero and give all major ion profiles an anomalous appearance. In the two underlying zones, most constituents display a steady change with increasing depth. Increased salinity below 400 mbsf suggests an influence of deep-seated saline fluids, similar to Site 1003. A shift in many profiles marks the boundary between geochemical Zones 3 and 4 at approximately 520 mbsf. At this time it is not known to what extent the shifts are influenced by diagenetic alterations within lithologic units, or lateral fluid movement within sequence boundaries.

In summary, the geochemical profiles of Site 1005, in conjunction with Sites 1003 and 1004, provide further evidence for fluid flow through the slopes of GBB. The consistency of changes in geochemical gradients at distinct stratigraphic horizons indicates that the flow has a horizontal component in the upper 50 m of sediment superimposed on the vertical diffusion controlled by gradients in the lower portions of the sedimentary column. Changes in permeability associated with sequence boundaries probably impart considerable anisotropy to the sediments causing diffusion and water movement laterally along sequence boundaries.

#### REFERENCES

- Baker, P.A., and Bloomer, S.H., 1988. The origin of celestite in deep-sea carbonate sediments. *Geochim. Cosmochim. Acta*, 52:335–339.
- Baker, P.A., and Kastner, M., 1981. Constraints on the formation of sedimentary dolomite. *Science*, 213:215–216.
- Claypool, G.E., and Kvenvolden, K.A., 1983. Methane and other hydrocarbon gases in marine sediment. *Annu. Rev. Earth Planet. Sci.*, 11:299–327.
- Droxler, A.W., Bruce, C.H., Sager, W.W., and Watkins, D.H., 1988. Pliocene–Pleistocene variations in aragonite content and planktonic oxygen-isotope record in Bahamian periplatform ooze, Hole 633A. In Austin Jr., J.A., Schlager, W., Palmer, A.A., et al. (Eds.). *Proc. ODP, Sci. Results*, 101, College Station, TX (Ocean Drilling Program): 221–244.
- Droxler, A.W., and Schlager, W., 1985. Glacial versus interglacial sedimentation rates and turbidite frequency in the Bahamas. *Geology*, 13:799–802.
- Droxler, A.W., and Schlager, W., and Whallon, C.C., 1983. Quaternary aragonite cycles and oxygen-isotope record in Bahamian carbonate ooze. *Geology*, 11:799–802.
- Eberli, G.P., and Ginsburg, R.N., 1989. Cenozoic progradation of NW Great Bahama Bank: a record of lateral platform growth and sea fluctuations. In Crevello, P.D., et al. (Eds.), *Controls on Carbonate Platform and Basin Evolution*. Spec. Publ.—Soc. Econ. Paleontol. Mineral., 44:339–355.
- Grammer, G.M., and Ginsburg, R.N., 1992. Highstand versus lowstand deposition on carbonate platform margins: insight from Quaternary fore-slopes in the Bahamas. *Mar. Geol.*, 103:125–136.
- Grammer, G.M., Ginsburg, R.N., and Harris, P.M., 1993. Timing of deposition, diagenesis, and failure of steep carbonate slopes in response to a high-amplitude/high-frequency fluctuation in sea level, Tongue of the Ocean, Bahamas. In Loucks, R.G., and Sarg, J.F. (Eds.), *Carbonate Sequence Stratigraphy: Recent Developments and Applications*. AAPG Mem., 57:107–131.
- Haak, A.B., and Schlager, W., 1989. Compositional variations in calciturbidites due to sea-level fluctuations, Late Quaternary, Bahamas. *Geol. Rundsch.*, 78:477–486.
- Haddad, G.A., Droxler, A.W., Kroon, D., and Müller, D.W., 1993. Quaternary CaCO<sub>3</sub> input and preservation within Antarctic intermediate water: mineralogic and isotopic results from Holes 818B and 817A, Townsville Trough (northeastern Australia margin). In McKenzie, J.A., Davies, P.J., Palmer-Julson, A., et al., *Proc. ODP, Sci. Results*, 133: College Station, TX (Ocean Drilling Program), 203–233.
- Haq, B.U., Hardenbol, J., and Vail, P.R., 1987. Chronology of fluctuating sea levels since the Triassic. *Science*, 235:1156–1167.
- Katz, A., and Matthews, A., 1977. The dolomitization of CaCO<sub>3</sub>: an experimental study at 252–295°C. *Geochim. Cosmochim. Acta*, 36:481–496.
- Kier, J.S., and Pilkey, O.H., 1971. The influence of sea level changes on sediment carbonate mineralogy, Tongue of the Ocean, Bahamas. *Mar. Geol.*, 11:189–200.
- Loughnan, F.C., 1969. *Chemical Weathering of Siliclastic Minerals*: New York (Elsevier).
- Mackin, J.E., and Aller, R.C., 1984. Ammonium adsorption in marine sediments. *Limnol. Oceanogr.*, 29:250–257.
- Maher, B.A., 1988. Magnetic properties of some synthetic sub-micron magnetites. *Geophys. J. R. Astron. Soc.*, 94:83–96.
- Melim, L.A., Swart, P.K., and Maliva, R.G., 1997. Meteoric and marine burial diagenesis, Great Bahama Bank In Ginsburg, R.N. (Ed.), *The Bahamas Drilling Project*. Soc. Econ. Paleontol. Mineral. Contrib. Sedimentol.
- Reid, R.P., 1987. Nonskeletal peloidal precipitates in Upper Triassic reefs, Yukon Territory (Canada). *J. Sedimentol. Petrol.*, 57:893–900.
- Reymer, J.J.G., Schlager, W., and Droxler, A.W., 1988. Site 632: Pliocene–Pleistocene sedimentation cycles in a Bahamian basin. In Austin, J.A., Jr., Schlager, W., et al., *Proc. ODP, Sci. Results*, 101: College Station, TX (Ocean Drilling Program), 213–220.
- Schlager, W., and Ginsburg, R.N., 1981. Bahama carbonate platforms: the deep and the past. *Mar. Geol.*, 44:1–24.
- Schlager, W., Reijmer, J., and Droxler, A.W., 1994. Highstand shedding of carbonate platforms, *J. Sediment. Res.*, B64:270–281.
- Serra, O., 1986. *Fundamentals of Well-Log Interpretation* (Vol. 2): *The Interpretation of Logging Data*. Dev. Pet. Sci., 15B.
- Sheridan, R.E., 1974. Atlantic continental margin of North America. In Burk, C.D., and Drake, C.L. (Eds.), *Geology of Continental Margins*: New York (Springer Verlag), 391–407.
- Shipboard Scientific Party, 1991. Explanatory notes. In Davies, P.J., McKenzie, J.A., Palmer-Julson, A., et al., *Proc. ODP, Init. Repts.*, 133 (Pt. 1): College Station, TX (Ocean Drilling Program), 31–58.
- Swart, P.K., and Guzikowski, M., 1988. Interstitial-water chemistry and diagenesis of periplatform sediments from the Bahamas, ODP Leg 101. In Austin, J.A., Jr., Schlager, W., Palmer, A.A., et al., *Proc. ODP, Sci. Results*, 101: College Station, TX (Ocean Drilling Program), 363–380.
- van Morkhoven, F.P.C.M., Berggren, W.A., and Edwards, A.S., 1986. Cenozoic cosmopolitan deep-water benthic foraminifera. *Bull. Cent. Rech. Explor.-Prod. Elf-Aquitaine*, Mem. 11.
- Wilber, R.J., Milliman, J.D., and Halley, R.B., 1990. Accumulation of bank-top sediment on the western slope of Great Bahama Bank: rapid progradation of a carbonate megabank. *Geology*, 18:970–974.

Ms 166IR-108

**NOTE: Core description forms (“barrel sheets”) and core photographs can be found in Section 3, beginning on page 377. Forms containing smear slides can be found in Section 4, beginning on page 831. Thin sections can be found in Section 5, beginning on page 849. See the Table of Contents for material contained on CD-ROM.**

## SHORE-BASED LOG PROCESSING

## Hole 1005A

**Bottom felt:** 362 mbrf  
**Total penetration:** 462.4 mbsf  
**Total core recovered:** 61%

## Logging Runs

**Logging string 1:** DIT/SDT/GPIT/NGT  
**Logging string 2:** HLDS/APS/HNGS  
**Logging string 3:** WST

Wireline heave compensator was used to counter ship heave.

## Bottom-Hole Assembly

The following bottom-hole assembly depths are as they appear on the logs after differential depth shift (see "Depth shift" section) and depth shift to the seafloor. As such, there might be a discrepancy with the original depths given by the drillers on board. Possible reasons for depth discrepancies are ship heave, use of wireline heave compensator, and drill string and/or wireline stretch.

DIT/SDT/GPIT/NGT: Bottom-hole assembly at ~85.5 mbsf.

APS/HLDS/HNGS: Bottom-hole assembly at ~86 mbsf.

## Processing

**Depth shift:** Original logs have been interactively depth shifted with reference to HNGS from APS/HLDS/HNGS run and to the seafloor (~363 m). This amount differs 1.0 m from the "bottom felt" depth given by the drillers and is based on correlation between logs and lithologic markers seen on core.

**Gamma-ray environmental corrections:** Corrections for borehole size and type of drilling fluid were performed on the NGT data from the DIT/SDT/GPIT/NGT tool string. HNGS data from the APS/HLDS/HNGS tool string were corrected in real-time during the recording.

**Acoustic data processing:** The array sonic tool was operated in standard depth-derived, borehole compensated, long spacing (8–10 and 10–12 ft) and short spacing (3–5 and 5–7 ft) mode. The sonic logs from the long spacing mode have been processed to eliminate some of the noise and cycle skipping experienced during the recording.

## Quality Control

Data recorded through bottom-hole assembly such as the gamma ray data above 86 mbsf should be used only qualitatively because of the attenuation on the incoming signal. Invalid gamma ray spikes were recorded at 81–86 mbsf during the DIT/SDT/GPIT/NGT run.

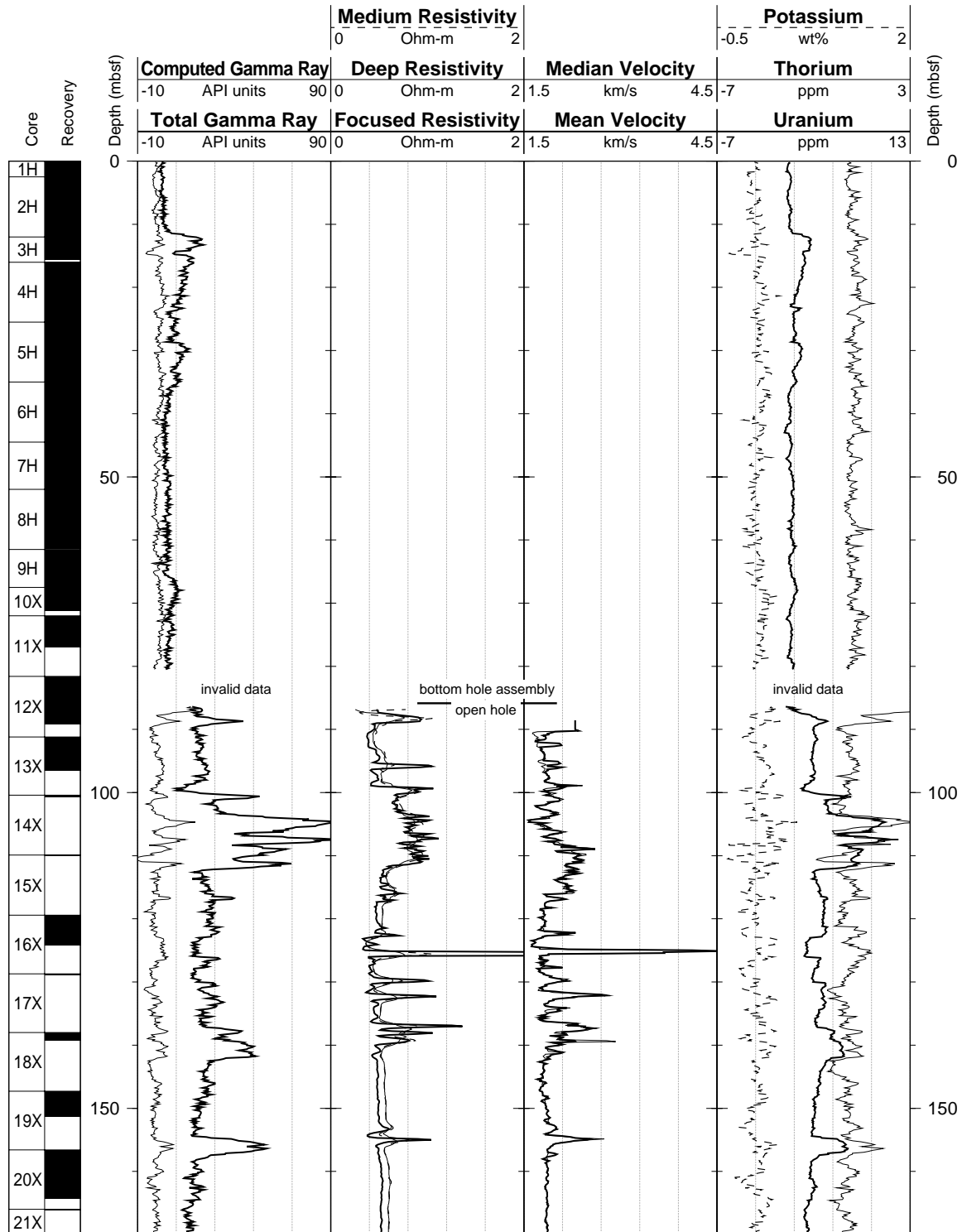
Hole diameter was recorded by the hydraulic caliper on the HLDS tool (LCAL).

Details of standard shore-based processing procedures are found in the "Explanatory Notes" chapter, this volume. For further information about the logs, please contact:

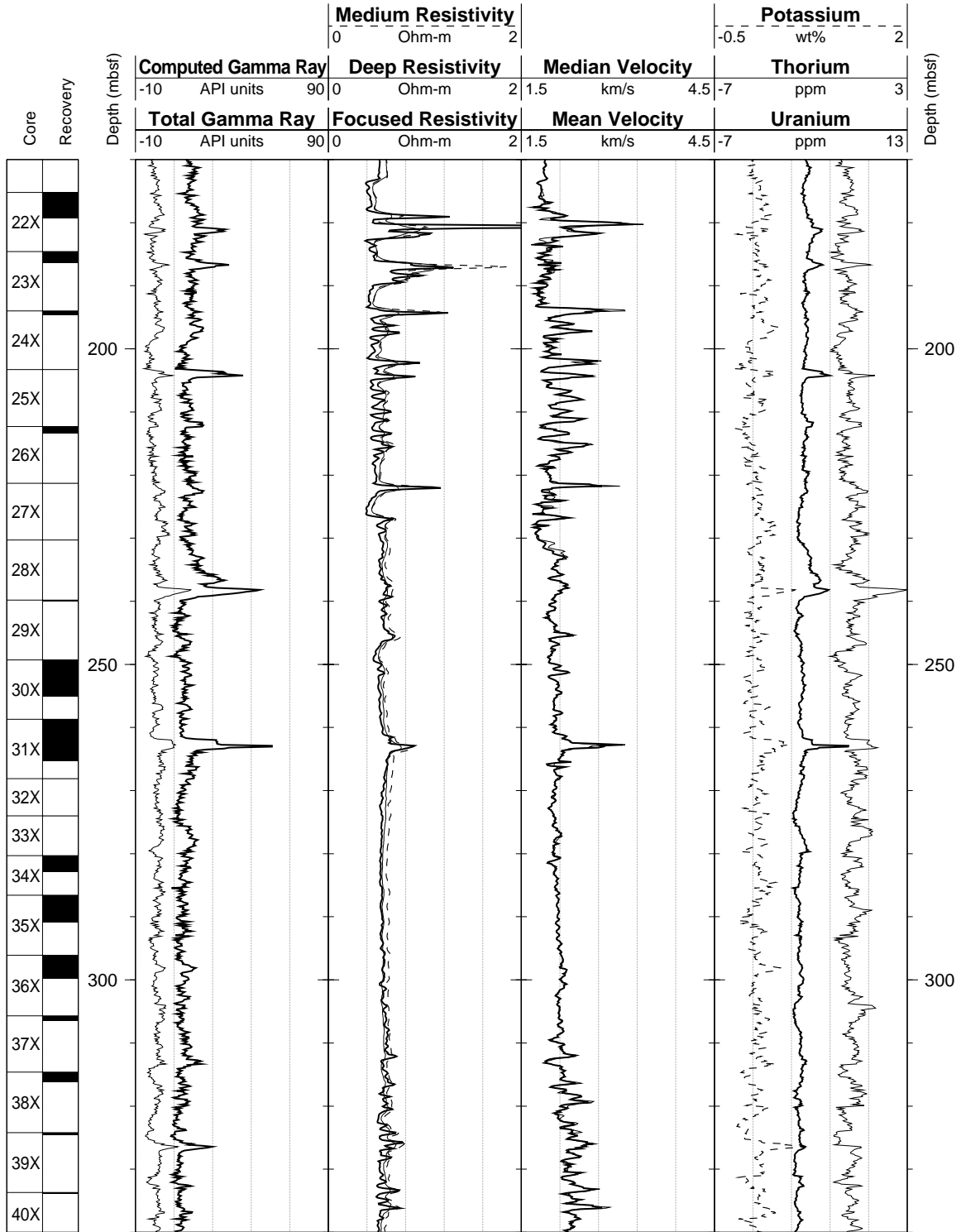
Cristina Broglia  
 Phone: 914-365-8343  
 Fax: 914-365-3182  
 E-mail: chris@ldeo.columbia.edu

Zhiping Tu  
 Phone: 914-365-8336  
 Fax: 914-365-3182  
 E-mail: ztu@ldeo.columbia.edu

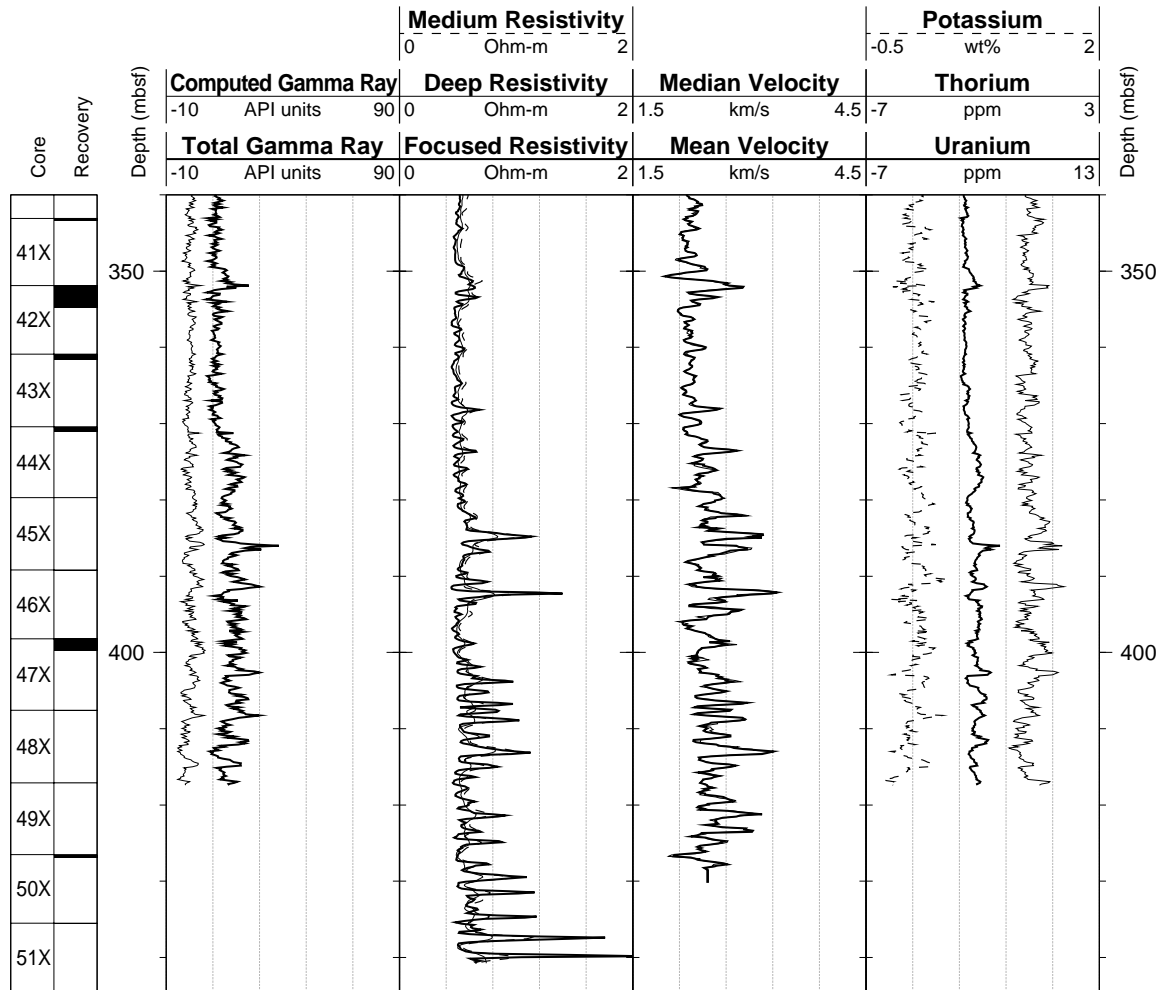
Hole 1005A: Natural Gamma Ray-Resistivity-Sonic Logging Data



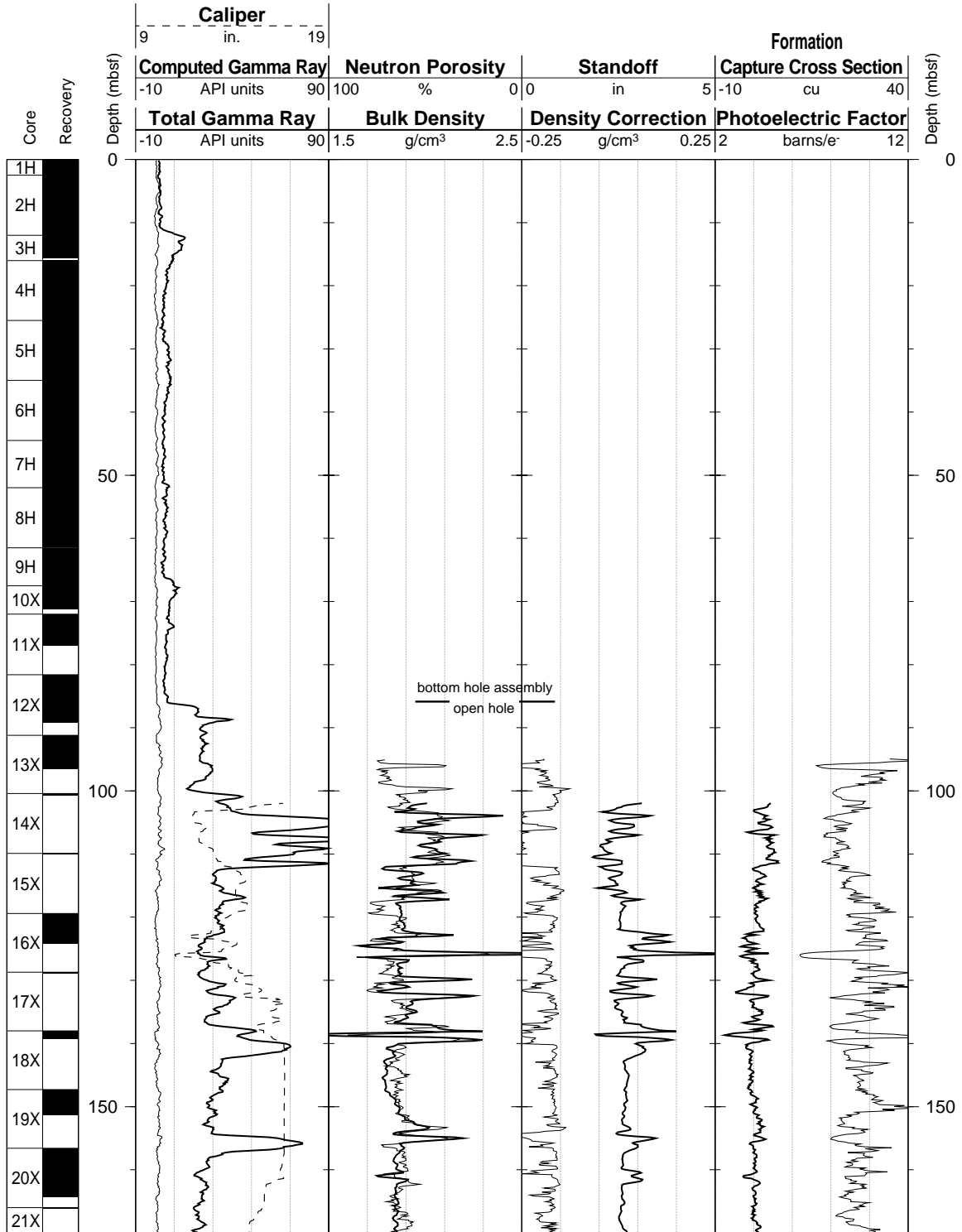
Hole 1005A: Natural Gamma Ray-Resistivity-Sonic Logging Data (cont.)



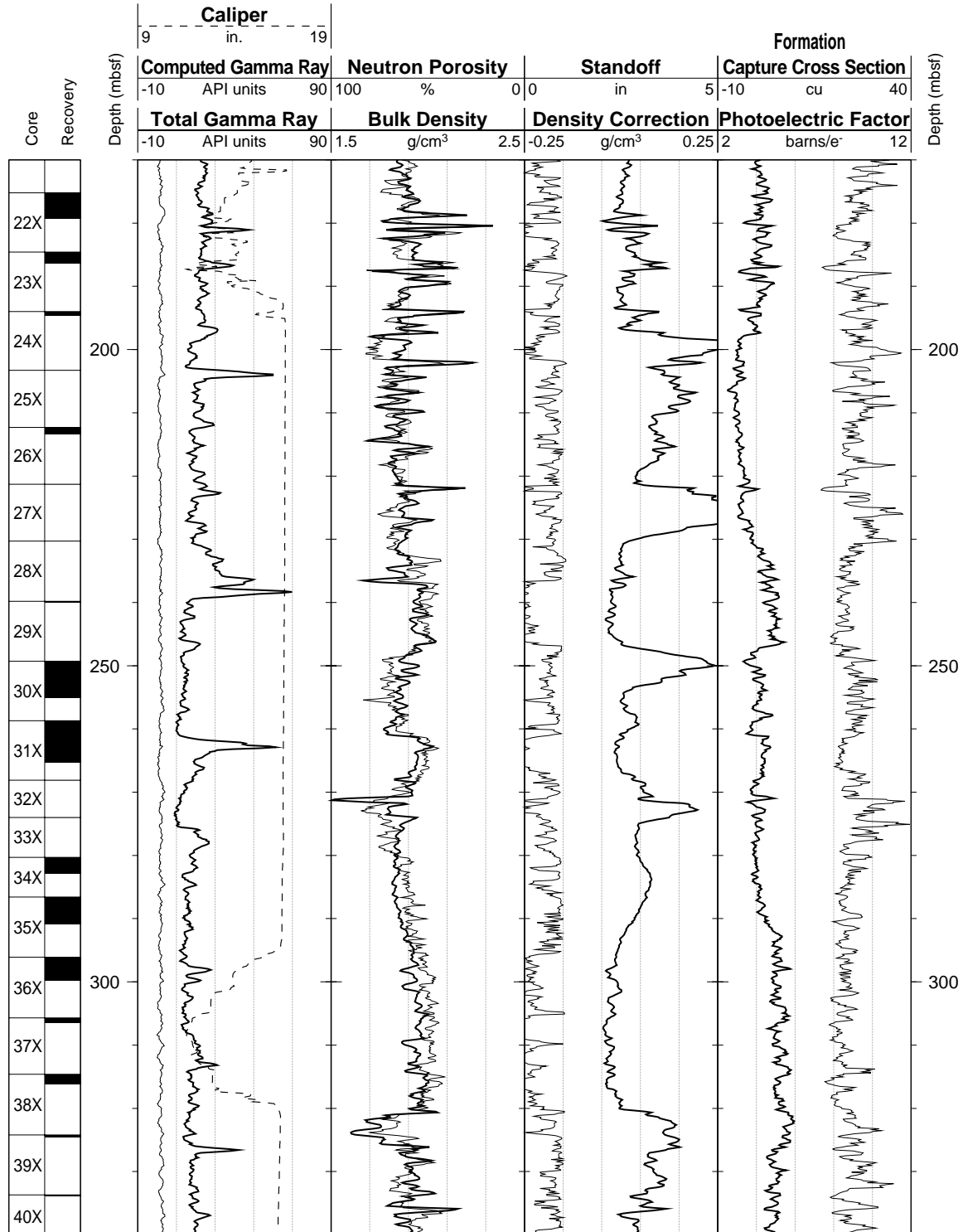
Hole 1005A: Natural Gamma Ray-Resistivity-Sonic Logging Data (cont.)



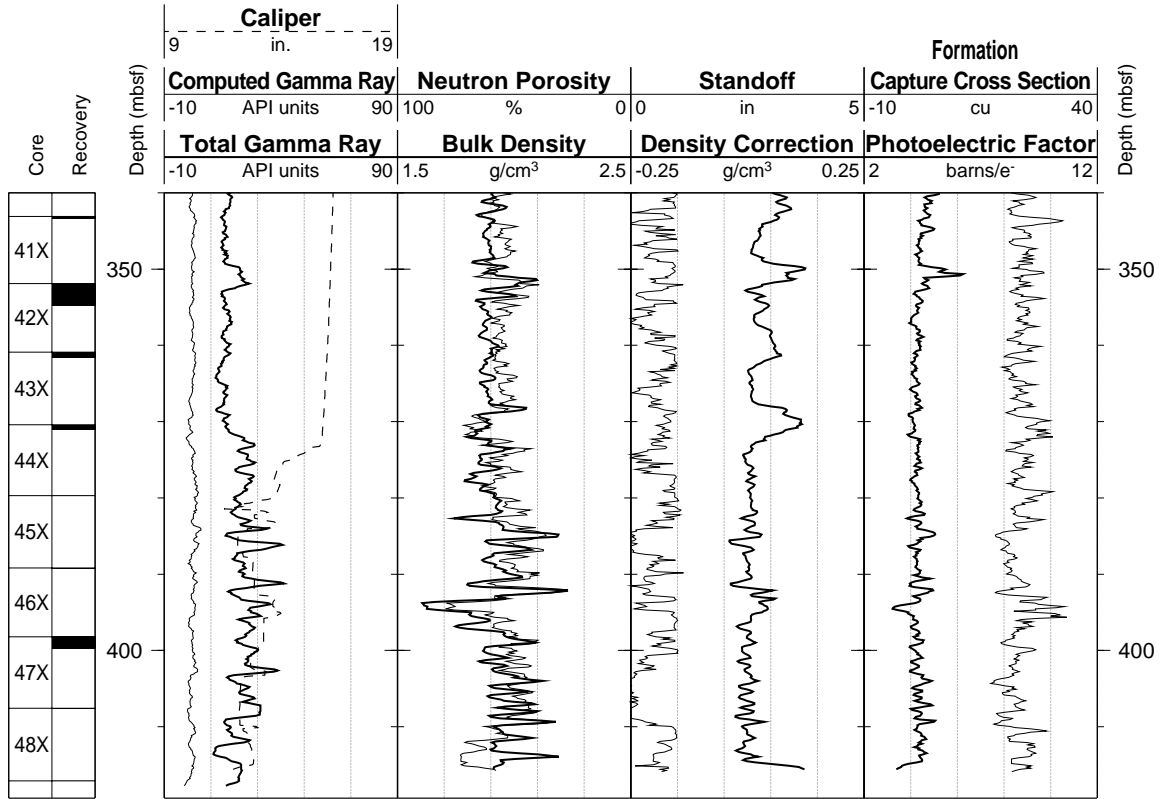
Hole 1005A: Natural Gamma Ray-Density-Porosity Logging Data



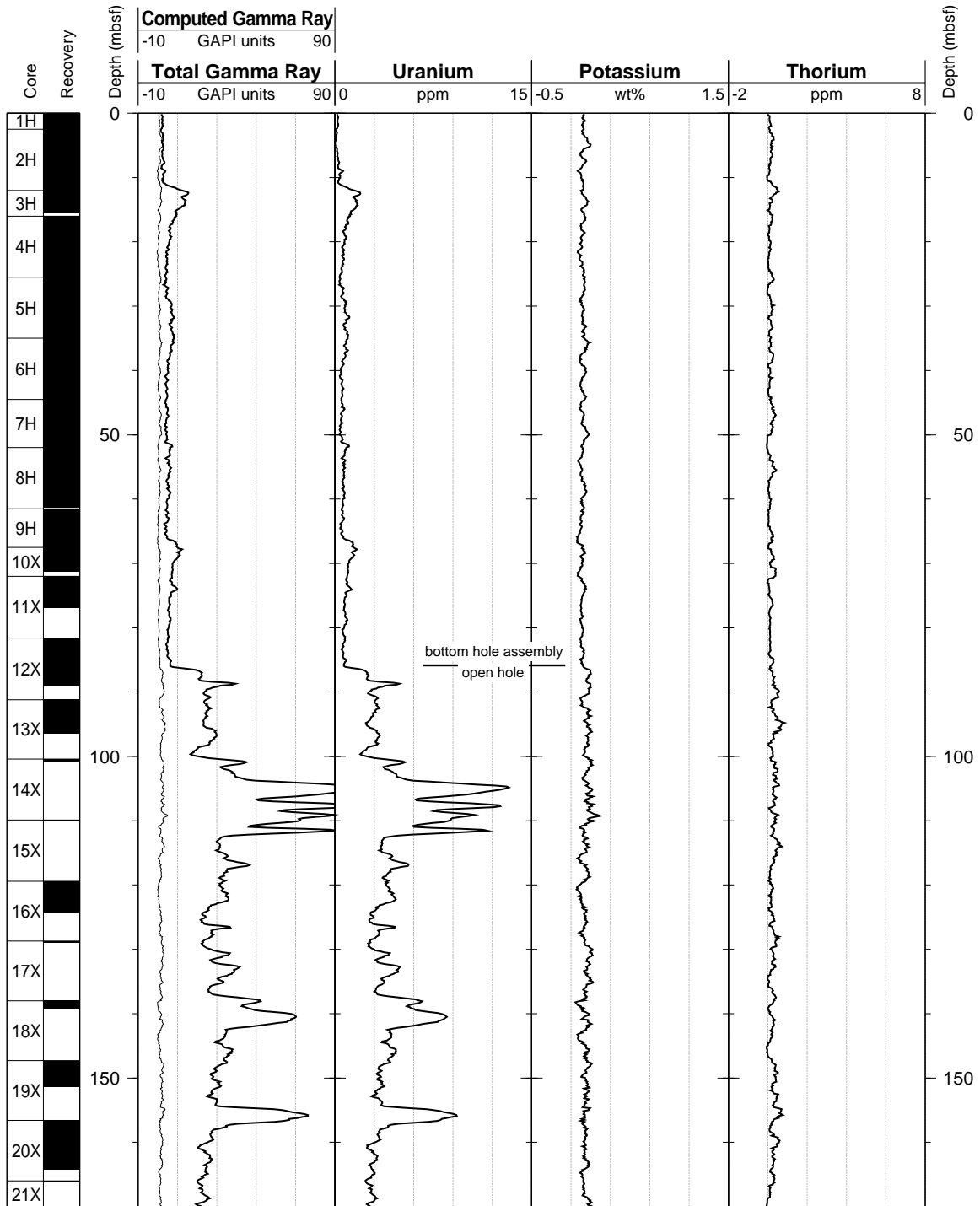
Hole 1005A: Natural Gamma Ray-Density-Porosity Logging Data (cont.)



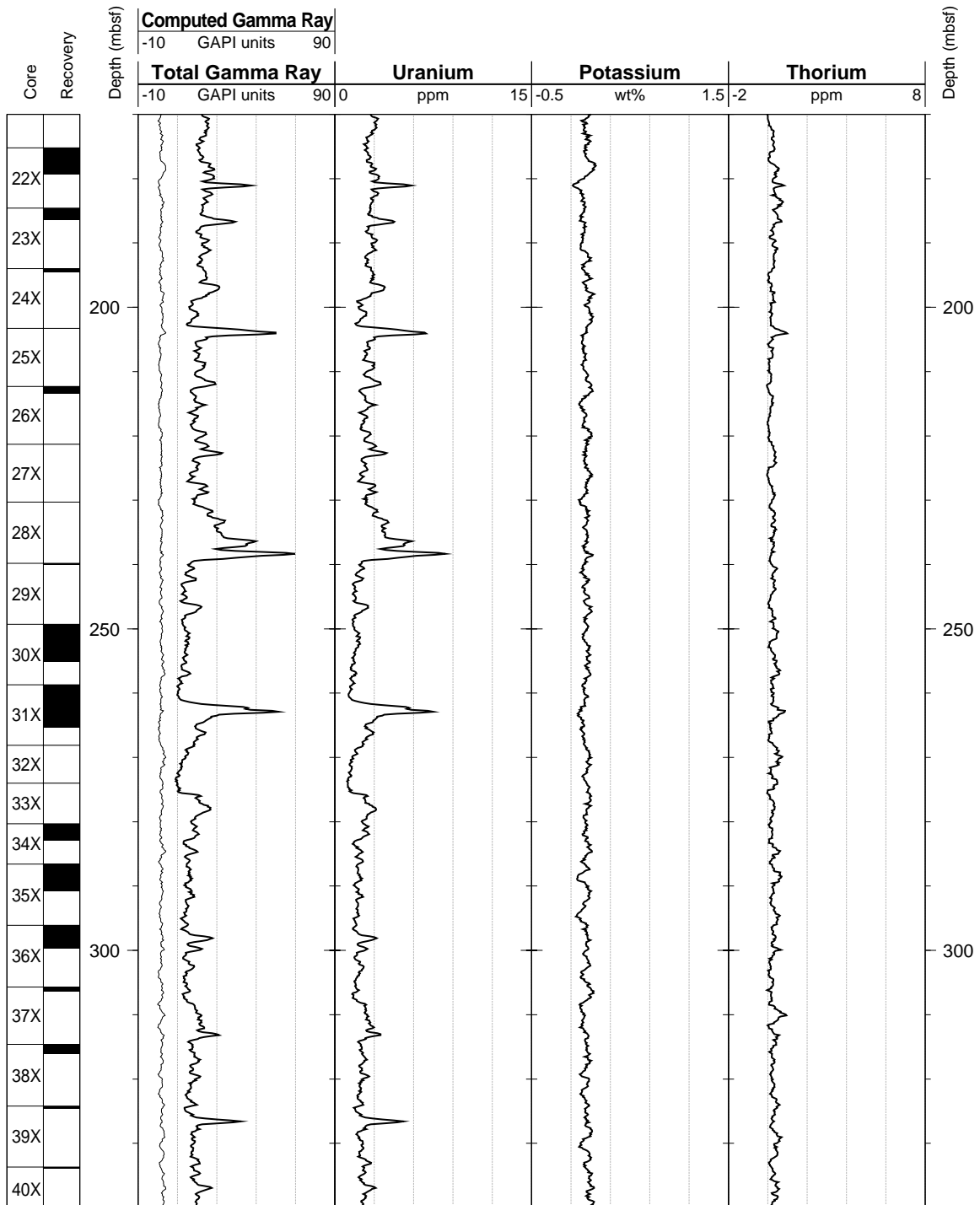
Hole 1005A: Natural Gamma Ray-Density-Porosity Logging Data (cont.)



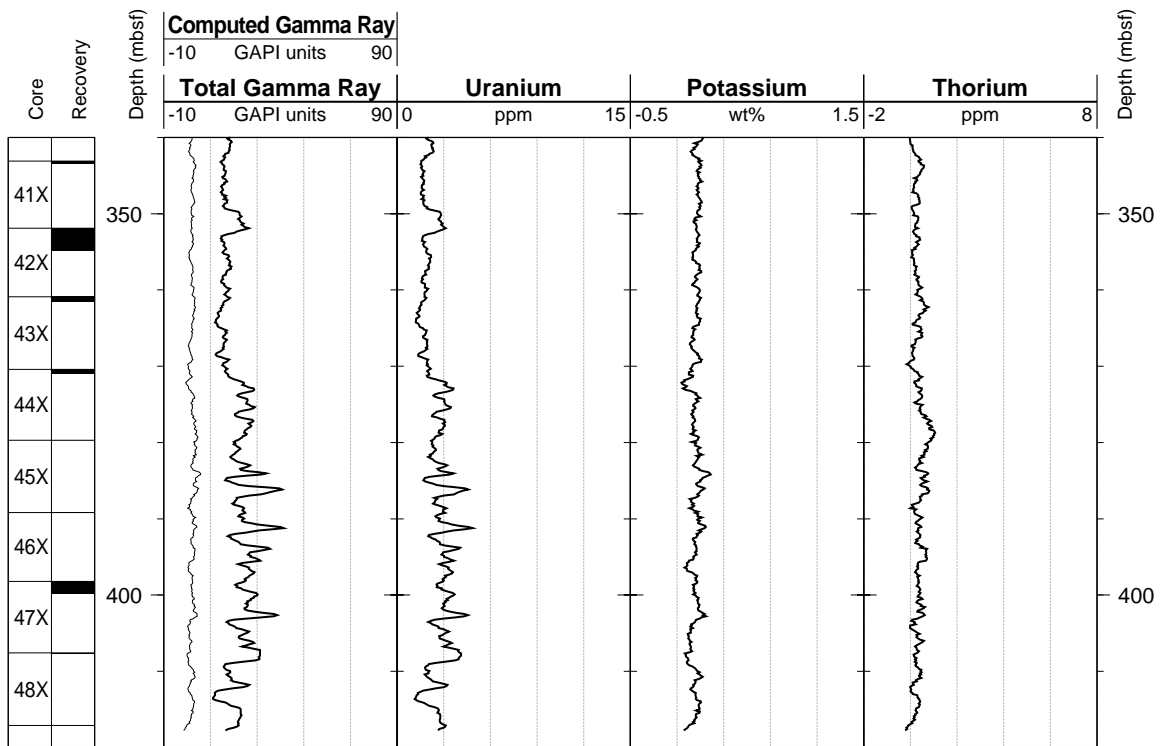
Hole 1005A: Natural Gamma Ray Logging Data



Hole 1005A: Natural Gamma Ray Logging Data (cont.)



Hole 1005A: Natural Gamma Ray Logging Data (cont.)



## SHORE-BASED LOG PROCESSING

## Hole 1005C

**Bottom felt:** 363 mbrf (used to depth shift to sea floor)

**Total penetration:** 700 mbsf

**Total core recovered:** 313.4 m (34.1%)

## Logging Runs

**Logging string 1:** APS/HLDS/HNGS

**Logging string 1:** DIT/SDT/GPIT/NGT

**Logging string 2:** FMS/GPIT/NGT

**Logging string 3:** WST

Wireline heave compensator was used to counter ship heave.

## Bottom-Hole Assembly

The following bottom-hole assembly depths are as they appear on the logs after differential depth shift (see "Depth shift" section) and depth shift to the seafloor. As such, there might be a discrepancy with the original depths given by the drillers on board. Possible reasons for depth discrepancies are ship heave, use of wireline heave compensator, and drill string and/or wireline stretch.

APS/HLDS/HNGS: Bottom-hole assembly at ~383 mbsf.

DIT/SDT/GPIT/NGT: Bottom-hole assembly at ~383 mbsf.

FMS/GPI/NGT: Bottom-hole assembly at ~383 mbsf.

APS/HLDS/HNGS: Drill pipe at ~219 mbsf.

## Processing

**Depth shift:** Original logs have been interactively depth shifted with reference to HNGS from APS/HLDS/HNGS run and to the seafloor (-363 m).

**Gamma-ray environmental corrections:** Corrections for borehole size and type of drilling fluid were performed on the NGT data from the FMS/GPIT/NGT and DIT/SDT/GPIT/NGT tool strings. HNGS data from the APS/HLDS/HNGS tool string were corrected in real-time during the recording.

**Acoustic data processing:** The array sonic tool was operated in standard depth-derived, borehole compensated, long spacing (8–10 and 10–12 ft) and short spacing (3–5 and 5–7 ft) mode. The sonic logs from the long spacing mode have been processed to eliminate some of the noise and cycle skipping experienced during the recording.

## Quality Control

Data recorded through bottom-hole assembly such as the gamma ray data above 376 mbsf should be used only qualitatively because of the attenuation on the incoming signal. Invalid gamma ray spikes were recorded at 366–371 and 376–382.5 mbsf during the DIT/SDT/GPIT/NGT run.

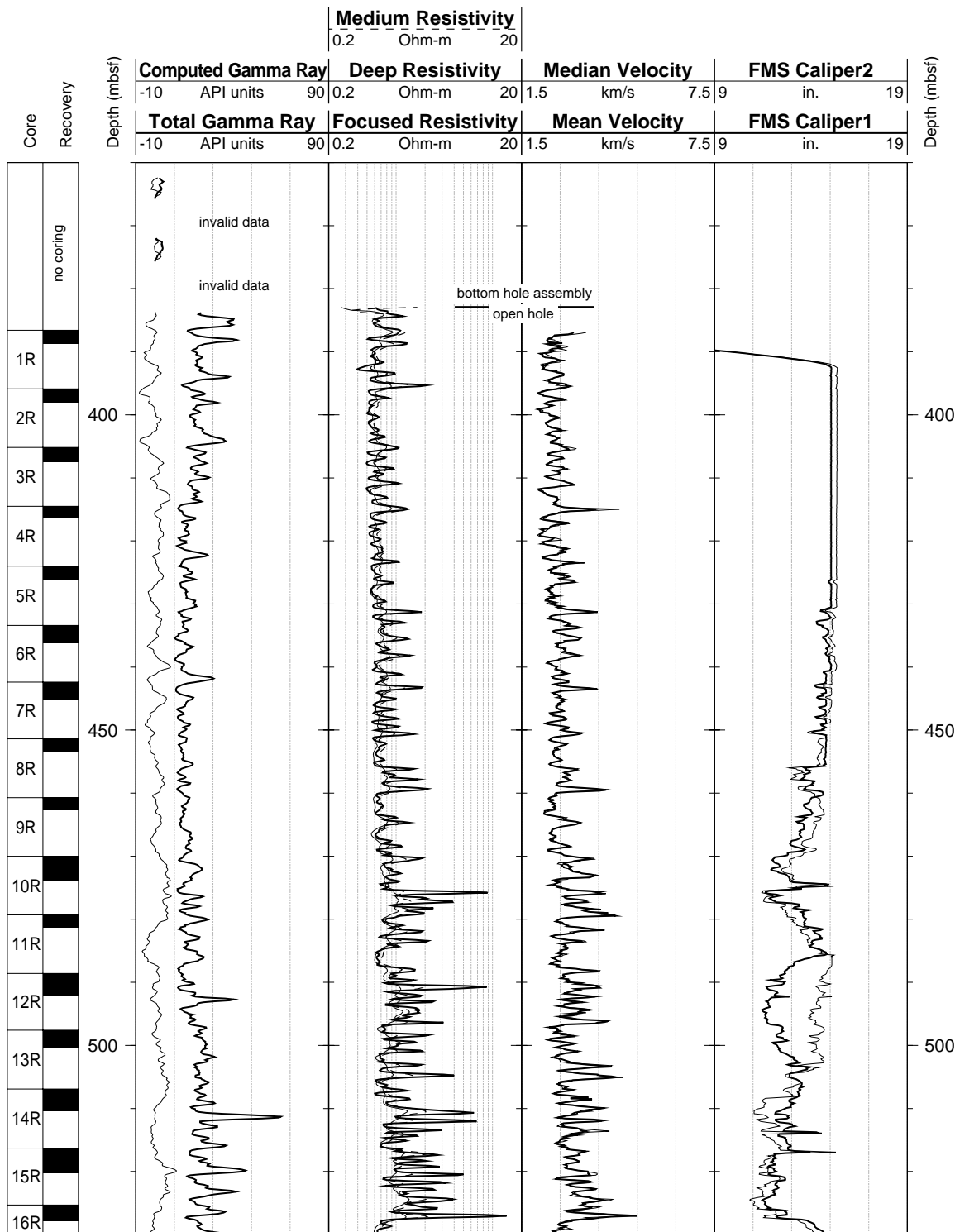
Hole diameter was recorded by the hydraulic caliper on the HLDS tool (LCAL) and the caliper on the FMS/GPIT tool string (C<sub>1</sub> and C<sub>2</sub>).

Details of standard shore-based processing procedures are found in the "Explanatory Notes" chapter, this volume. For further information about the logs, please contact:

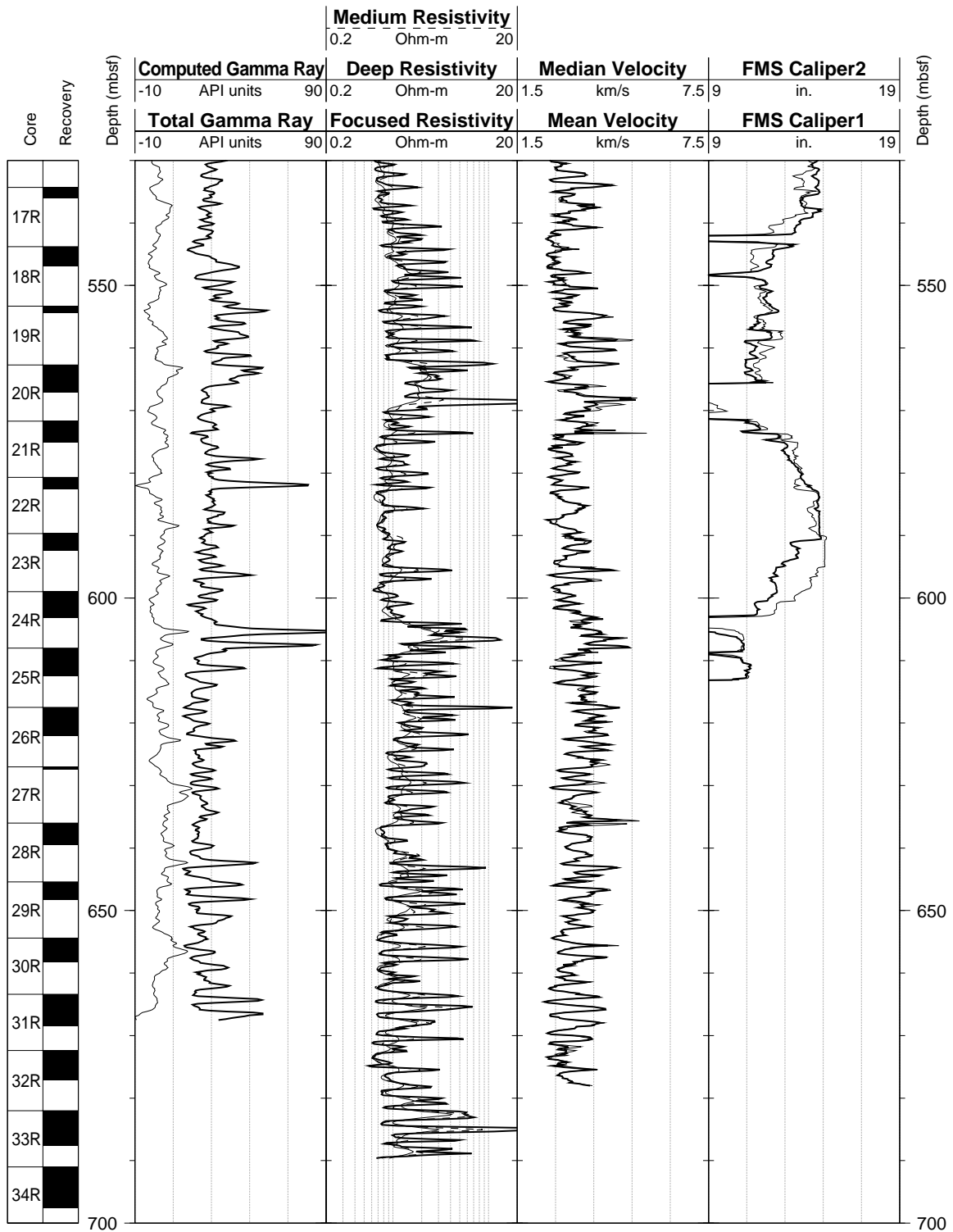
Cristina Broglia  
Phone: 914-365-8343  
Fax: 914-365-3182  
E-mail: chris@ldeo.columbia.edu

Zhiping Tu  
Phone: 914-365-8336  
Fax: 914-365-3182  
E-mail: ztu@ldeo.columbia.edu

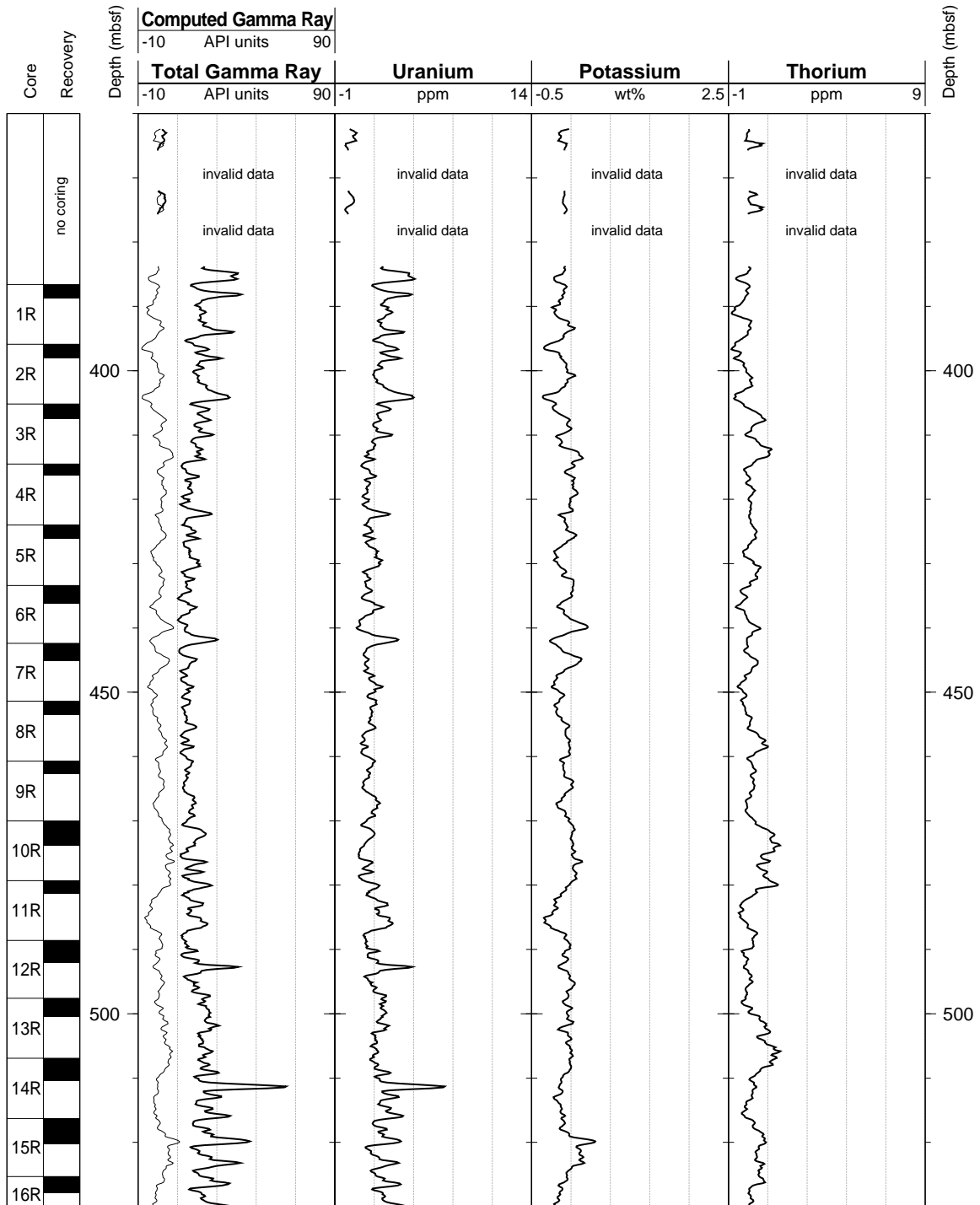
Hole 1005C: Natural Gamma Ray-Resistivity-Sonic Logging Data



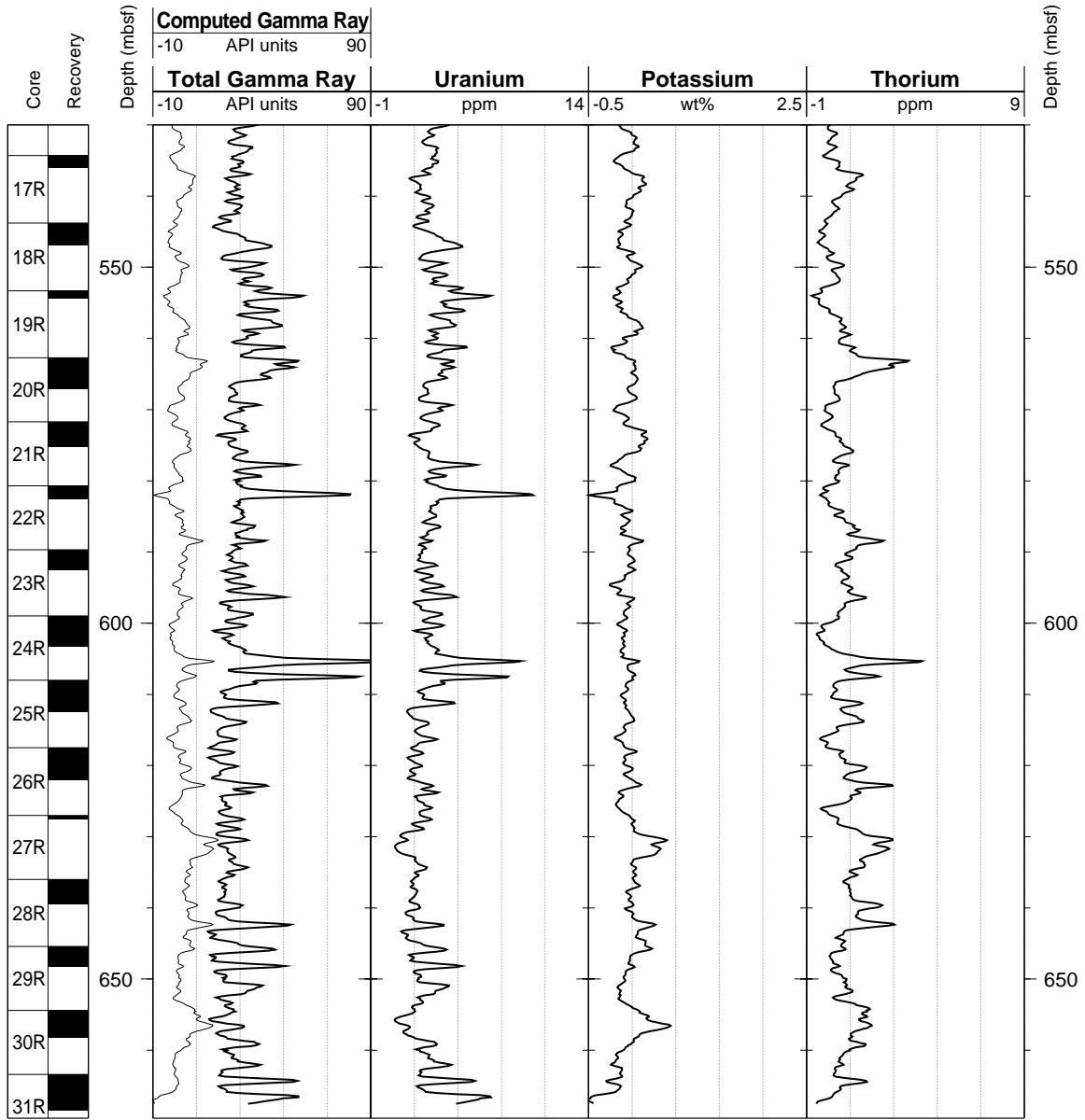
Hole 1005C: Natural Gamma Ray-Resistivity-Sonic Logging Data (cont.)



Hole 1005C: Natural Gamma Ray Logging Data

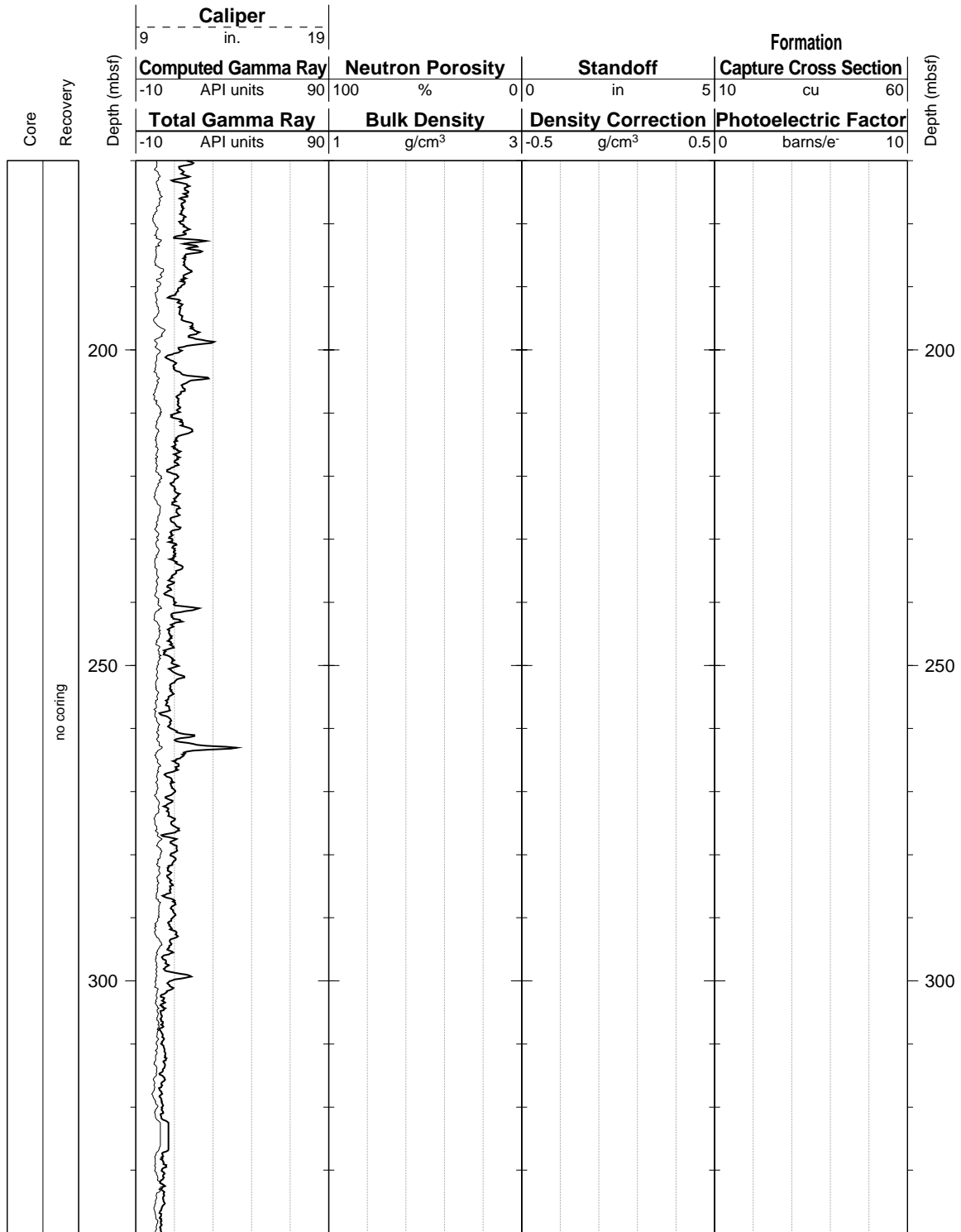


Hole 1005C: Natural Gamma Ray Logging Data (cont.)

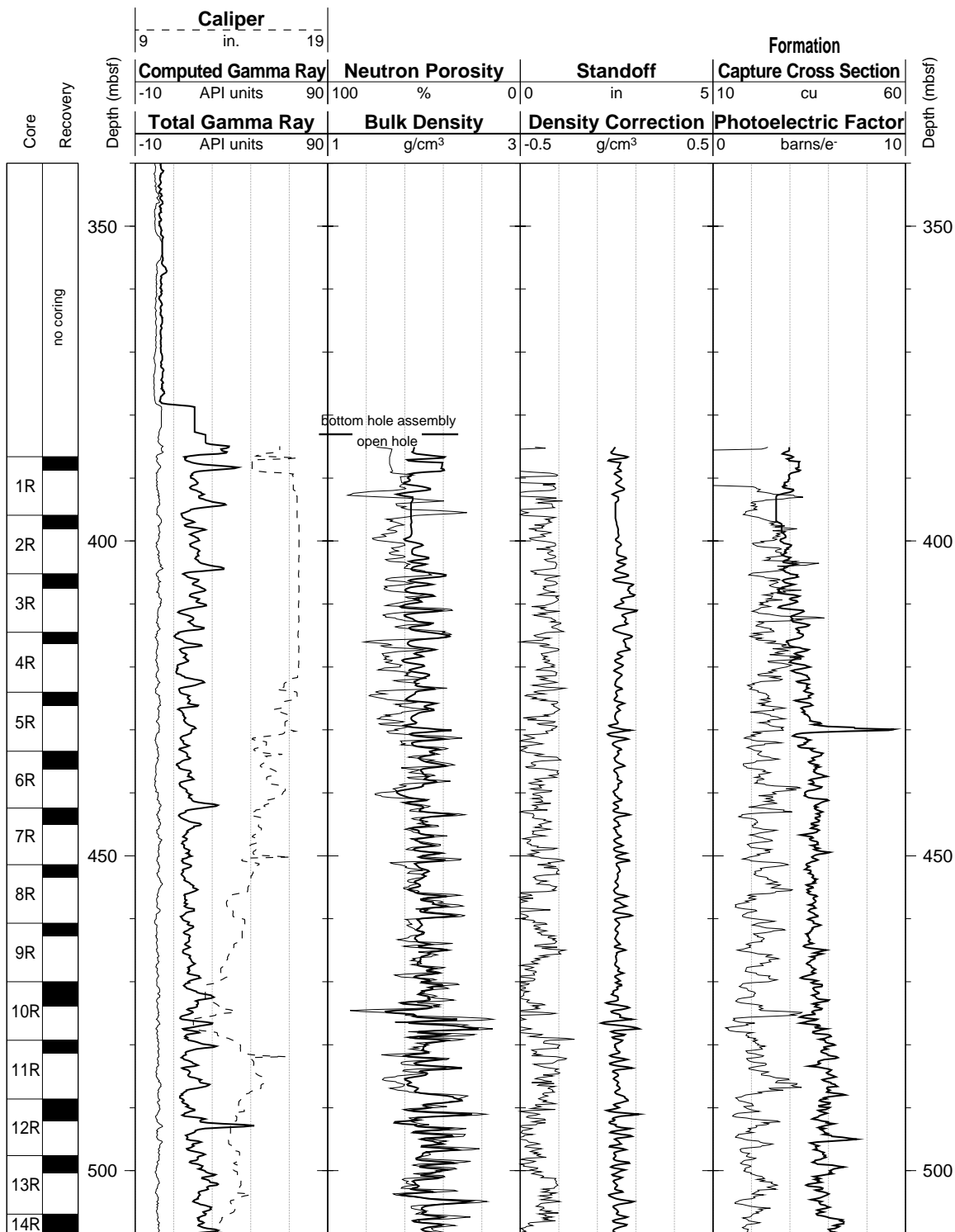




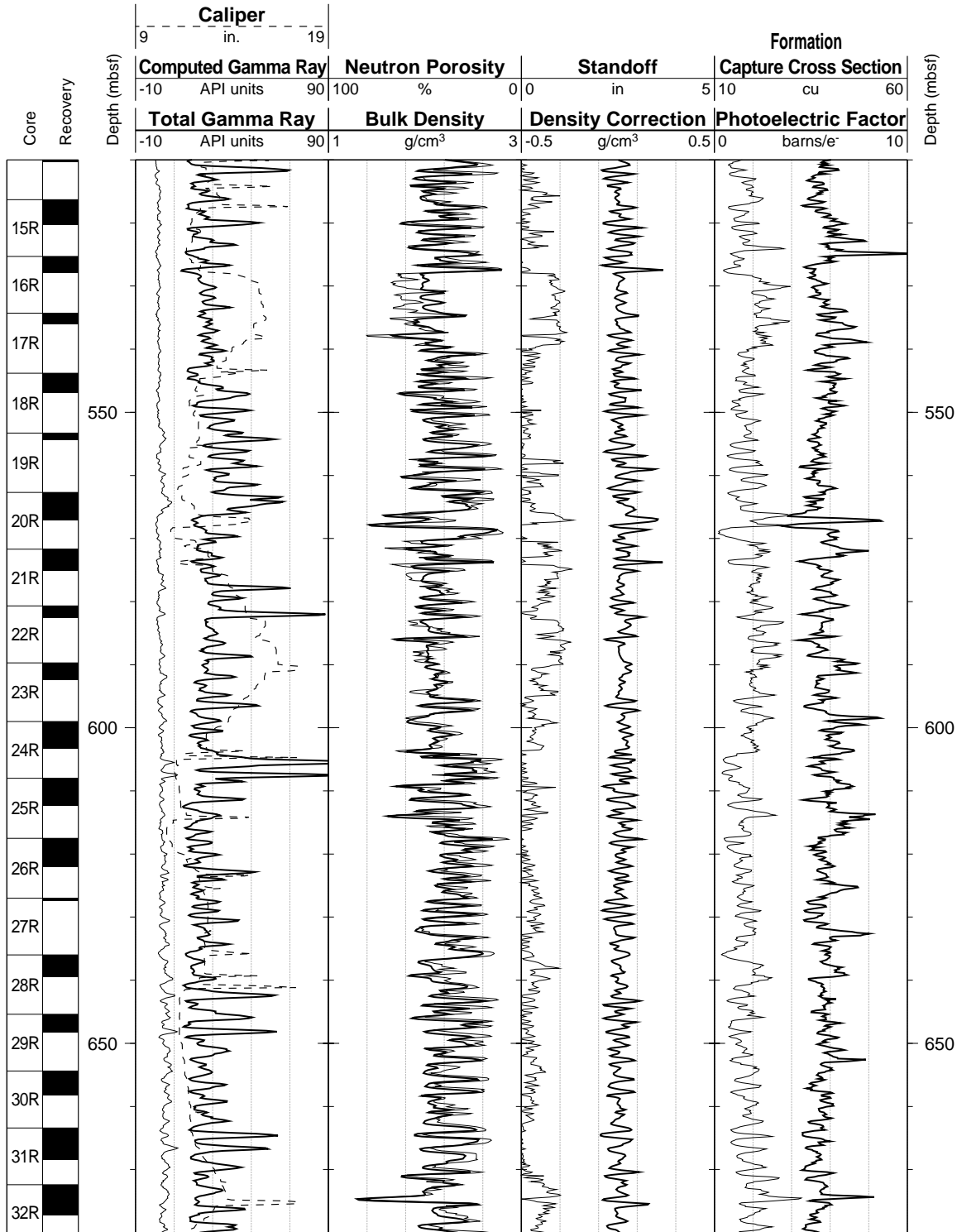
Hole 1005C: Natural Gamma Ray-Density-Porosity Logging Data (cont.)



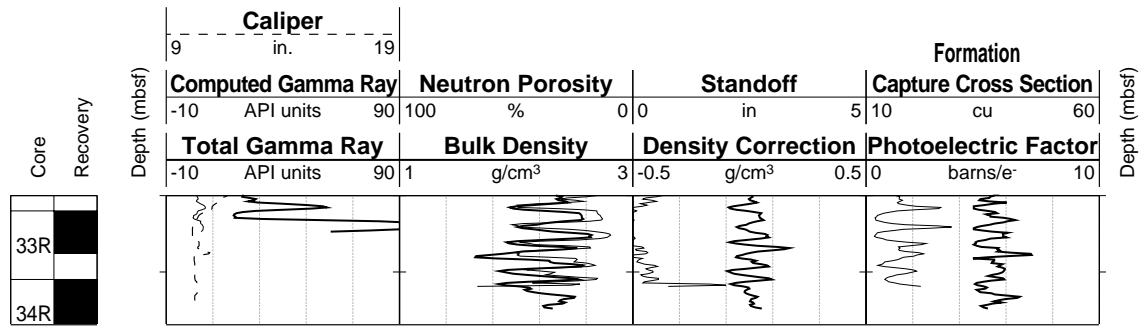
Hole 1005C: Natural Gamma Ray-Density-Porosity Logging Data (cont.)



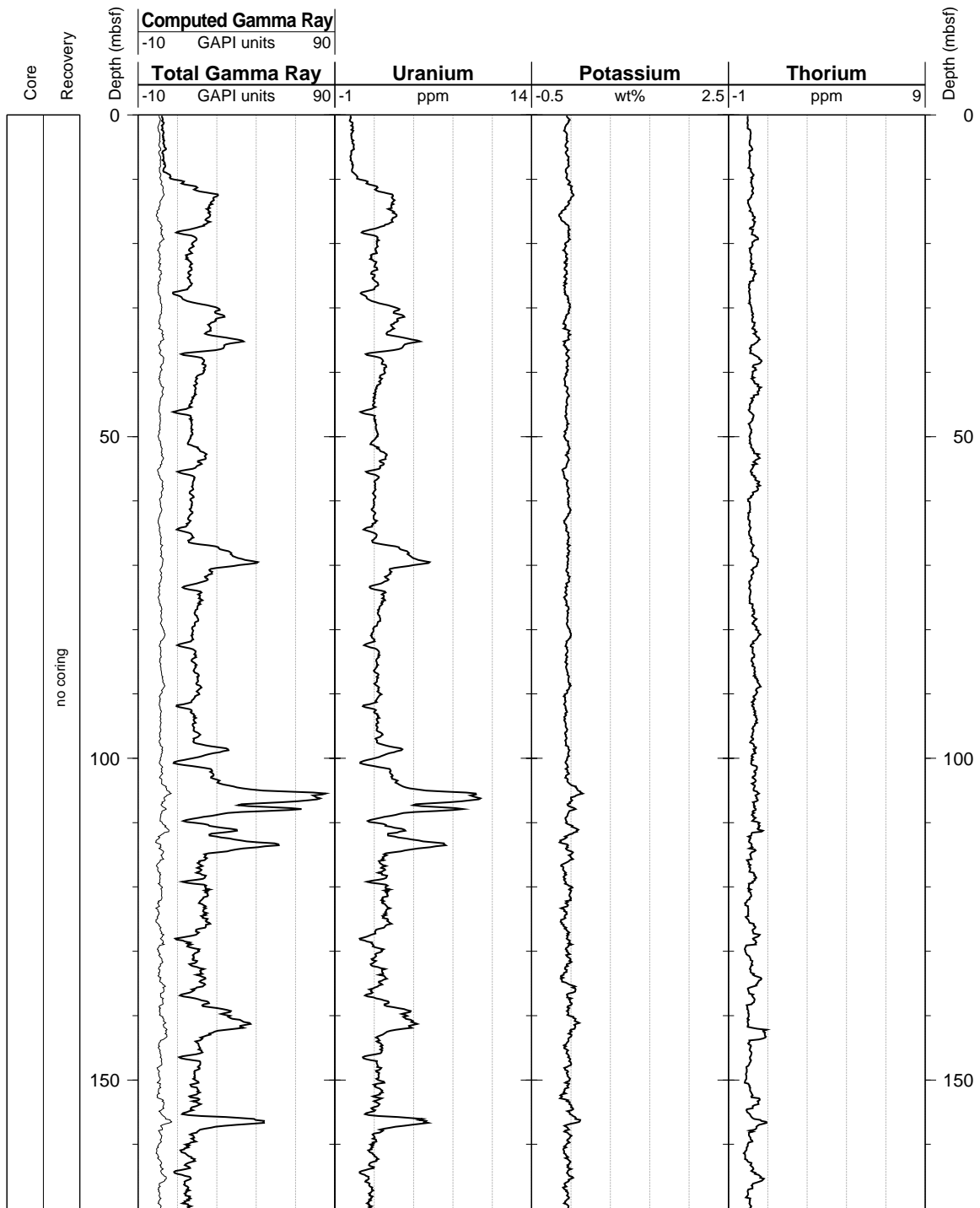
Hole 1005C: Natural Gamma Ray-Density-Porosity Logging Data (cont.)



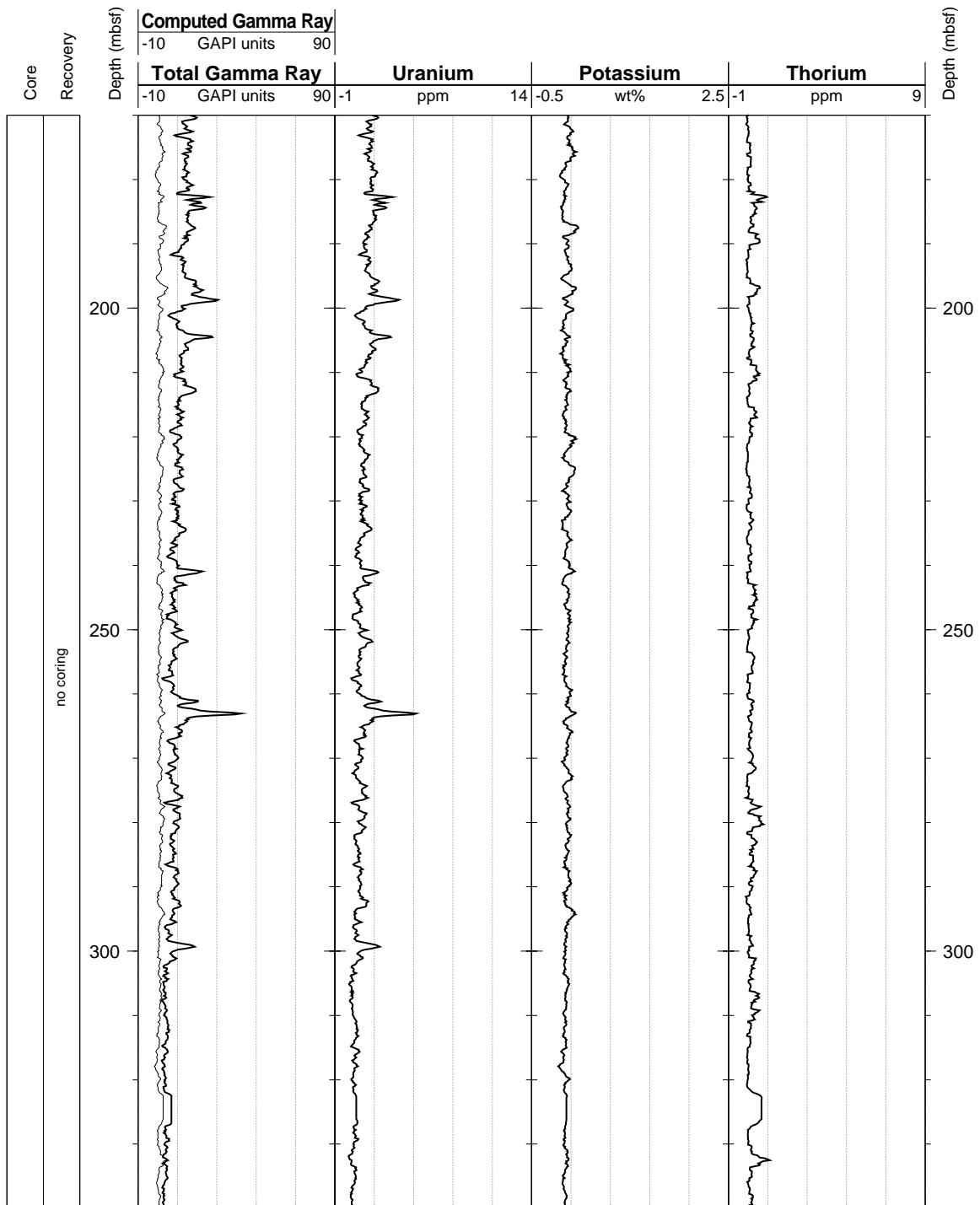
Hole 1005C: Natural Gamma Ray-Density-Porosity Logging Data (cont.)



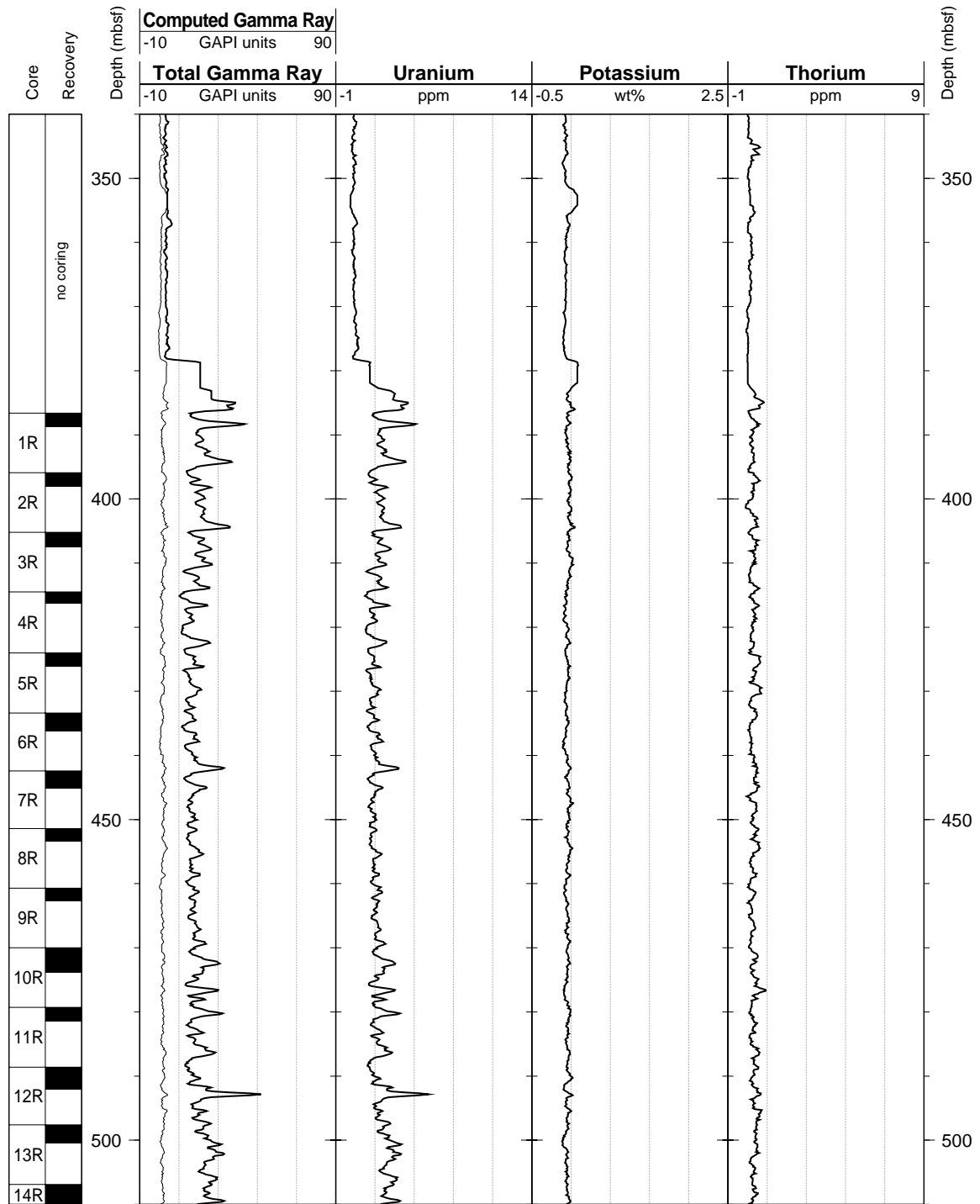
Hole 1005C: Natural Gamma Ray Logging Data



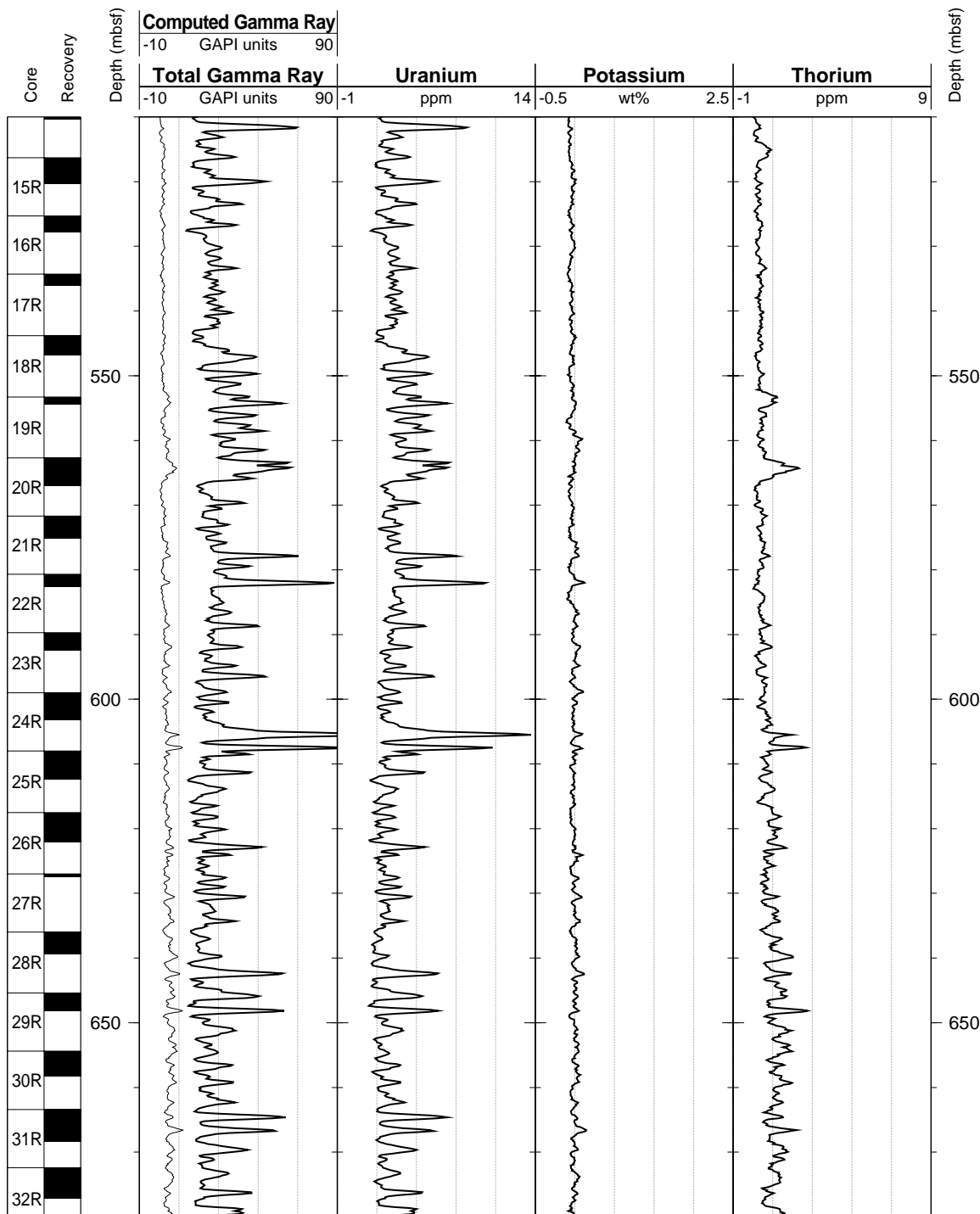
Hole 1005C: Natural Gamma Ray Logging Data (cont.)



Hole 1005C: Natural Gamma Ray Logging Data (cont.)



Hole 1005C: Natural Gamma Ray Logging Data (cont.)



Hole 1005C: Natural Gamma Ray Logging Data (cont.)

